การไหลที่มีผิวอิสระผ่านประตูน้ำเอียง

ว่าที่ ร้อยตรี ภณัฐ ก้วยเจริญพานิชก์

วิทยานิพนธ์นี้เป็นส่วนหนึ่งของการศึกษาตามหลักสูตรปริญญาวิทยาศาสตรมหาบัณฑิต
สาขาวิชาวิทยาการคณนา ภาควิชาคณิตศาสตร์
คณะวิทยาศาสตร์ จุฬาลงกรณ์มหาวิทยาลัย
ปีการศึกษา 2546

ISBN 974-17-5205-9

FREE-SURFACE FLOWS UNDER AN INCLINED SLUICE GATE

Acting Sec. Lt. Panat Guayjarernpanishk

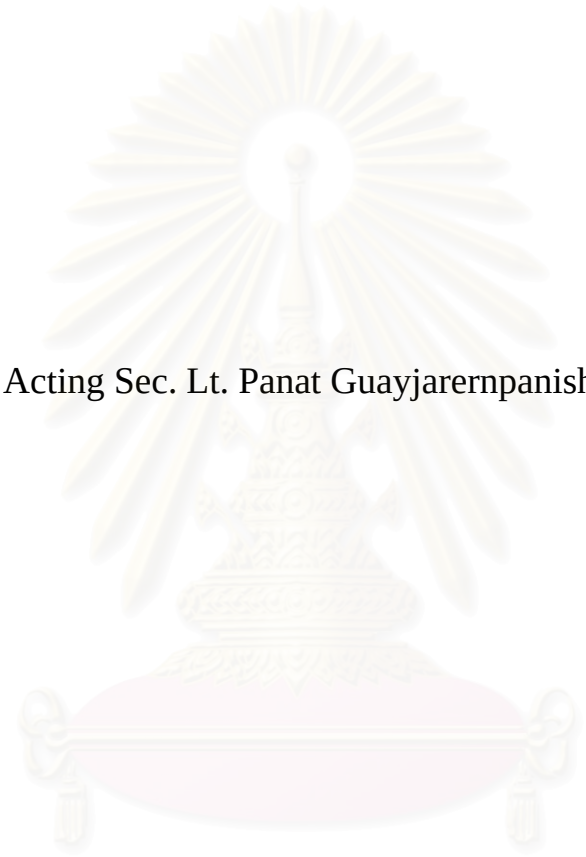

A Thesis Submitted in Partial Fulfillment of the Requirements
for the Degree of Master of Science in Computational Science
Department of Mathematics
Faculty of Science
Chulalongkorn University
Academic Year 2003
ISBN 974-17-5205-9

Thesis title	Free-surface flows under an inclined sluice gate
By	Acting Sec. Lt. Panat Guayjarernpanishk
Field of study	Computational Science
Thesis advisor	Associate Professor Jack Asavanant, Ph.D.

Accepted by the Faculty of Science, Chulalongkorn University in Partial Fulfillment of the Requirements for the Master's Degree

……..…… Dean of the Faculty of Science
(Professor Piamsak Menasveta, Ph.D.)

Thesis Committee

……..…… Chairman
(Associate Professor Pornpote Piumsomboon, Ph.D.)

……..……Thesis Advisor
(Associate Professor Jack Asavanant, Ph.D.)

……..…… Member
(Assistant Professor Pornchai Satravaha, Ph.D.)

……..…… Member
(Assistant Professor Vimolrat Ngamaramvarangnul, Ph.D.)

ภณัฐ ก้วยเจริญพานิชก์ : การไหลที่มีผิวอิสระผ่านประตูน้ำเอียง (FREE-SURFACE FLOWS UNDER AN INCLINED SLUICE GATE)
อ.ที่ปรึกษา : รองศาสตราจารย์ ดร. จักษ์ อัศวานันท์, จำนวนหน้า 81 หน้า. ISBN 974-17-5205-9

ในวิทยานิพนธ์ฉบับนี้ เราพิจารณาปัญหาการไหลที่มีผิวอิสระผ่านประตูน้ำ โดยประตูน้ำเอียงทำมุม γ กับแนวราบ ของไหลที่พิจารณาเป็นของไหลที่ไม่มีความหนืดและไม่มีการบีบอัดตัว สำหรับสมมติฐานเกี่ยวกับการไหล คือ การไหลเป็นการไหลแบบสม่ำเสมอ ใน 2 มิติ และการไหลไม่มีการหมุนวน ในที่นี้จะไม่พิจารณาผลกระทบจากแรงตึงผิว ส่วนเงื่อนไขขอบแบบพลศาสตร์บนผิวอิสระด้านต้นน้ำและท้ายน้ำนั้น จะพิจารณาแรงที่เกิดจากแรงโน้มถ่วงของโลกด้วย สำหรับเทคนิคเชิงตัวเลขที่ใช้ในการคำนวณหาคำตอบของปัญหานี้คือ เทคนิคของสมการปริพันธ์เชิงขอบ (boundary integral equation technique) และหลังจากการทำปัญหาให้เป็นแบบภินทนะแล้ว เราจะหาคำตอบของระบบสมการไม่เชิงเส้นนี้ด้วยระเบียบวิธีของนิวตัน เมื่อจุดแยกระหว่างต้นน้ำและประตูน้ำเป็นจุดหยุดนิ่ง (stagnation point) ค่ามุมเอียงของประตูน้ำที่สามารถคำนวณหาคำตอบเชิงตัวเลขได้นั้นจะอยู่ในช่วง $\left(\chi, \frac{\pi}{2}\right)$ โดยที่ χ คือ ค่าขอบเขตน้อยสุดของมุมเอียงของประตูน้ำ ซึ่งแปรผันตาม ความยาวของประตูน้ำ และสอดคล้องกับจำนวนของฟรุด (Froude number) เมื่อความยาวของประตูน้ำลดลง คลื่นที่เกิดขึ้นทางด้านต้นน้ำจะมีลักษณะเป็นคลื่นที่ไม่เชิงเส้นมากยิ่งขึ้น กล่าวคือ ยอดคลื่นจะมีลักษณะแคบส่วนท้องคลื่นจะมีลักษณะกว้าง และการคำนวณหาคำตอบเชิงตัวเลขของปัญหานี้ จะมีความยุ่งยากมากยิ่งขึ้น เมื่อมุมเอียงของประตูน้ำเข้าใกล้ค่าของ χ เหตุที่เป็นเช่นนี้ก็เพราะว่า ผิวอิสระบริเวณใกล้จุดแยกของต้นน้ำและประตูน้ำประพฤติตัวไม่สอดคล้องกับสมบัติของจุดหยุดนิ่ง นอกเหนือจากนี้แล้ว เรายังพบคำตอบเชิงตัวเลขของปัญหาการไหลผ่านประตูน้ำเอียงในกรณีที่ผิวอิสระบริเวณจุดแยกทั้งสองของประตูน้ำ มีลักษณะต่อเนื่องกับแนวของเส้นสัมผัสของประตูน้ำ (smooth attachment)

ภาควิชา **คณิตศาสตร์** ลายมือชื่อนิสิต.....
สาขาวิชา **วิทยาการคณนา** ลายมือชื่ออาจารย์ที่ปรึกษา.....
ปีการศึกษา **2546**

4472358023 : MAJOR COMPUTATIONAL SCIENCE
KEYWORDS : FREE-SURFACE FLOWS / INCLINED SLUICE GATE / BOUNDARY INTEGRAL METHOD / STAGNATION POINT / SMOOTH ATTACHMENT

PANAT GUAYJARERNPANISHK : FREE-SURFACE FLOWS UNDER AN INCLINED SLUICE GATE. THESIS ADVISOR: ASSOCIATE PROFESSOR JACK ASAVANANT, Ph. D, 81 pp. ISBN 974-17-5205-9

In this thesis we consider the problem of free-surface flows under a gate that is inclined at an angle γ. The fluid is treated as inviscid and incompressible. The flow is assumed to be steady two-dimensional and irrotational. The effect of surface tension is neglected. Dynamic boundary condition is applied on both upstream and downstream free surfaces subject to gravitational force. The problem is solved numerically by using boundary integral equation technique. After the discretization, we obtain a system of nonlinear algebraic equations which can be solved by the Newton's method. When the upstream free surface separates at a stagnation point, numerical results for inclined gate are presented for various values of γ. These solutions exist for certain values of gate inclination, in particular, $\chi < \gamma \leq \frac{\pi}{2}$. Here χ is the lower bound for gate inclination depending on the gate length and the corresponding Froude number. As the gate length decreases, nonlinear effect on the upstream waves becomes more pronounced in that the waves tend to develop narrow crests and broad troughs. Difficulties arise in the numerical computation as we attempt to calculate solutions for $\gamma \downarrow \chi$. This is because the free surface near upstream separation can no longer satisfy the prescribed stagnation point behavior. We also investigate the problem of flows past an inclined gate with smooth attachment. It is found that there are solutions for which the flows have been continuously tangent at both ends of the gate at which separation occurs.

Department **Mathematics** Student's signature.....

Field of study **Computational Science** Advisor's signature.....

Academic year **2003**

ACKNOWLEDGEMENTS

I should like to express my deep gratitude to the many contributors to this thesis Associate Professor Dr. Jack Asavanant, who is my thesis adviser, very kindly read and edited the thesis and offered many useful suggestion. Also, I would like to thank the chairman and members of the committee of this thesis, Associate Professor Dr. Pornpote Piumsomboon, Assistant Professor Dr. Pornchai Satravaha and Assistant Professor Dr. Vimolrat Ngamaramvaranggul, who made helpful comments on the suitability of thesis content. Besides, I feel very thankful to all of my teachers who have taught me for my knowledge and skill.

This research was supported in parts by the University Development Commission (U.D.C.) Scholarship and Chulalongkorn University's Research Division. I must also extend my thanks to Advanced Visualization and Intelligent Computing Center-AVIC and Department of mathematics for various forms of help.

In particular, I would like express my sincere gratitude to my beloved parents for their kind encouragement throughout my study.

TABLE OF CONTENTS

page

ABSTRACT IN THAI iv

ABSTRACT IN ENGLISH v

ACKNOWLEDGEMENTS vi

TABLE OF CONTENTS vii

LIST OF TABLES ix

LIST OF FIGURES x

CHAPTER

I INTRODUCTION 1

II FORMULATION OF FREE-SURFACE FLOWS UNDER AN INCLINED SLUICE GATE 4

2.1 Dynamic and Kinematic Boundary Conditions 4

2.2 Dimensionless Variables 6

2.3 Potential Function and Stream Function 6

2.4 Conformal Mapping 9

2.5 Boundary Integral Equation 11

III NUMERICAL PROCEDURE OF FREE-SURFACE FLOWS UNDER AN INCLINED SLUICE GATE 17

IV NUMERICAL RESULTS OF FREE-SURFACE FLOWS UNDER AN INCLINED SLUICE GATE WITH STAGNATION POINT 23

4.1 The Vertical Sluice Gate 24

4.2 The Gate Inclination between 60° and 90° ($60° \leq \gamma < 90°$) 33

4.3 The Gate Inclination between 0° and 60° ($0° \leq \gamma < 60°$) 49

TABLE OF CONTENTS (Continued)

CHAPTER page

V NUMERICAL RESULTS OF FREE-SURFACE FLOWS UNDER AN INCLINED SLUICE GATE WITH SMOOTH ATTACHMENT . 61

VI CONCLUSIONS 74

REFERENCES 76

APPENDIX 78

VITA 81

LIST OF TABLES

TABLE page

Table 2.1 Values of major points in f - plane and ζ - plane. 9

Table 4.1 Numerical values of the downstream Froude number F between ours and Vandan-Broeck. 32

LIST OF FIGURES

FIGURE page

Figure 2.1 Sketch of free-surface flows under an inclined sluice gate. 4

Figure 2.2 Flow configurations in the complex potential f - plane. 8

Figure 2.3 The flow in the complex ζ - plane. 10

Figure 2.4 Contour Γ in the complex ζ - plane. 12

Figure 4.1 Profiles of the free surfaces and the gate when $\gamma = 90°$. The symbol $\circ$ indicates the position of the points at which the upstream and downstream free surfaces separate from the gate. . 25

Figure 4.2 Upstream free surface of $\phi_C = 1.00$. 29

Figure 4.3 Values of the contraction coefficient C_c versus $\frac{y_C}{y_B}$. The symbols crosses and squares correspond to the calculation of Fangmeier and Strelkoff (1968) and Vanden-Broeck (1997), respectively. 30

Figure 4.4 Values of the contraction coefficient C_c versus F^2. 30

Figure 4.5 Profiles of the upstream free surface with $\Delta_1 = 0.01$ (broken line) and $\Delta_1 = 0.02$ (solid curve) for $\phi_C = 0.19$. 32

Figure 4.6 Profiles of the free surfaces and the gate when $\gamma = 80°$. 34

Figure 4.7 Profiles of the free surfaces and the gate when $\gamma = 70°$. 38

Figure 4.8 Profiles of the free surfaces and the gate when $\gamma = 60°$. 42

Figure 4.9 Profiles of the upstream free surface with $\Delta_1 = 0.01$ (broken line) and $\Delta_1 = 0.02$ (solid curve) for $\phi_C = 0.26$ and $\gamma = 60°$. 46

Figure 4.10 Relationship between the contraction coefficient C_c and $\frac{y_C}{y_B}$. 46

Figure 4.11 Relationship between the contraction coefficient C_c and F^2. 47

Figure 4.12 The gate inclination γ is shown as a function of F^2. 48

LIST OF FIGURES (Continued)

FIGURE page

Figure 4.13 The length L of the gate is shown as a function of F^2. 48

Figure 4.14 Profiles of the free surfaces and the gate when $\gamma = 55°$. 50

Figure 4.15 Profiles of the free surfaces and the gate when $\gamma = 45°$. 53

Figure 4.16 Profiles of the free surfaces and the gate when $\gamma = 35°$. 56

Figure 4.17 The amplitude A of the waves versus F. 58

Figure 4.18 Values of the contraction coefficient C_c versus $\frac{y_C}{y_B}$. 58

Figure 4.19 Values of the contraction coefficient C_c versus F^2. 59

Figure 4.20 The length L of the gate versus F^2. 59

Figure 4.21 The gate inclination γ versus F^2. 60

Figure 5.1 Profiles of the free surfaces and the gate when $\gamma = 6°$. 63

Figure 5.2 Profiles of the free surfaces and the gate when $\gamma = 7°$. 65

Figure 5.3 Profiles of the free surfaces and the gate when $\gamma = 8°$. 68

Figure 5.4 Blow up of the free surface near upstream separation point of Figure 5.2 (a), (c) and (e). 70

Figure 5.5 Blow up of the free surface near upstream separation point of Figure 5.3 (a), (c) and (e). 70

Figure 5.6 Values of the contraction coefficient C_c versus F^2. 71

Figure 5.7 Values of the contraction coefficient C_c versus $\frac{y_C}{y_B}$. 71

Figure 5.8 Numerical value of y at waves crests versus F^2 for $\gamma = 7°$. As $y^* = \frac{F^2}{2} + 1$ is the maximum level. 72

Figure 5.9 The amplitude A of the waves versus the upstream Froude number F_U. 72

LIST OF FIGURES (Continued)

FIGURE page

Figure 5.10 The steepness s of the waves versus the upstream Froude number F_U. The dot-dash curve corresponds the limiting cases characterized by a 120° angle at the crests (Cokelet 1977). 73

CHAPTER I

Introduction

Free-surface flow under a sluice gate is one of the well known classical problem in fluid mechanics. Analytical and numerical results have been proposed for different flow configurations by many researchers. Such mathematical and numerical techniques for solving this problem are, for examples, finite difference method, finite element method, boundary integral method, conformal transformation and etc.

Free streamline solutions of flow under a gate were studied by Rayleigh in the mid nineteenth century. He neglected the effect of gravity and solved by using conformal transformations. Pajer (1937) was the first to consider the influence of gravity on this problem. Seriously numerical solutions of free-surface flows were introduced by Southwell and Vaisey (1946). They included the effect of gravity on the upstream free surface. The flow was governed by Laplaces equation for which it was solved by finite difference method with relaxation procedures. In 1952, Binnie suggested the use of nondimensional parameter, the Froude number, and gave a tentative argument indicating that waves cannot be present on the downstream side of the gate. McCorquodale and Li (1955) was among the first to use finite element method to solve this problem. Approximately analytic solutions were derived by Benjamin (1956) using the theories of jets and solitary wave and compared with experimental results for the same sluice gate opening. Fangmeier and Strelkoff (1968) formulated the problem via complex function theory as nonlinear integral equations and solved numerically. Cheng, et al. (1981) was one

of the first to formulate the problem using Boundary Integral Equation Method (BIEM). He showed that to achieve the same solution accuracy as the results from finite element technique, BIEM requires fewer numbers of iteration process. A boundary-fitted coordinate method for vertical and radial sluice gates was employed by Masliyah, et al. (1985). This method can be used when the problem has initial unknown discharge and unknown free surfaces. In 1986, Naghdi and Vongsarnpigoon gave a thorough analysis of solutions of this problem using an inviscid theory for a fluid sheet. Vanden-Broeck (1986) computed numerical solution for various values of the downstream Froude number F by the method of series truncation. He found that there are two solutions for $1.80 \leq F \leq 1.87$, one solution for $F > 1.87$, and no solutions for $F < 1.80$. Xianyun and Chigong (1987) used Muskelishvili's theory to derive a system of nonsingular boundary integral equation in the physical plane and solved by an iterative method. In 1996, Asavanant and Vanden-Broeck considered the complete sluice gate problem with two free surfaces and constructed solutions for which the free surface leave tangentially at both separation points by series truncation procedure. Their results could be obtained only for small values of gate inclination γ. Vanden-Broeck (1997) computed numerical solution for the fully nonlinear vertical sluice gate problem using boundary integral method. He showed that there exist solutions for which the flow does not approach a uniform stream far upstream. These solutions are characterized by a train of waves on the upstream free surface. Analytic solution of the smooth attachment problem was presented in the implicit form by Petrila (2002). He reduced the problem to a boundary value problem of the Hilbert type and employed Muskelishvili's technique. Defina and Susin (2003) used conservations of energy and momentum to predict behaviors of upstream and downstream free surfaces and compared with experimental results.

In this study, we consider fully nonlinear problem of the steady free-surface flows under an inclined sluice gate with possibilities of either a stagnation point or a smooth attachment to occur. The fluid domain in the physical plane is transformed onto the complex plane. Dynamic boundary condition (Bernoulli equation) is applied on both upstream and downstream free surfaces subject to gravitational force. We solve the problem numerically by the boundary integral method introduced by Vanden-Broeck (1997). This integral equation provides a relationship between the flow variables on the free surfaces. One of the advantages of the technique is that mesh points in the numerical scheme need only be placed on the free surface rather than throughout the entire flow domain. We obtain the numerical solutions by solving a system of nonlinear algebraic equations on the free surface using Newton's method. Details of the formulation and the numerical procedure are given in chapters II and III, respectively. In chapter IV, we discuss the numerical results of free-surface flows under an inclined sluice gate with stagnation point. The case in which the free surfaces leave tangentially at both separation points, the so called *smooth attachment*, is discussed in Chapter V. Finally, the concluding remarks are presented in Chapter VI.

CHAPTER II

Formulation of Free-Surface Flows under an Inclined Sluice Gate

2.1 Dynamic and Kinematic Boundary Conditions

We consider the steady two-dimensional flow under an inclined sluice gate. The fluid is treated as inviscid and incompressible and the flow is assumed to be irrotational. The flow domain is bounded below by a rigid wall $A'D'$ and above by the free surfaces AB and CD and the gate BC (see Figure 2.1).

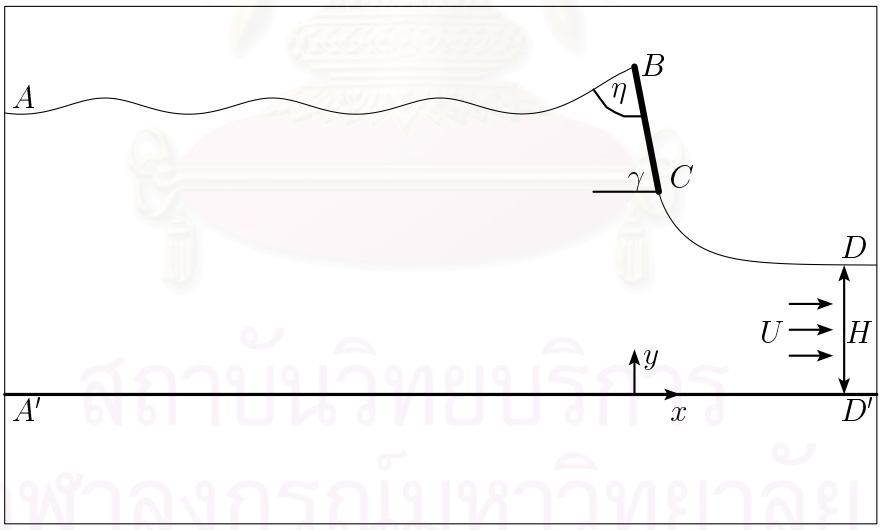

Figure 2.1: Sketch of free-surface flows under an inclined sluice gate.

Let us introduce Cartesian coordinates with the x - axis along the bottom and the y - axis directed vertically upwards through the upstream contact point between the free surface and the gate, i.e. the point B. Gravity g is acting in the negative y - direction. The gate inclination is denoted by γ measured clockwise

from the negative x - axis. At the point B, we denote by η the angle between free surface and gate (see Figure 2.1). The velocity components in the x - and y - direction are denoted by u and v, respectively. The flow is subcritical far upstream and is supercritical far downstream. As $x \to \infty$, the flow is assumed to approach a uniform stream with constant velocity U and constant depth H.

For inviscid fluid, it is well known that the governing equation for fluid motion are Euler equation. Due to the incompressibility and irrotationality of fluid flow, we have

$$\frac{1}{2}(u^2 + v^2) + \frac{p}{\rho} + gy = B^* \tag{2.1}$$

on the free surfaces. This result is known as **Bernoulli equation** or *dynamic boundary condition.* Here p is the constant atmospheric pressure, y is the vertical displacement measured from the bottom to the free surface, ρ is the constant fluid density and B^* is the Bernoulli constance. Equation (2.1) can be rewritten as

$$\frac{1}{2}(u^2 + v^2) + gy = B^{**} \tag{2.2}$$

where $B^{**} = B^* - \frac{p}{\rho}$. On the rigid wall $A'D'$ and the gate, the normal velocity must be zero. This is called *kinematic boundary condition.* They are, on the rigid wall $A'D'$,

$$v = 0, \qquad -\infty < x < \infty \quad \text{and} \quad y = 0, \tag{2.3}$$

and on the gate,

$$u \sin\gamma + v \cos\gamma = 0 \tag{2.4}$$

or

$$v = -u \tan\gamma. \tag{2.5}$$

2.2 Dimensionless Variables

It is convenient to normalize the physical problem by introducing appropriate scaling variables. This is done by choosing downstream velocity U as the unit velocity and downstream depth H as the unit depth. The dimensionless variables are

$$u^* = \frac{u}{U}, \qquad v^* = \frac{v}{U}, \qquad x^* = \frac{x}{H}, \qquad y^* = \frac{y}{H}. \tag{2.6}$$

Hence, after dropping *, equation (2.2) can be expressed in nondimensional form as

$$u^2 + v^2 + \frac{2}{F^2} y = B \tag{2.7}$$

where $F = \frac{U}{\sqrt{gH}}$ is the downstream Froude number, and $B = \frac{B^{**}}{U^2}$ is the dimensionless Bernoulli constance.

2.3 Potential Function and Stream Function

The problem is generally difficult to solve. However it can be simplified further by using complex function theory. Due to the incompressibility of the fluid it follows that

$$\frac{\partial u}{\partial x} + \frac{\partial v}{\partial y} = 0. \tag{2.8}$$

A suitably differentiable function $\psi(x, y)$ can be chosen such that

$$u = \frac{\partial \psi}{\partial y} \quad \text{and} \quad v = -\frac{\partial \psi}{\partial x}. \tag{2.9}$$

Thus (2.8) is automatically satisfied. The function ψ is known as the stream function and is useful in the problem formulation. For irrotational flow, we have the following relationship

$$\nabla \times \mathbf{q} = \frac{\partial v}{\partial x} - \frac{\partial u}{\partial y} = 0. \tag{2.10}$$

where $\mathbf{q} = (u, v)$ is the velocity vector. This equation can be satisfied by letting

$$\mathbf{q} = u(x, y)\mathbf{i} + v(x, y)\mathbf{j} = \nabla\phi = \frac{\partial\phi}{\partial x}\mathbf{i} + \frac{\partial\phi}{\partial y}\mathbf{j} \tag{2.11}$$

where ϕ is known as the potential function. From (2.9) and (2.11), we can deduce that

$$\frac{\partial\phi}{\partial x} = \frac{\partial\psi}{\partial y} \quad \text{and} \quad \frac{\partial\phi}{\partial y} = -\frac{\partial\psi}{\partial x}. \tag{2.12}$$

Relations (2.12) are the well known **Cauchy-Riemann equations** from the theory of functions of complex variables.

We introduce the complex potential function f by

$$f = \phi(x, y) + i\psi(x, y) \tag{2.13}$$

and the complex velocity w by

$$w = \frac{df}{dz} = u - iv \tag{2.14}$$

where $z = x + iy$. Both f and w are analytic functions of z.

Without loss of generality, we choose $\phi = 0$ at B and $\psi = 0$ on the streamline $ABCD$ and the bottom defines another streamline on which $\psi = -UH$. By the choice of our dimensionless variables we will have $\psi = -1$ on the bottom $A'D'$. We denote by ϕ_C the value of the potential function at the separation point C. The flow configurations in the f - plane is sketched in Figure 2.2. The flow domain in the complex f - plane is simply an infinite strip defined by

$$D = \{(\phi, \psi) | -\infty < \phi < \infty, -1 < \psi < 0\}.$$

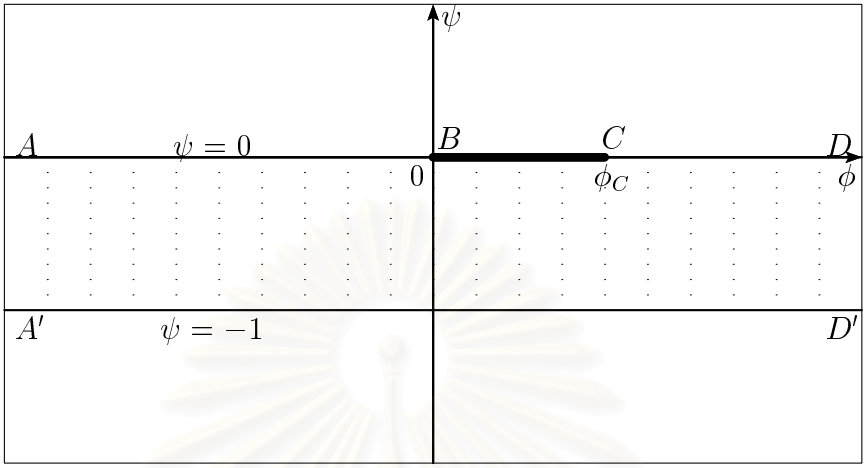

Figure 2.2: Flow configurations in the complex potential f - plane.

The nonlinear free surface condition for this problem can be expressed by the Bernoulli equation (2.7). We determine the constant term on the right hand side of (2.7) by using flow condition in the far field, i.e., $x \to \infty$, so $|\mathbf{q}| = \sqrt{u^2 + v^2} = 1$ and $y = 1$. That is,

$$u^2 + v^2 + \frac{2}{F^2} y = 1 + \frac{2}{F^2}$$
$$u^2 + v^2 + \frac{2}{F^2}(y - 1) = 1. \tag{2.16}$$

In the complex potential f - plane, the kinematic boundary conditions (2.3) and (2.5) become

$$v = 0 \quad \text{on} \quad \psi = -1 \quad \text{and} \quad -\infty < \phi < \infty \tag{2.17}$$

on the rigid wall $A'D'$ and

$$v = -u \tan\gamma \quad \text{on} \quad \psi = 0 \quad \text{and} \quad 0 < \phi < \phi_C \tag{2.18}$$

on the gate BC.

This concludes the mathematical formulation of the problem. We seek w as an analytic function of f in the strip $-1 < \psi < 0$. This function must approach 1 as $\phi \to \infty$ and satisfy (2.16) - (2.18).

2.4 Conformal Mapping

We map the flow domain from the complex potential f - plane onto the lower half plane in the complex ζ - plane. It can be done by using the conformal mapping

$$\begin{aligned}\zeta = \alpha + i\beta &= e^{\pi f} \\ &= e^{\pi(\phi+i\psi)} \\ &= e^{\pi\phi}(\cos(\pi\psi) + i\sin(\pi\psi)).\end{aligned} \tag{2.19}$$

Table 2.1 shows the position of the major points in the complex potential f - plane and the complex ζ - plane.

Cartesian plane	f - plane	ζ - plane
A	$\psi = 0, \phi = \phi_A = -\infty$	$\alpha = \alpha_A = 0, \beta = 0$
B	$\psi = 0, \phi = \phi_B = 0$	$\alpha = \alpha_B = 1, \beta = 0$
C	$\psi = 0, \phi = \phi_C > 0$	$\alpha = \alpha_C > 1, \beta = 0$
D	$\psi = 0, \phi = \phi_D = \infty$	$\alpha = \alpha_D = \infty, \beta = 0$
A'	$\psi = -1, \phi = \phi_{A'} = -\infty$	$\alpha = \alpha_{A'} = 0, \beta = 0$
D'	$\psi = -1, \phi = \phi_{D'} = -\infty$	$\alpha = \alpha_{D'} = -\infty, \beta = 0$

Table 2.1: Values of major points in f - plane and ζ - plane.

Therefore, the gate and free surfaces have been mapped onto the positive real axis of the ζ - plane and the rigid wall has been mapped onto the negative real axis of the ζ - plane (see Figure 2.3).

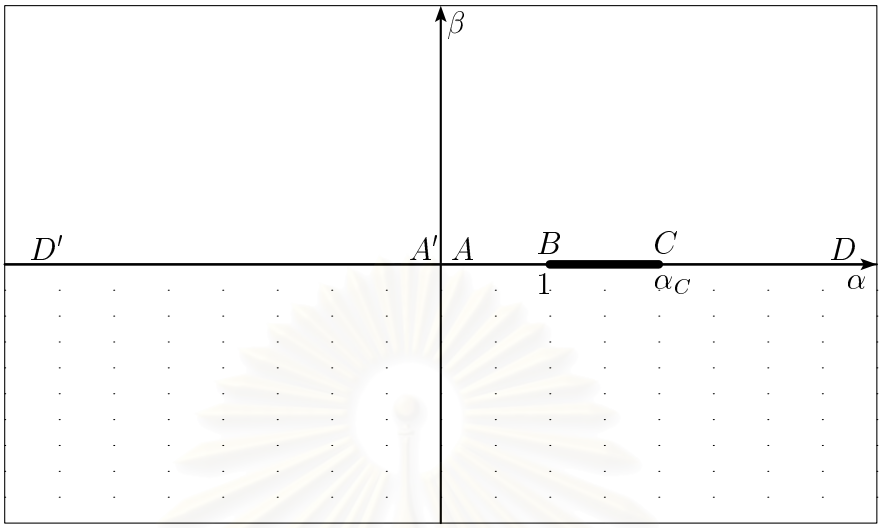

Figure 2.3: The flow in the complex ζ - plane.

A new complex function, $\tau - i\theta = \ln(\frac{df}{dz})$, is introduced, and is related to the complex velocity by

$$w = u - iv = e^{\tau - i\theta}. \tag{2.20}$$

This equation is used to express (2.7) in terms of new complex variables τ and θ. The first and second terms in (2.16) become

$$\begin{aligned} u^2 + v^2 &= |w|^2 \\ &= \left|e^{\tau - i\theta}\right|^2 \\ &= e^{2\tau}\left|e^{-2i\theta}\right| \\ &= e^{2\tau}. \end{aligned} \tag{2.21}$$

The final form of Bernoulli equation can now be rewritten as

$$e^{2\tau} + \frac{2}{F^2}(y - 1) = 1 \tag{2.22}$$

on free surfaces AB and CD.

On the ζ - plane, the kinematic boundary conditions (2.17) and (2.18) have to be conformally mapped to

$$\theta(\alpha) = 0 \quad \text{for} \quad \beta = 0 \quad \text{and} \quad \alpha < 0 \tag{2.23}$$

on the bottom $A'D'$ and

$$\theta(\alpha) = -\gamma \quad \text{for} \quad \beta = 0 \quad \text{and} \quad 1 < \alpha < \alpha_C \tag{2.24}$$

on the gate BC where $\alpha_C = e^{(\pi\phi_C)}$.

2.5 Boundary Integral Equation

In this section, integral equation relating τ and θ on the free surfaces is derived. Firstly, we consider a contour integral of the form

$$\oint_\Gamma \frac{\tau(\alpha,\beta) - i\theta(\alpha,\beta)}{\zeta - \alpha_0} d\zeta \tag{2.25}$$

where α_0 is a point on the free surface, i.e. $\alpha_0 \in AB$ or CD. The path Γ can be separated into 4 subpaths (see Figure 2.4):

C_1 := the semi-circular arc of radius R centered at the origin,

C_2 := the contour line between R to $\alpha_0 + \epsilon$,

C_3 := the semi-circular arc of radius ϵ centered at α_0, and

C_4 := the contour line between $\alpha_0 - \epsilon$ to $-R$.

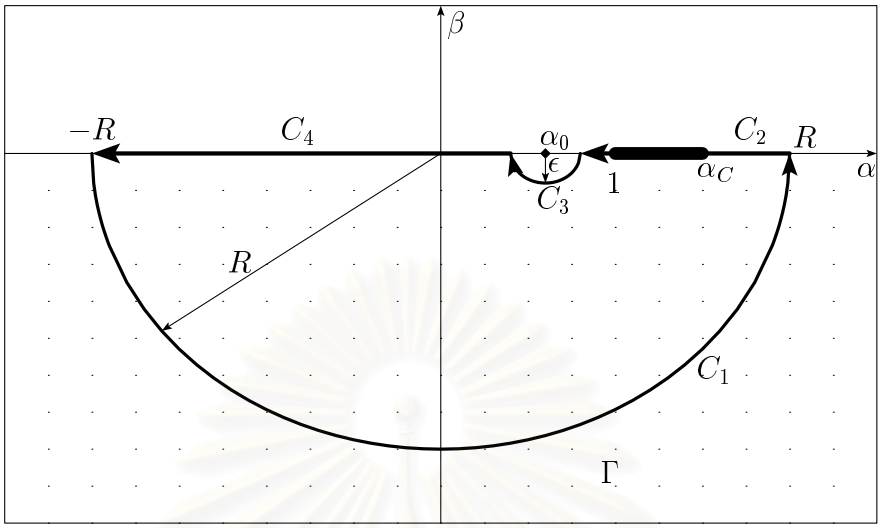

Figure 2.4: Contour Γ in the complex ζ - plane.

That is

$$\oint_{\Gamma} \frac{\tau(\alpha,\beta) - i\theta(\alpha,\beta)}{\zeta - \alpha_0} d\zeta = \int_{C_1} \frac{\tau(\alpha,\beta) - i\theta(\alpha,\beta)}{\zeta - \alpha_0} d\zeta + \int_{C_3} \frac{\tau(\alpha,\beta) - i\theta(\alpha,\beta)}{\zeta - \alpha_0} d\zeta + \int_{R}^{\alpha_0+\epsilon} \frac{\tau(\alpha,0) - i\theta(\alpha,0)}{\alpha - \alpha_0} d\alpha + \int_{\alpha_0-\epsilon}^{-R} \frac{\tau(\alpha,0) - i\theta(\alpha,0)}{\alpha - \alpha_0} d\alpha. \tag{2.26}$$

Cauchy theorem states that a contour integral along any closed contour not enclosing a singularity, of an analytic and single-valued function, is equal to zero. That is

$$\int_{C_1} \frac{\tau(\alpha,\beta) - i\theta(\alpha,\beta)}{\zeta - \alpha_0} d\zeta + \int_{C_3} \frac{\tau(\alpha,\beta) - i\theta(\alpha,\beta)}{\zeta - \alpha_0} d\zeta + \int_{R}^{\alpha_0+\epsilon} \frac{\tau(\alpha,0) - i\theta(\alpha,0)}{\alpha - \alpha_0} d\alpha + \int_{\alpha_0-\epsilon}^{-R} \frac{\tau(\alpha,0) - i\theta(\alpha,0)}{\alpha - \alpha_0} d\alpha = 0. \tag{2.27}$$

Consider the second integral in (2.27), the integral involving C_3.

Let $\zeta = \alpha + i\beta = \alpha_0 + \epsilon e^{i\lambda}$, so

$$\lambda = 0 \quad \text{at} \quad \zeta = \alpha_0 + \epsilon,$$

$$\lambda = -\pi \quad \text{at} \quad \zeta = \alpha_0 - \epsilon$$

and $$d\zeta = i\epsilon e^{i\lambda} d\lambda.$$

Then

$$\begin{aligned}
&\int_{C_3} \frac{\tau(\alpha,\beta) - i\theta(\alpha,\beta)}{\zeta - \alpha_0} d\zeta \\
&\quad = \int_0^{-\pi} \frac{\tau(\alpha_0 + \epsilon\cos\lambda, \epsilon\sin\lambda) - i\theta(\alpha_0 + \epsilon\cos\lambda, \epsilon\sin\lambda)}{\epsilon e^{i\lambda}} i\epsilon e^{i\lambda} d\lambda \\
&\quad = i\int_0^{-\pi} \left[(\tau(\alpha_0 + \epsilon\cos\lambda, \epsilon\sin\lambda) - i\theta(\alpha_0 + \epsilon\cos\lambda, \epsilon\sin\lambda)\right] d\lambda. \qquad (2.28)
\end{aligned}$$

Substituting (2.28) into (2.27), gives

$$\begin{aligned}
&\int_{C_1} \frac{\tau(\alpha,\beta) - i\theta(\alpha,\beta)}{\zeta - \alpha_0} d\zeta + i\int_0^{-\pi} \left[(\tau(\alpha_0 + \epsilon\cos\lambda, \epsilon\sin\lambda) - i\theta(\alpha_0 + \epsilon\cos\lambda, \epsilon\sin\lambda)\right] d\lambda \\
&\quad + \int_R^{\alpha_0+\epsilon} \frac{\tau(\alpha,0) - i\theta(\alpha,0)}{\alpha - \alpha_0} d\alpha + \int_{\alpha_0-\epsilon}^{-R} \frac{\tau(\alpha,0) - i\theta(\alpha,0)}{\alpha - \alpha_0} d\alpha = 0. \qquad (2.29)
\end{aligned}$$

Taking limit as $\epsilon \to 0$,

$$\begin{aligned}
&\int_{C_1} \frac{\tau(\alpha,\beta) - i\theta(\alpha,\beta)}{\zeta - \alpha_0} d\zeta + i\left[(\tau(\alpha_0,0) - i\theta(\alpha_0,0)\right] \int_0^{-\pi} d\lambda \\
&\qquad + \int_R^{-R} \frac{\tau(\alpha,0) - i\theta(\alpha,0)}{\alpha - \alpha_0} d\alpha = 0
\end{aligned}$$

$$\int_{C_1} \frac{\tau(\alpha,\beta) - i\theta(\alpha,\beta)}{\zeta - \alpha_0} d\zeta - i\pi\left[(\tau(\alpha_0,0) - i\theta(\alpha_0,0)\right] + \int_R^{-R} \frac{\tau(\alpha,0) - i\theta(\alpha,0)}{\alpha - \alpha_0} d\alpha = 0.$$

Then

$$\begin{aligned}
&\tau(\alpha_0,0) - i\theta(\alpha_0,0) \\
&\qquad = \frac{1}{i\pi}\int_{C_1} \frac{\tau(\alpha,\beta) - i\theta(\alpha,\beta)}{\zeta - \alpha_0} d\zeta + \frac{1}{i\pi}\int_R^{-R} \frac{\tau(\alpha,0) - i\theta(\alpha,0)}{\alpha - \alpha_0} d\alpha \\
&\qquad = \frac{1}{i\pi}\int_{C_1} \frac{\tau(\alpha,\beta) - i\theta(\alpha,\beta)}{\zeta - \alpha_0} d\zeta - \frac{1}{i\pi}\int_{-R}^{R} \frac{\tau(\alpha,0) - i\theta(\alpha,0)}{\alpha - \alpha_0} d\alpha. \qquad (2.30)
\end{aligned}$$

Taking limit as $R \to \infty$, the second integral on the right hand side of (2.30) becomes

$$\lim_{R\to\infty} \frac{1}{i\pi}\int_{-R}^{R} \frac{\tau(\alpha,0) - i\theta(\alpha,0)}{\alpha - \alpha_0} d\alpha = \frac{1}{i\pi}\int_{-\infty}^{\infty} \frac{\tau(\alpha,0) - i\theta(\alpha,0)}{\alpha - \alpha_0} d\alpha. \qquad (2.31)$$

This integral is of Cauchy principal values.

As $\phi \to \infty$, we have $w \to 1$ or $e^{\tau - i\theta} \to 1$ implying $\tau - i\theta \to 0$. Hence, the first integral on the right hand side of (2.30), vanishes as $R \to \infty$

$$\lim_{R\to\infty} \frac{1}{i\pi} \int_{C_1} \frac{\tau(\alpha,\beta) - i\theta(\alpha,\beta)}{\zeta - \alpha_0} d\zeta = 0. \tag{2.32}$$

Equation (2.30) can now be reduced to

$$\tau(\alpha_0, 0) - i\theta(\alpha_0, 0) = -\frac{1}{i\pi} \int_{-\infty}^{\infty} \frac{\tau(\alpha,0) - i\theta(\alpha,0)}{\alpha - \alpha_0} d\alpha. \tag{2.33}$$

By taking the real part of (2.33) we obtain

$$\tau(\alpha_0) = \frac{1}{\pi} \int_{-\infty}^{\infty} \frac{\theta(\alpha)}{\alpha - \alpha_0} d\alpha, \tag{2.34}$$

where $\tau(\alpha)$ and $\theta(\alpha)$ denote the value of τ and θ on the free surfaces.

The kinematic boundary conditions (2.23) and (2.24) can be applied to (2.34) for further simplification. First, we write the integral as

$$\begin{aligned}\int_{-\infty}^{\infty} \frac{\theta(\alpha)}{\alpha - \alpha_0} d\alpha = \int_{-\infty}^{0} \frac{\theta(\alpha)}{\alpha - \alpha_0} d\alpha + \int_{0}^{1} \frac{\theta(\alpha)}{\alpha - \alpha_0} d\alpha \\ + \int_{1}^{\alpha_C} \frac{\theta(\alpha)}{\alpha - \alpha_0} d\alpha + \int_{\alpha_C}^{\infty} \frac{\theta(\alpha)}{\alpha - \alpha_0} d\alpha.\end{aligned} \tag{2.35}$$

The first integral on the right hand side vanishes due to the kinematic boundary condition (2.23). The third integral reduce to

$$\begin{aligned}\int_{1}^{\alpha_C} \frac{\theta(\alpha)}{\alpha - \alpha_0} d\alpha &= \int_{1}^{\alpha_C} \frac{-\gamma}{\alpha - \alpha_0} d\alpha \\ &= -\gamma \ln \frac{|\alpha_C - \alpha_0|}{|1 - \alpha_0|}\end{aligned} \tag{2.36}$$

by using (2.24). Equation (2.34) can be rewritten as

$$\begin{aligned}\tau(\alpha_0) = \frac{1}{\pi} \int_{-\infty}^{\infty} \frac{\theta(\alpha)}{\alpha - \alpha_0} d\alpha = -\frac{\gamma}{\pi} \ln \frac{|\alpha_C - \alpha_0|}{|1 - \alpha_0|} + \frac{1}{\pi} \int_{0}^{1} \frac{\theta(\alpha)}{\alpha - \alpha_0} d\alpha \\ + \frac{1}{\pi} \int_{\alpha_C}^{\infty} \frac{\theta(\alpha)}{\alpha - \alpha_0} d\alpha.\end{aligned} \tag{2.37}$$

This provides a relation between τ and θ on the free surfaces.

Finally, we determine the free surface boundary by integrating the identity

$$\frac{d}{df}(x+iy) = w^{-1} \tag{2.38}$$

or

$$\begin{aligned}\frac{d}{d\zeta}(x+iy) &= \frac{d}{df}(x+iy)\frac{df}{d\zeta} \\ &= \frac{w^{-1}}{\pi e^{\pi f}} \\ &= \frac{(e^{\tau-i\theta})^{-1}}{\pi\zeta} \\ &= \frac{e^{-\tau}}{\pi\zeta}(\cos\theta + i\sin\theta).\end{aligned} \tag{2.39}$$

Taking the real and imaginary part of (2.39) for $\beta = 0$ gives

$$\frac{\partial x}{\partial \alpha} = \frac{e^{-\tau}}{\pi\alpha}\cos\theta \tag{2.40}$$

and

$$\frac{\partial y}{\partial \alpha} = \frac{e^{-\tau}}{\pi\alpha}\sin\theta. \tag{2.41}$$

Hence, the x - coordinate on free surface AB $(0 < \alpha < 1)$ is

$$\int_{x_B}^{x(\alpha)} dx = \frac{1}{\pi}\int_1^{\alpha} \frac{e^{-\tau(\alpha_0)}}{\alpha_0}\cos\theta(\alpha_0)d\alpha_0$$

$$x(\alpha) - x_B = \frac{1}{\pi}\int_1^{\alpha} \frac{e^{-\tau(\alpha_0)}}{\alpha_0}\cos\theta(\alpha_0)d\alpha_0.$$

At B, $\alpha = 1$. By choosing $x_B = 0$, we have

$$x(\alpha) = \frac{1}{\pi}\int_1^{\alpha} \frac{e^{-\tau(\alpha_0)}}{\alpha_0}\cos\theta(\alpha_0)d\alpha_0. \tag{2.42}$$

The y - coordinate on free surface AB $(0 < \alpha < 1)$ is

$$\int_{y_B}^{y(\alpha)} dy = \frac{1}{\pi}\int_1^{\alpha} \frac{e^{-\tau(\alpha_0)}}{\alpha_0}\sin\theta(\alpha_0)d\alpha_0$$

$$y(\alpha) - y_B = \frac{1}{\pi}\int_1^{\alpha} \frac{e^{-\tau(\alpha_0)}}{\alpha_0}\sin\theta(\alpha_0)d\alpha_0. \tag{2.43}$$

From Bernoulli equation (2.22)

$$e^{2\tau(\alpha_B)} + \frac{2}{F^2}(y_B - 1) = 1$$

$$y_B = 1 + \frac{F^2}{2}(1 - e^{2\tau(\alpha_B)}). \tag{2.44}$$

Substituting (2.44) into (2.43), we obtain

$$y(\alpha) = 1 + \frac{F^2}{2}(1 - e^{2\tau(\alpha_B)}) + \frac{1}{\pi}\int_1^{\alpha} \frac{e^{-\tau(\alpha_0)}}{\alpha_0}\sin\theta(\alpha_0)d\alpha_0. \tag{2.45}$$

The x - coordinate on free surface CD $(\alpha_C < \alpha < \infty)$ is

$$\int_{x_C}^{x(\alpha)} dx = \frac{1}{\pi}\int_{\alpha_C}^{\alpha} \frac{e^{-\tau(\alpha_0)}}{\alpha_0}\cos\theta(\alpha_0)d\alpha_0$$

$$x(\alpha) - x_C = \frac{1}{\pi}\int_{\alpha_C}^{\alpha} \frac{e^{-\tau(\alpha_0)}}{\alpha_0}\cos\theta(\alpha_0)d\alpha_0$$

$$x(\alpha) = x_C + \frac{1}{\pi}\int_{\alpha_C}^{\alpha} \frac{e^{-\tau(\alpha_0)}}{\alpha_0}\cos\theta(\alpha_0)d\alpha_0 \tag{2.46}$$

where x_C is the position of separation point C.

The y - coordinate on free surface CD $(\alpha_C < \alpha < \infty)$ is

$$\int_{y_D}^{y(\alpha)} dy = \frac{1}{\pi}\int_{\infty}^{\alpha} \frac{e^{-\tau(\alpha_0)}}{\alpha_0}\sin\theta(\alpha_0)d\alpha_0$$

$$y(\alpha) - y_D = \frac{1}{\pi}\int_{\infty}^{\alpha} \frac{e^{-\tau(\alpha_0)}}{\alpha_0}\sin\theta(\alpha_0)d\alpha_0.$$

Since $y_D = 1$ far downstream, then

$$y(\alpha) = 1 + \frac{1}{\pi}\int_{\infty}^{\alpha} \frac{e^{-\tau(\alpha_0)}}{\alpha_0}\sin\theta(\alpha_0)d\alpha_0. \tag{2.47}$$

Equations (2.22), (2.37), (2.42), (2.45), (2.46) and (2.47) define a system of nonlinear equations for the unknowns $\theta(\alpha)$ on the free surfaces $0 < \alpha < 1$ and $\alpha > \alpha_C$.

CHAPTER III

Numerical Procedure of Free-Surface Flows under an Inclined Sluice Gate

In this chapter, we describe the numerical procedure to seek the nonlinear solutions of (2.22) and (2.37) derived in chapter II. From

$$\alpha = e^{\pi\phi}$$

on free surfaces, we can write (2.37) as

$$\tau'(\phi_0) = -\frac{\gamma}{\pi}\ln\frac{|e^{\pi\phi_C} - e^{\pi\phi_0}|}{|1 - e^{\pi\phi_0}|} + \int_{-\infty}^{0}\frac{\theta'(\phi)e^{\pi\phi}}{e^{\pi\phi} - e^{\pi\phi_0}}d\phi + \int_{\phi_C}^{\infty}\frac{\theta'(\phi)e^{\pi\phi}}{e^{\pi\phi} - e^{\pi\phi_0}}d\phi. \tag{3.1}$$

On the free surface AB, where $-\infty < \phi < 0$ and $\psi = 0$, we have

$$x'(\phi) = \int_0^{\phi} e^{-\tau'(\phi_0)}\cos\theta'(\phi_0)d\phi_0 \tag{3.2}$$

and

$$y'(\phi) = 1 + \frac{F^2}{2}(1 - e^{2\tau'(\phi_B)}) + \int_0^{\phi} e^{-\tau'(\phi_0)}\sin\theta'(\phi_0)d\phi_0. \tag{3.3}$$

Similarly on free surface CD, where $\phi_C < \phi < \infty$ and $\psi = 0$, we have

$$x'(\phi) = x_C + \int_{\phi_C}^{\phi} e^{-\tau'(\phi_0)}\cos\theta'(\phi_0)d\phi_0 \tag{3.4}$$

and

$$y'(\phi) = 1 + \int_{\infty}^{\phi} e^{-\tau'(\phi_0)}\sin\theta'(\phi_0)d\phi_0. \tag{3.5}$$

Here $\tau'(\phi) = \tau(e^{\pi\phi})$, $\theta'(\phi) = \theta(e^{\pi\phi})$, $x'(\phi) = x(e^{\pi\phi})$ and $y'(\phi) = y(e^{\pi\phi})$.

Next we introduce the equally spaced mesh points

$$\phi_I^U = -(I-1)\Delta_1, \qquad I = 1, ..., N_1 \tag{3.6}$$

and

$$\phi_I^D = \phi_C + (I-1)\Delta_2, \qquad I = 1, ..., N_2 \tag{3.7}$$

on the upstream and downstream free surfaces, respectively. Here $\Delta_1 > 0$ and $\Delta_2 > 0$ are the mesh sizes. The corresponding unknowns are

$$\theta_I^U = \theta'(\phi_I^U), \qquad I = 1, ..., N_1 \tag{3.8}$$

and

$$\theta_I^D = \theta'(\phi_I^D), \qquad I = 1, ..., N_2. \tag{3.9}$$

We assign the values $\theta_1^U = \delta$ and $\theta_1^D = -\gamma$, where δ will be defined in chapters IV and V. There are $N_1 + N_2 - 2$ unknowns: θ_I^U, $I = 2, ..., N_1$ and θ_I^D, $I = 2, ..., N_2$.

We evaluate the values τm_I^U and τm_I^D of $\tau'(\phi)$ at the midpoints

$$\phi m_I^U = \frac{\phi_I^U + \phi_{I+1}^U}{2}, \qquad I = 1, ..., N_1 - 1 \tag{3.10}$$

and

$$\phi m_I^D = \frac{\phi_I^D + \phi_{I+1}^D}{2}, \qquad I = 1, ..., N_2 - 1 \tag{3.11}$$

by applying the trapezoidal rule to the first and second integrals in (3.1) with summations over the $\phi_{N_1}^U$ and $\phi_{N_2}^D$, respictively . Since the spacings are symmetric with respect to the pole, the singularity is subtracted from the Cauchy principal value integral (see Appendix). Next we replace (3.1) by

$$\tau'(\phi_0) = -\frac{\gamma}{\pi} \ln \frac{|e^{\pi\phi_C} - e^{\pi\phi_0}|}{|1 - e^{\pi\phi_0}|} + \int_{\phi_{N_1}^U}^{0} \frac{\theta'(\phi) e^{\pi\phi}}{e^{\pi\phi} - e^{\pi\phi_0}} d\phi + \int_{\phi_C}^{\phi_{N_2}^D} \frac{\theta'(\phi) e^{\pi\phi}}{e^{\pi\phi} - e^{\pi\phi_0}} d\phi. \tag{3.12}$$

Following Hocking and Vanden-Broeck (1996), we write the last integral in (3.12) as

$$\begin{aligned}\int_{\phi_C}^{\phi_{N_2}^D} \frac{\theta'(\phi)e^{\pi\phi}}{e^{\pi\phi}-e^{\pi\phi_0}}d\phi &= \int_{\phi_C}^{\phi_{N_2}^D} \frac{(\theta'(\phi)-\theta'(\phi_0))e^{\pi\phi}}{e^{\pi\phi}-e^{\pi\phi_0}}d\phi + \int_{\phi_C}^{\phi_{N_2}^D} \frac{\theta'(\phi_0)e^{\pi\phi}}{e^{\pi\phi}-e^{\pi\phi_0}}d\phi \\ &= \int_{\phi_C}^{\phi_{N_2}^D} \frac{(\theta'(\phi)-\theta'(\phi_0))e^{\pi\phi}}{e^{\pi\phi}-e^{\pi\phi_0}}d\phi \\ &\quad + \frac{\theta'(\phi_0)}{\pi}\ln\frac{|e^{\pi\phi_{N_2}^D}-e^{\pi\phi_0}|}{|e^{\pi\phi_C}-e^{\pi\phi_0}|} \end{aligned} \tag{3.13}$$

before applying the trapezoidal rule. The value of τ' at the midpoints can be calculate from

$$\begin{aligned}\tau m_I^U = \tau'(\phi m_I^U) &= -\frac{\gamma}{\pi}\ln\frac{|e^{\pi\phi_C}-e^{\pi\phi m_I^U}|}{|1-e^{\pi\phi m_I^U}|} + \frac{\theta'(\phi m_I^U)}{\pi}\ln\frac{|e^{\pi\phi_{N_2}^D}-e^{\pi\phi m_I^U}|}{|e^{\pi\phi_C}-e^{\pi\phi m_I^U}|} \\ &\quad + \sum_{j=1}^{N_1}\frac{\theta_j^U e^{\pi\phi_j^U}}{e^{\pi\phi_j^U}-e^{\pi\phi m_I^U}}\Delta_1 w_j^U \\ &\quad + \sum_{j=1}^{N_2}\frac{(\theta_j^D-\theta'(\phi m_I^U))e^{\pi\phi_j^D}}{e^{\pi\phi_j^D}-e^{\pi\phi m_I^U}}\Delta_2 w_j^D \end{aligned} \tag{3.14}$$

on the upstream free surface, and

$$\begin{aligned}\tau m_I^D = \tau'(\phi m_I^D) &= -\frac{\gamma}{\pi}\ln\frac{|e^{\pi\phi_C}-e^{\pi\phi m_I^D}|}{|1-e^{\pi\phi m_I^D}|} + \frac{\theta'(\phi m_I^D)}{\pi}\ln\frac{|e^{\pi\phi_{N_2}^D}-e^{\pi\phi m_I^D}|}{|e^{\pi\phi_C}-e^{\pi\phi m_I^D}|} \\ &\quad + \sum_{j=1}^{N_1}\frac{\theta_j^U e^{\pi\phi_j^U}}{e^{\pi\phi_j^U}-e^{\pi\phi m_I^D}}\Delta_1 w_j^U \\ &\quad + \sum_{j=1}^{N_2}\frac{(\theta_j^D-\theta'(\phi m_I^D))e^{\pi\phi_j^D}}{e^{\pi\phi_j^D}-e^{\pi\phi m_I^D}}\Delta_2 w_j^D \end{aligned} \tag{3.15}$$

on the downstream free surface. Here

$$w_j^U[w_j^D] = \begin{cases} \frac{1}{2} & \text{if } \ j=0 \ \text{ and } \ N_1[N_2], \\ 1 & \text{otherwise.} \end{cases} \tag{3.16}$$

The $\theta'(\phi m_I^U)$ and $\theta'(\phi m_I^D)$ are values of θ' at the midpoints (3.10) and (3.11) and are evaluated by the four-point interpolation, denote by θm_I^U and θm_I^D, respectively. That is

$$\theta m_1^U = \frac{5}{16}\theta_1^U + \frac{15}{16}\theta_2^U - \frac{5}{16}\theta_3^U + \frac{1}{16}\theta_4^U, \tag{3.17}$$

$$\theta m_I^U = -\frac{1}{16}\theta_{I-1}^U + \frac{9}{16}\theta_I^U + \frac{9}{16}\theta_{I+1}^U - \frac{1}{16}\theta_{I+2}^U, \qquad I = 2, 3, ..., N_1 - 2 \tag{3.18}$$

and

$$\theta m_{N_1-1}^U = \frac{5}{16}\theta_{N_1}^U + \frac{15}{16}\theta_{N_1-1}^U - \frac{5}{16}\theta_{N_1-2}^U + \frac{1}{16}\theta_{N_1-3}^U \tag{3.19}$$

and θm_I^D is similar to (3.17) - (3.19) with N_1 replaced by N_2.

Next we evaluate

$$x_I^U = x'(\phi_I^U),$$

$$y_I^U = y'(\phi_I^U),$$

$$x_I^D = x'(\phi_I^D)$$

and

$$y_I^D = y'(\phi_I^D)$$

by integrating (3.2) - (3.5) numerically. This yields

$$x_1^U = 0.0, \tag{3.20}$$

$$y_1^U = 1 + \frac{1}{2}F^2(1 - e^{2\tau_1^U}), \tag{3.21}$$

$$x_I^U = x_{I-1}^U - e^{(-\tau m_{I-1}^U)}\cos(\theta m_{I-1}^U)\Delta_1, \tag{3.22}$$

$$y_I^U = y_{I-1}^U - e^{(-\tau m_{I-1}^U)}\sin(\theta m_{I-1}^U)\Delta_1 \tag{3.23}$$

$$\text{for} \quad I = 2, 3, ..., N_1$$

where τ_1^U is $\frac{3}{2}\tau m_1^U - \frac{1}{2}\tau m_2^U$, and

$$x_1^D = x_C, \tag{3.24}$$

$$x_I^D = x_{I-1}^D + e^{(-\tau m_{I-1}^D)}\cos(\theta m_{I-1}^D)\Delta_2, \qquad I = 2, 3, ..., N_2, \tag{3.25}$$

$$y_{N_2}^D = 1.0, \tag{3.26}$$

$$y_I^D = y_{I+1}^D - e^{(-\tau m_I^D)}\sin(\theta m_I^D)\Delta_2, \qquad I = N_2 - 1, N_2 - 2..., 1. \tag{3.27}$$

We use y_I^U and y_I^D to evaluate $y'(\phi)$ at the midpoints (3.10) and (3.11) by four-point interpolation formula, denote by ym_I^U and ym_I^D, respectively. We obtain $N_1 + N_2 - 2$ nonlinear equations by satisfying Bernoulli equation (2.22) at the midpoints (3.10) and (3.11).

The last equation is obtained by fixing the length L of the gate BC. Using (2.20), (2.24) and (2.38), we obtain

$$\frac{\partial x}{\partial \phi} = e^{-\tau} \cos \gamma \tag{3.28}$$

and

$$\frac{\partial y}{\partial \phi} = e^{-\tau} \sin \gamma \tag{3.29}$$

on $0 < \phi < \phi_C$.

We use (3.1) to evaluate $\tau'(\phi)$ for $0 < \phi < \phi_C$ and integrate (3.28) and (3.29) numerically. This yields the length L of the gate BC in terms on the unknows. The last equation is then

$$L - \sqrt{(x_1^U - x_1^D)^2 + (y_1^U - y_1^D)^2} = 0. \tag{3.30}$$

For given values of ϕ_C and γ, we solve this system of N_1+N_2-1 nonlinear algebraic equations with $N_1 + N_2 - 1$ unknowns, i.e., $F, \theta_I^U, I = 2, ..., N_1$ and $\theta_I^D, I = 2, ..., N_2$ by Newton's method. It is convenient to write this system of equations in the form

$$h_i(\chi_1, \chi_2, ..., \chi_{N_1+N_2-1}) = e^{2\tau m_i^U} + \frac{2}{F^2}(ym_i^U - 1) - 1 = 0,$$
$$i = 1, 2, ..., N_1 - 1; \tag{3.31}$$

$$h_{N_1+j-1}(\chi_1, \chi_2, ..., \chi_{N_1+N_2-1}) = e^{2\tau m_j^D} + \frac{2}{F^2}(ym_j^D - 1) - 1 = 0,$$
$$j = 1, 2, ..., N_2 - 1 \tag{3.32}$$

and

$$h_{N_1+N_2-1}(\chi_1, \chi_2, ..., \chi_{N_1+N_2-1}) = L - \sqrt{(x_1^U - x_1^D)^2 + (y_1^U - y_1^D)^2} = 0 \qquad (3.33)$$

where

$$\{\chi_j\}_{j=1}^{N_1-1} = \{\theta_i^U\}_{i=2}^{N_1},$$
$$\{\chi_j\}_{j=N_1}^{N_1+N_2-2} = \{\theta_i^D\}_{i=2}^{N_2}$$

and

$$\chi_{N_1+N_2-1} = F.$$

Thus if $\chi_j^{(k)}$ is an approximation to the solution, the next approximation $\chi_j^{(k+1)}$ can be obtained from

$$\chi_j^{(k+1)} = \chi_j^{(k)} + \Delta_j^{(k)}, \qquad j = 1, ..., N_1 + N_2 - 1 \qquad (3.34)$$

where the corrections $\Delta_j^{(k)}$ are calculated from

$$\sum_{j=1}^{N_1+N_2-1} \left[\frac{\partial h_i}{\partial \chi_j}\right]^{(k)} \Delta_j^{(k)} = -h_i^{(k)}, \qquad i = 1, ..., N_1 + N_2 - 1. \qquad (3.35)$$

The Jacobians $\frac{\partial h_i}{\partial \chi_j}$ are determined by exact differentiation of (3.31) - (3.33), and $h_i^{(k)} = h_i(\chi_1^{(k)}, \ldots, \chi_{N_1+N_2-1}^{(k)})$.

CHAPTER IV

Numerical Results of Free-Surface Flows under an Inclined Sluice Gate with Stagnation Point

We use the numerical scheme described in the previous chapter to compute solutions for two cases:

I. Separation point between the upstream free surface and the gate is a stagnation point.

II. Free surfaces leave tangentially at both separation points (see chapter V).

Dagan and Tulin (1972) investigated the intersection angle η between the free surface and a rigid boundary for small Froude number by using perturbation technique. For a stagnation point to occur, there are two possible angles between the free surface and the rigid boundary as follows.

(1) If the rigid boundary is inclined at an angle larger than 60° ($\gamma \geq 60^\circ$), then the free surface in the neighborhood of the stagnation point is horizontal or $\theta_1^U = 0$.

(2) If the rigid boundary is inclined at an angle between 0° and 60° ($0^\circ \leq \gamma < 60^\circ$), then the intersection angle between the free surface and the rigid boundary is 120° ($\eta = 120^\circ$) or $\theta_1^U = \frac{\pi}{3} - \gamma$.

For case (1), we consider 3 possible subcases:

1. The gate inclination is 90° ($\gamma = 90^\circ$) which is the vertical sluice gate problem,

2. The gate inclination is between 60° and 90° ($60^\circ \leq \gamma < 90^\circ$), and

3. The gate inclination is between 0° and 60° ($0^\circ \leq \gamma < 60^\circ$).

In section 4.1 and 4.2, we present and discuss numerical results of the vertical sluice gate problem and the gate inclination between 60° and 90° ($60° \leq \gamma < 90°$), respectively. In this case the free surface is horizontal at the stagnation point C, so $\theta_1^U = 0$. The case of gate inclination between 0° and 60° ($0° \leq \gamma < 60°$) is discussed in section 4.3. In this case, $\theta_1^U = \frac{\pi}{3} - \gamma$. Most of the results are obtained with $N_1 = 841$, $N_2 = 501$, $\Delta_1 = 0.01$ and $\Delta_2 = 0.01$.

4.1 The Vertical Sluice Gate

As mentioned in Chapter III, we calculate solution of the system of nonlinear algebraic equations (3.31) - (3.33) for various values of ϕ_C and $\gamma = 90°$. In this case, we fully recover the results obtained by Vanden-Broeck (1997).

Typical free-surface profiles are shown in Figure 4.1 (a) - (i). The symbol $\circ$ for all figures indicates the position of the points at which the upstream and downstream free surfaces separate from the gate. There is a train of waves on the upstream free surface. For large values of F ($F > 2.40$), the waves are too small to observe in the figures (see Figure 4.1 (a) - (e)). When $F < 2.40$, the waves are noticeable on the profiles (see Figure 4.1 (f) - (i)). As F decreases, amplitude of the wave increases with broad troughs and narrow crests (see Figure 4.1 (i)). Additionally the wavelength of these waves increases as F decreases (see Figures 4.1 (f) - (i)).

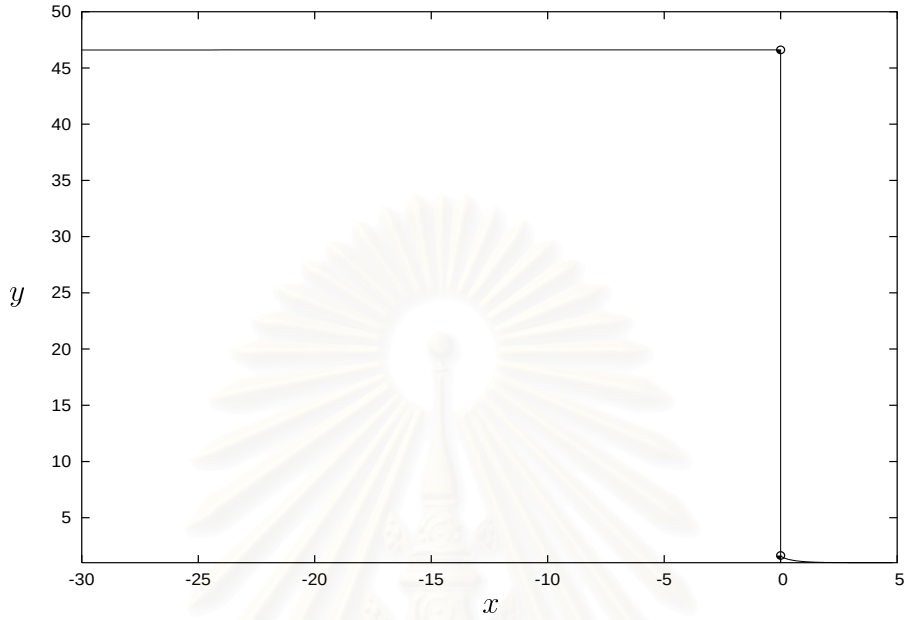

Figure 4.1 (a): $\phi_C = 2.00$ ($F = 9.5511$).

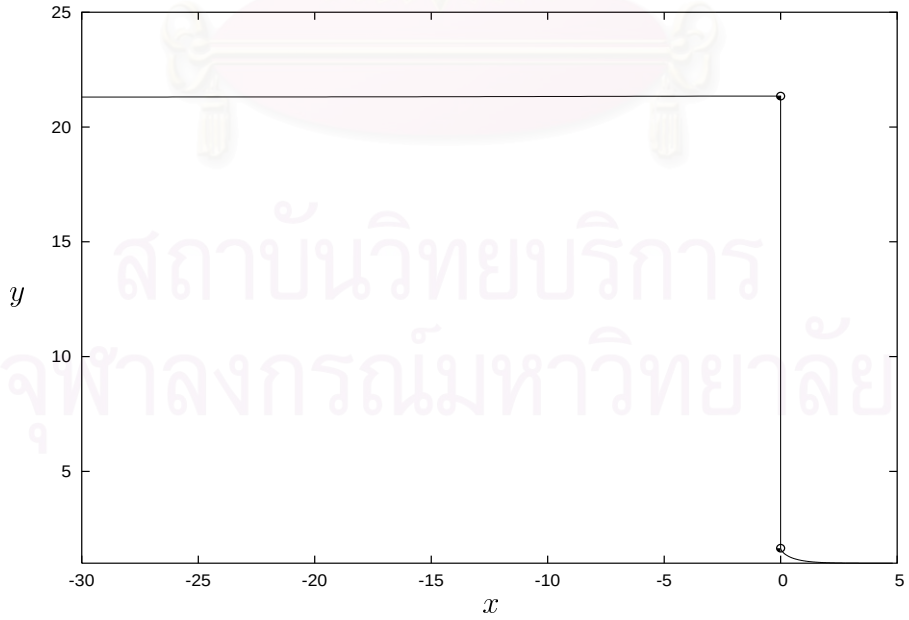

Figure 4.1 (b): $\phi_C = 1.50$ ($F = 6.3795$).

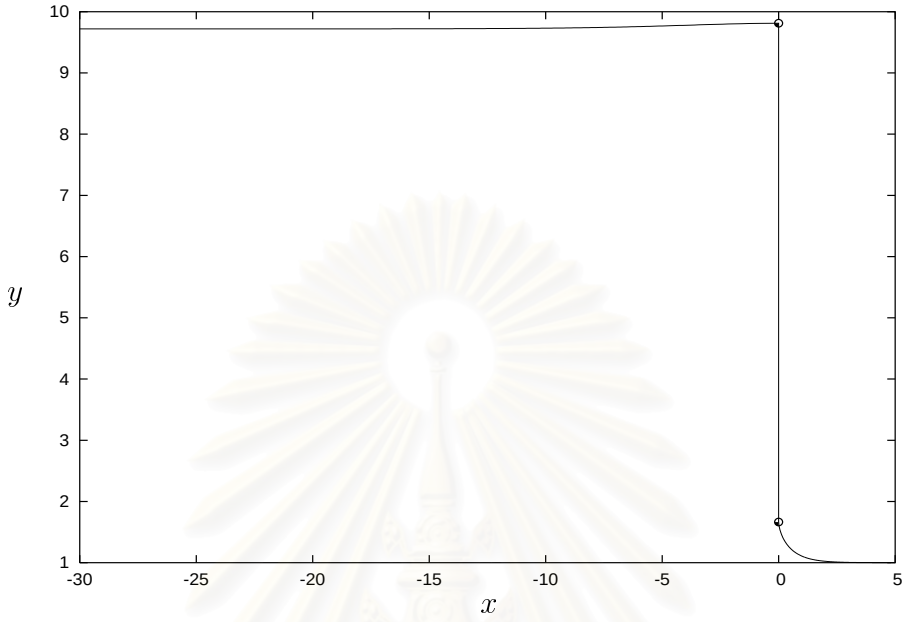

Figure 4.1 (c): $\phi_C = 1.00$ ($F = 4.1982$).

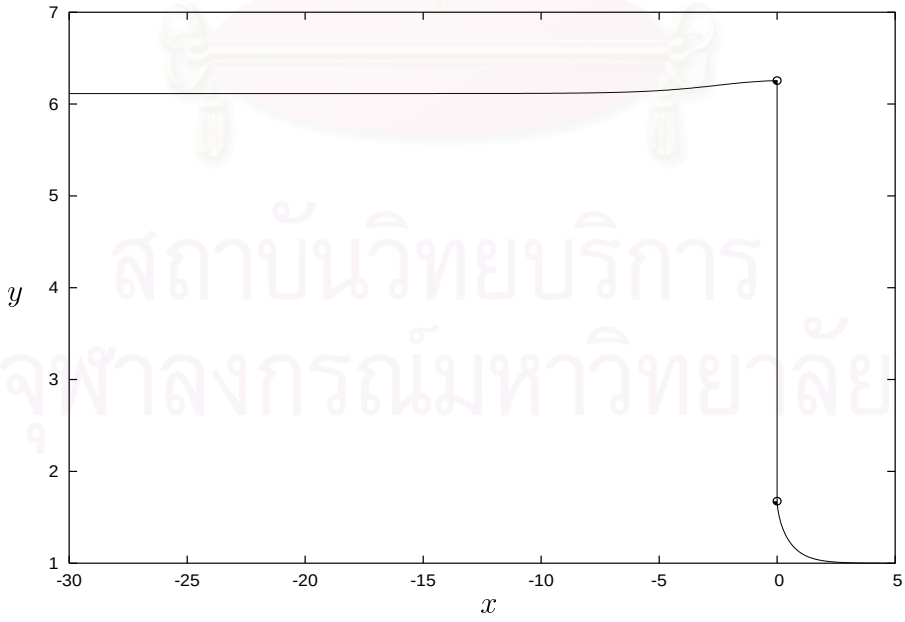

Figure 4.1 (d): $\phi_C = 0.71$ ($F = 3.2419$).

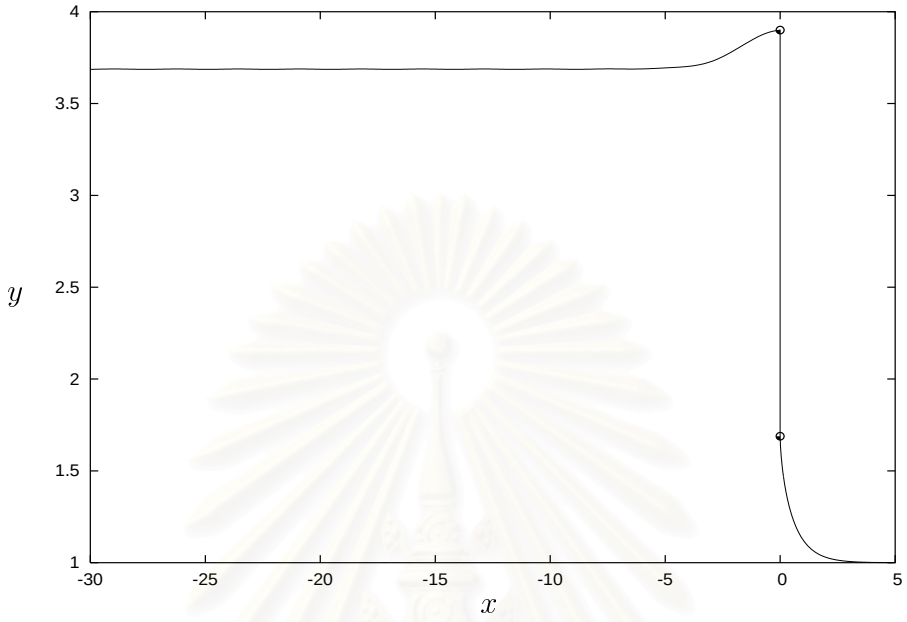

Figure 4.1 (e): $\phi_C = 0.41$ ($F = 2.4084$).

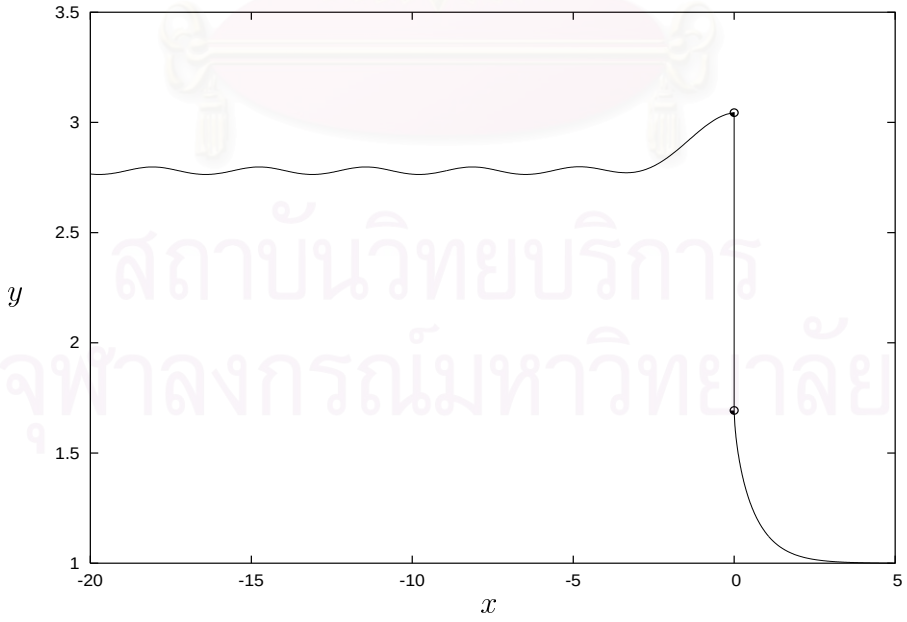

Figure 4.1 (f): $\phi_C = 0.26$ ($F = 2.0221$).

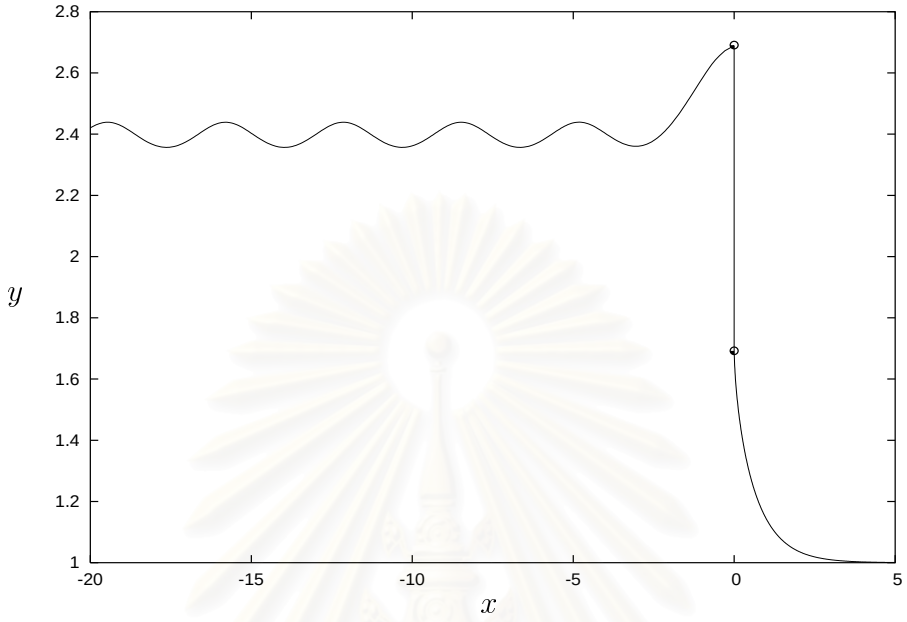

Figure 4.1 (g): $\phi_C = 0.19$ ($F = 1.8389$).

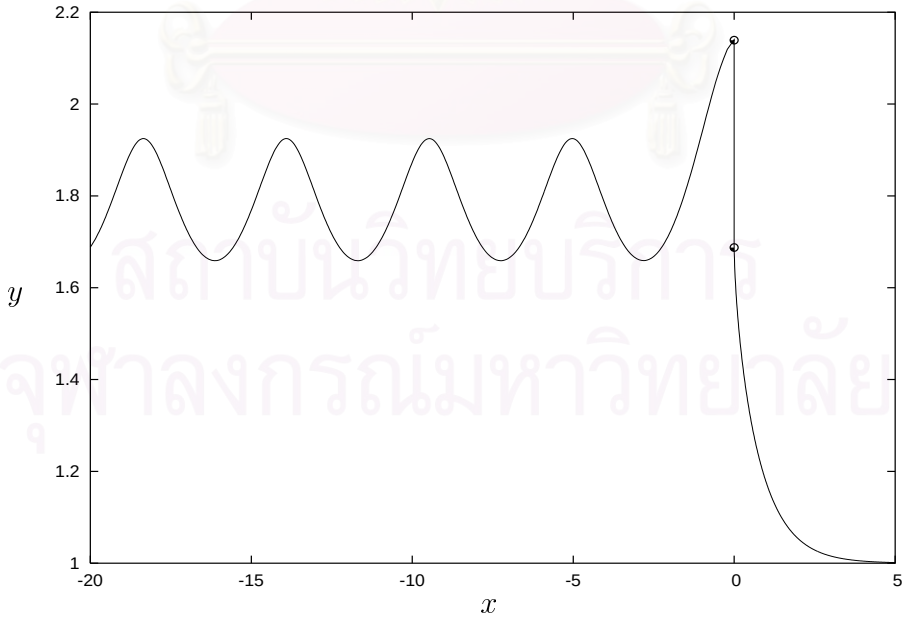

Figure 4.1 (h): $\phi_C = 0.075$ ($F = 1.5094$).

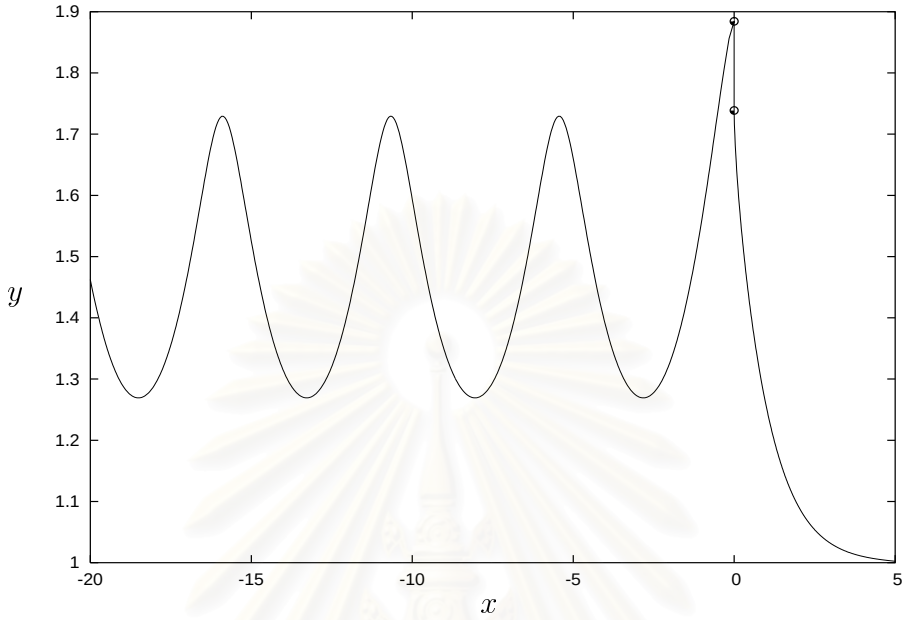

Figure 4.1 (i): $\phi_C = 0.016$ ($F = 1.3299$).

Figure 4.1: Profiles of the free surfaces and the gate when $\gamma = 90°$. The symbol $\circ$ indicates the position of the points at which the upstream and downstream free surfaces separate from the gate.

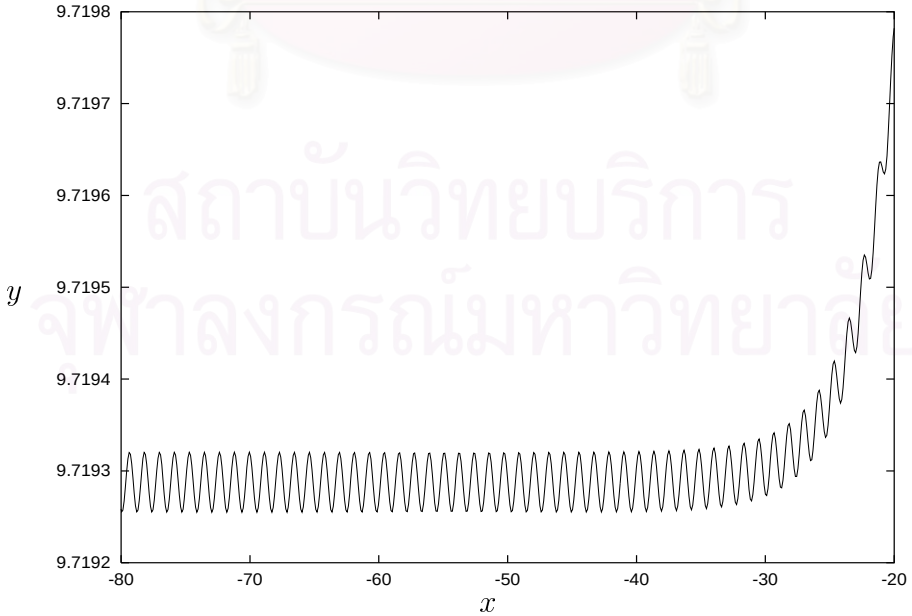

Figure 4.2: Upstream free surface of $\phi_C = 1.00$.

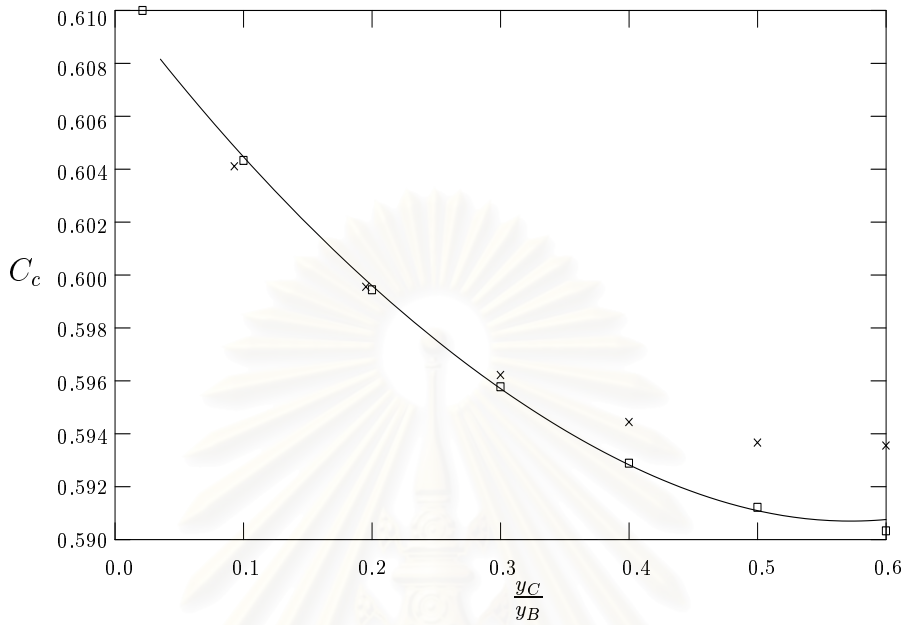

Figure 4.3: Values of the contraction coefficient C_c versus $\frac{y_C}{y_B}$. The symbols crosses and squares correspond to the calculation of Fangmeier and Strelkoff (1968) and Vanden-Broeck (1997), respectively.

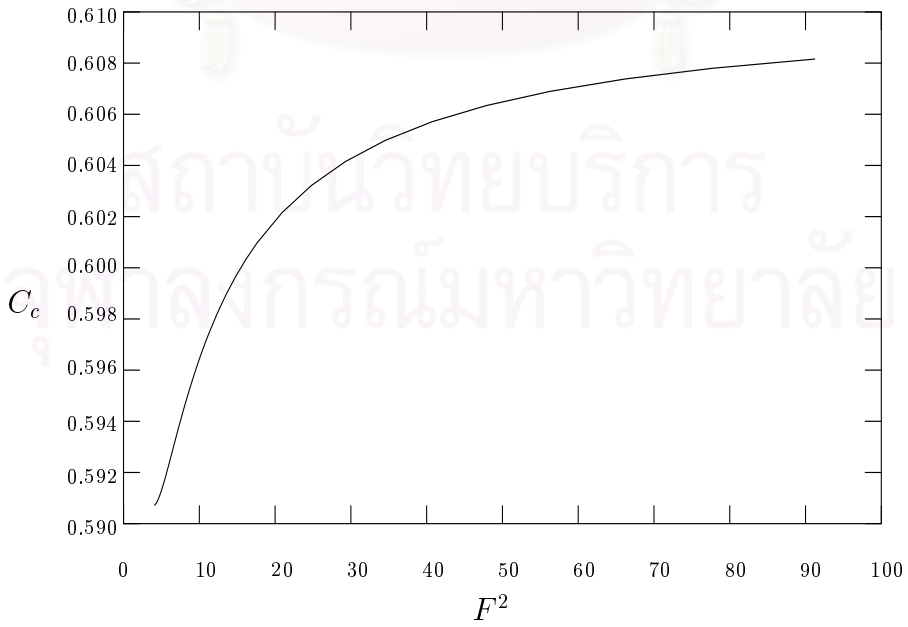

Figure 4.4: Values of the contraction coefficient C_c versus F^2.

In Figure 4.2, we enlarge the upstream free surface for the case of $\phi_C = 1.0$ so that the oscillations can clearly be seen. The amplitude of these waves is finitely small. In Figure 4.3, we show the relationship between the contraction coefficient C_c, defined as the ratio of depth far downstream and y_C (gate opening), and $\frac{y_C}{y_B}$. Here y_B and y_C are the distance from the point B and C to the bottom, respectivity. The contraction coefficient C_c constitutes an important check on our numerical scheme. In case of zero gravity (Batchelor, 1967), the contraction coefficient C_c for the free-streamline solution is:

$$C_c = \frac{\pi}{\pi + 2}$$
$$\approx 0.611015.$$

The crosses and squares in Figure 4.3 are represented numerical values taken from the Figure 13 in Fangmeier and Strelkoff (1968) and Figure 5 in Vanden-Broeck (1997). Fangmeier and Strelkoff assumed that the flow is uniform across a vertical section far upstream. Our results agree with Fangmeier and Strelkoff for $\frac{y_C}{y_B}$ smaller than 0.3. The difference between our calculations and those of Vanden-Broeck is approximately 0.44%. Table 4.1 show the numerical values of F between ours and Vanden-Broeck for some values of ϕ_C.

From Figures 4.3 and 4.4, we can see that $C_c \to C_c$ of free-streamline $= \frac{\pi}{\pi+2}$ as $\frac{y_C}{y_B} \to 0$ or $F^2 \to \infty$. Figure 4.5 shows the effect of mesh size on the upstream free surface profile corresponding to $\phi_C = 0.19$. This shows that our results are independent of Δ_1.

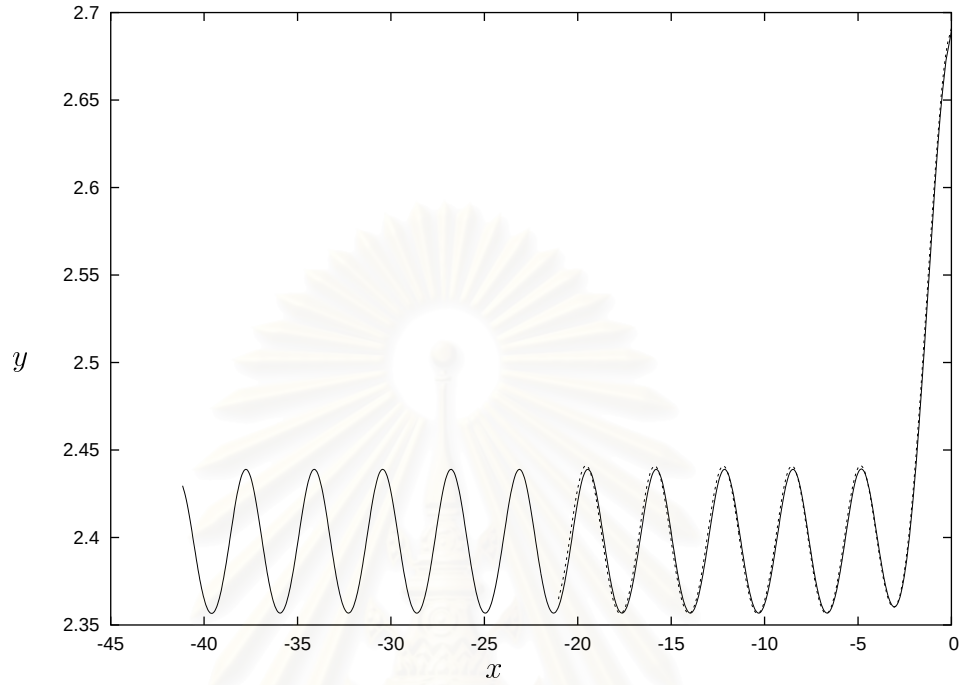

Figure 4.5: Profiles of the upstream free surface with $\Delta_1 = 0.01$ (broken line) and $\Delta_1 = 0.02$ (solid curve) for $\phi_C = 0.19$.

ϕ_C	F(Vanden-Broeck)	F
0.71	3.25	3.2419
0.41	2.41	2.4084
0.26	2.03	2.0221
0.19	1.83	1.8389
0.075	1.51	1.5094

Table 4.1: Numerical values of the downstream Froude number F between ours and Vanden-Broeck.

4.2 The Gate Inclination between 60° and 90° ($60^\circ \leq \gamma < 90^\circ$)

In this case, the free surface is horizontal in the neighborhood of stagnation point, so $\theta_1^U = 0$. The numerical results are shown that there exist solutions depending on two parameter, γ and ϕ_C.

Typical free-surface profiles are displayed in Figures 4.6, 4.7 and 4.8 for $\gamma = 80^\circ$, 70° and 60°, respectively. We find that there is a train of waves on the upstream free surface similar to the results of the vertical sluice gate problem. For a fixed value of γ, the amplitude of waves increases with broad troughs and narrow crests as F decreases (see Figures 4.6 (e) - (h), 4.7 (e) - (h) and 4.8 (e) - (h)). In Figure 4.9, we present an example of the checks so we used to test the accuracy of the numerical results. Both curves show the computed profiles when $\phi_C = 0.26$ and $\gamma = 60^\circ$ for $\Delta_1 = 0.01$ and $\Delta_1 = 0.02$.

In Figure 4.10, we present numerical values of the contraction coefficient C_c versus $\frac{y_C}{y_B}$ for $\gamma = 80^\circ$, 70° and 60°. For a fixed ratio of y_C and y_B, the value of C_c increases as γ decreases. This relationship shows that the contraction coefficient C_c is function of $\frac{y_C}{y_B}$ and γ. Numerical values of C_c versus F^2 for $\gamma = 80^\circ$, 70° and 60° are shown in Figure 4.11 (a) for $F^2 > 2$ and Figure 4.11 (b) for $F^2 \leq 2$. As C_c decreases, F^2 is close to 1.70 (see Figure 4.11 (b)).

In Figure 4.12, we present numerical values of the gate inclination γ versus F^2 for various values of ϕ_C. For a fixed ϕ_C, F^2 decreases as γ decreases. As ϕ_C is very small, there is little variation in F^2 for difference values of γ. Numerical values of the gate length L versus F^2 are shown in Figure 4.13. For a fixed F^2, the gate length L increases as γ decreases. This gives the length L of the gate as functions of F and γ.

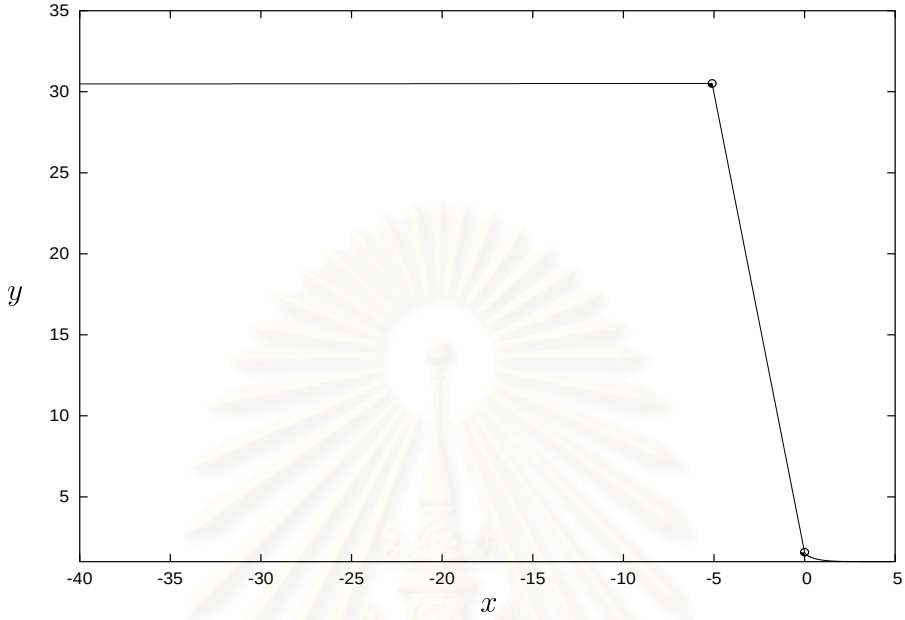

Figure 4.6 (a): $\phi_C = 2.00$ ($F = 7.6830$).

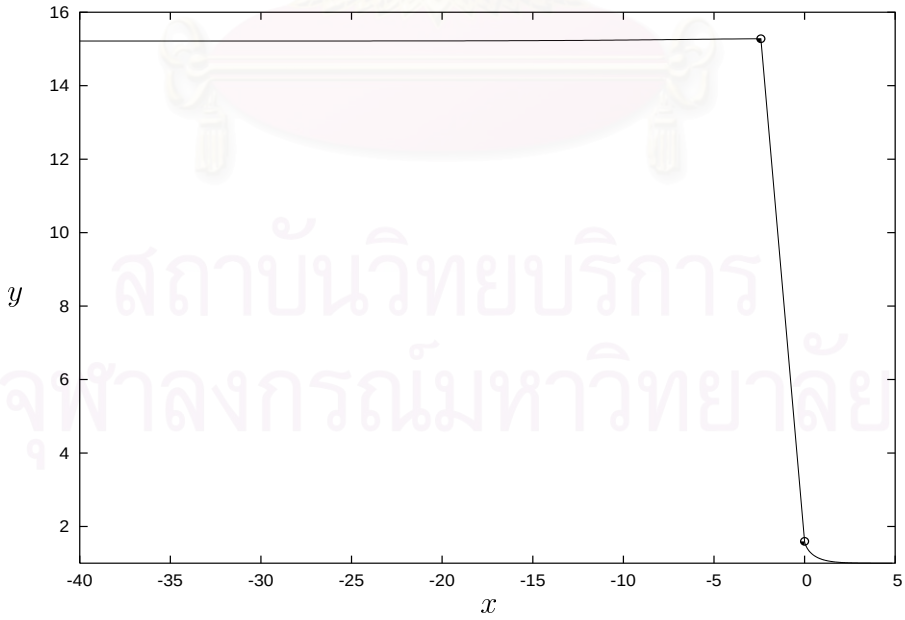

Figure 4.6 (b): $\phi_C = 1.50$ ($F = 5.3437$).

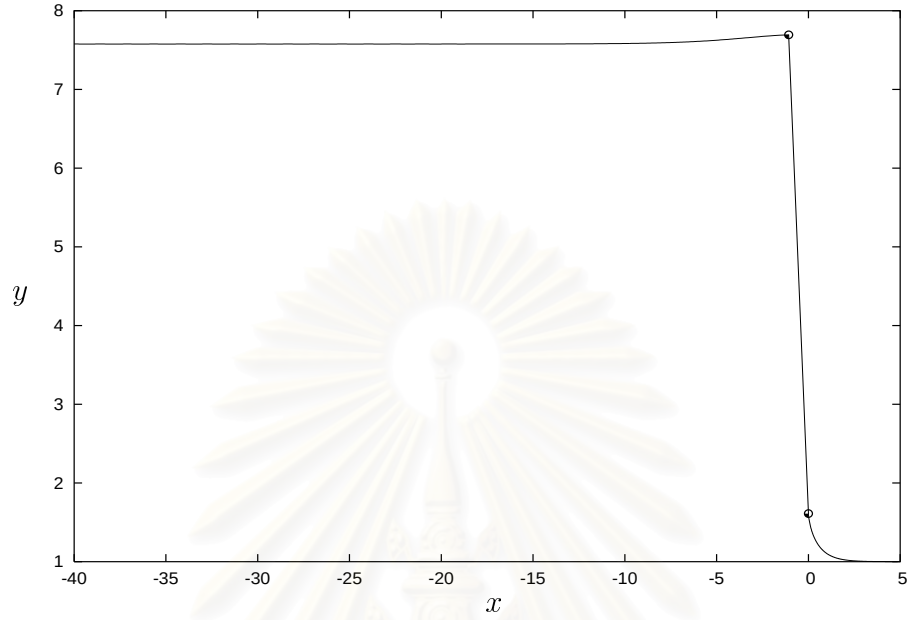

Figure 4.6 (c): $\phi_C = 1.00$ ($F = 3.6588$).

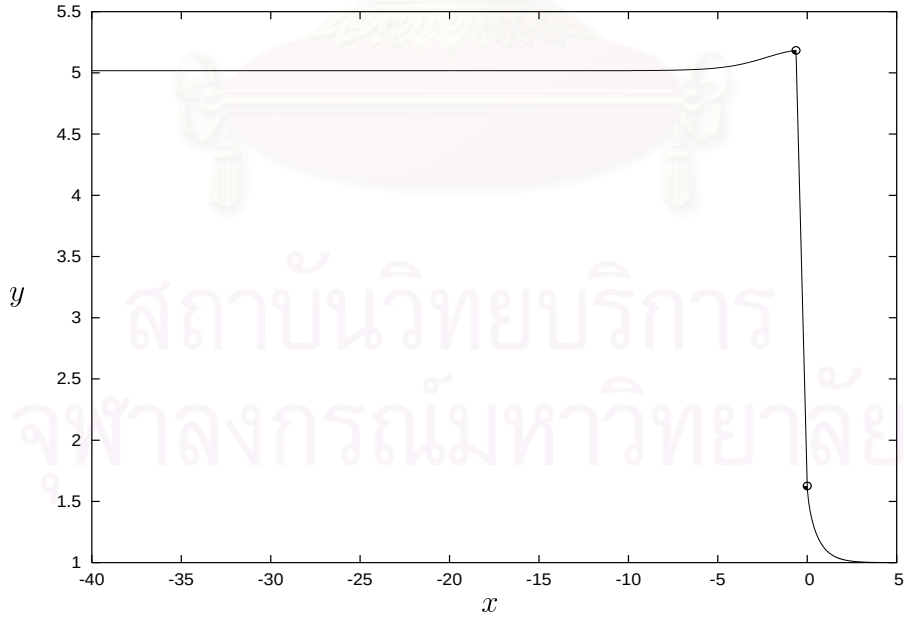

Figure 4.6 (d): $\phi_C = 0.71$ ($F = 2.8926$).

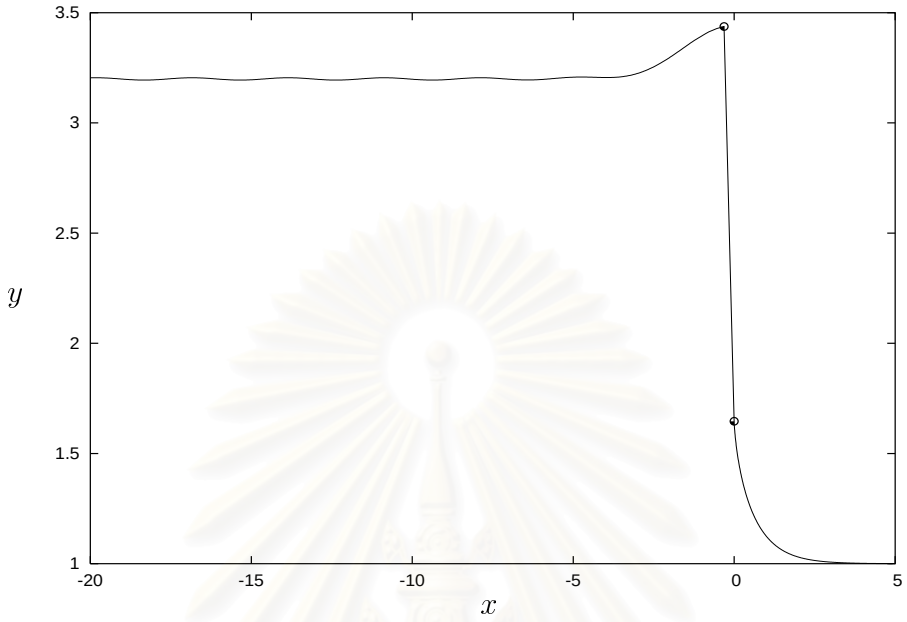

Figure 4.6 (e): $\phi_C = 0.41$ ($F = 2.2078$).

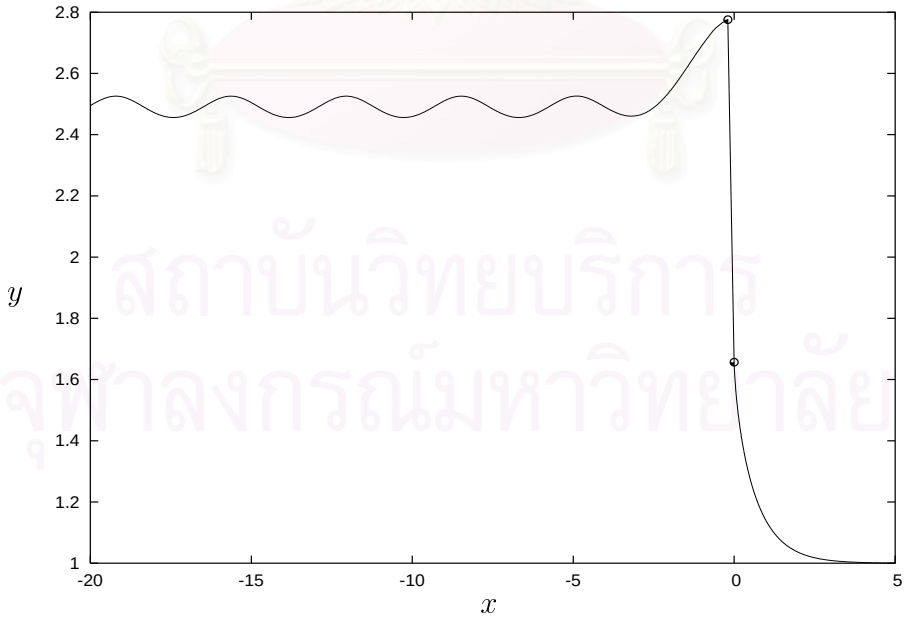

Figure 4.6 (f): $\phi_C = 0.26$ ($F = 1.8844$).

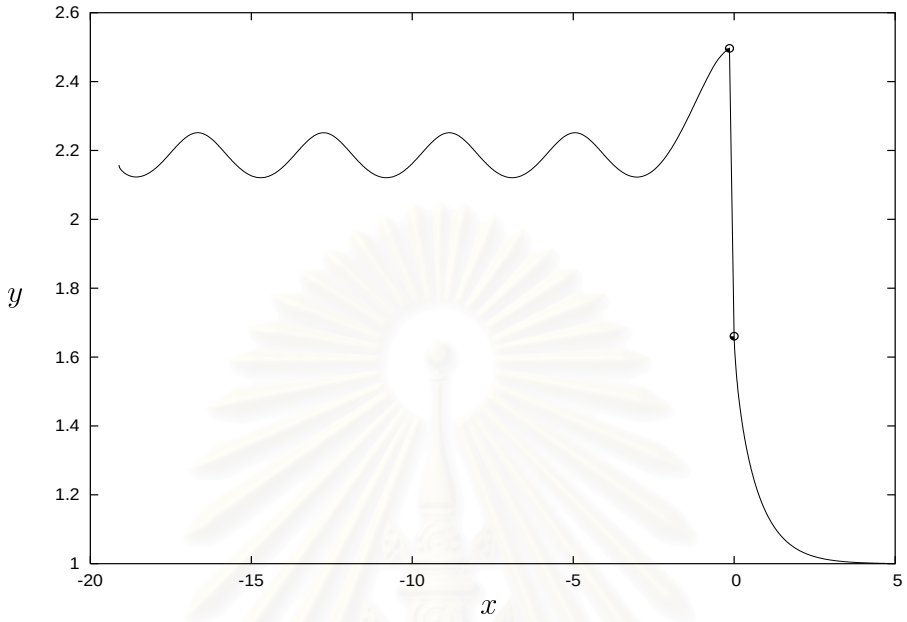

Figure 4.6 (g): $\phi_C = 0.19$ ($F = 1.7300$).

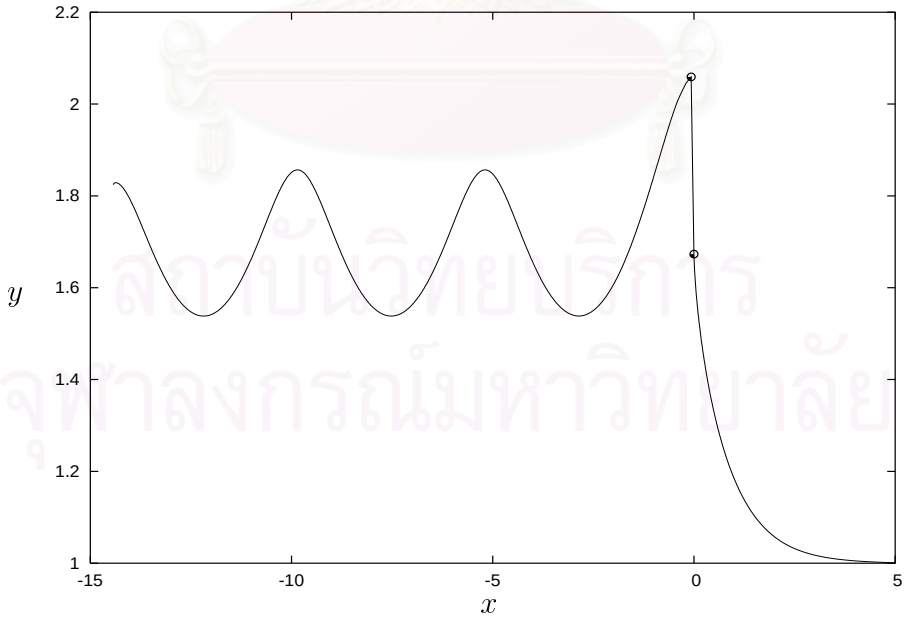

Figure 4.6 (h): $\phi_C = 0.075$ ($F = 1.4554$).

Figure 4.6: Profiles of the free surfaces and the gate when $\gamma = 80°$.

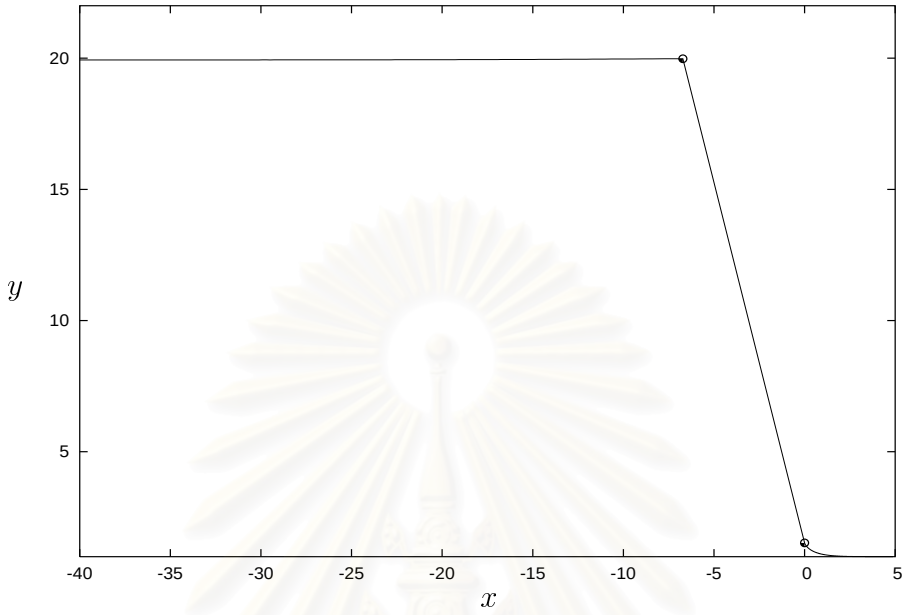

Figure 4.7 (a): $\phi_C = 2.00$ ($F = 6.1613$).

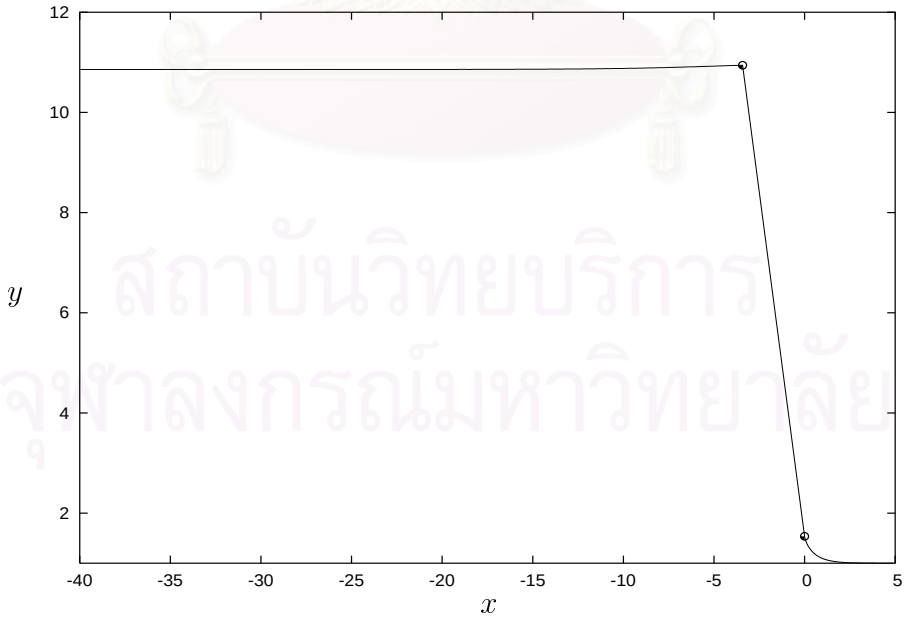

Figure 4.7 (b): $\phi_C = 1.50$ ($F = 4.4590$).

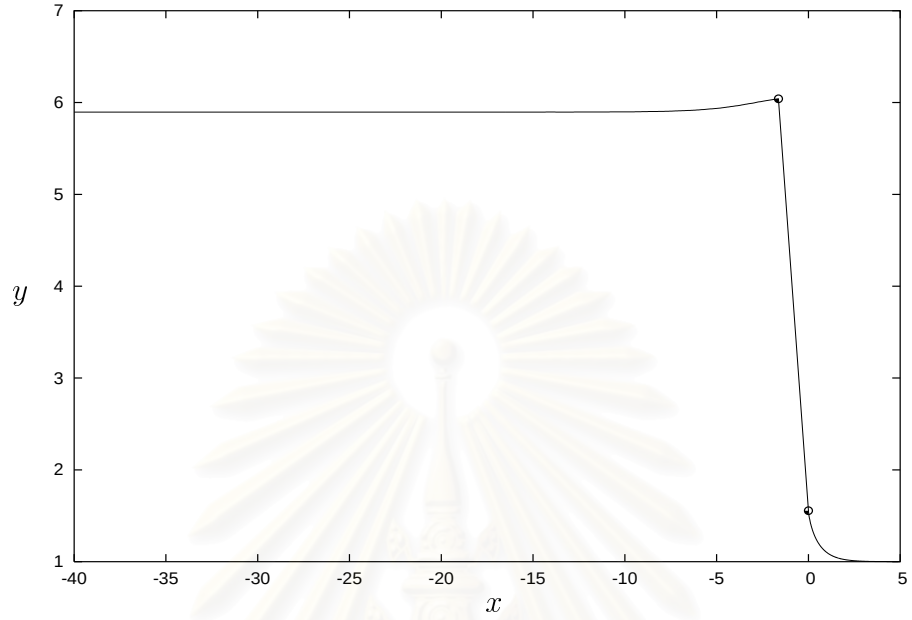

Figure 4.7 (c): $\phi_C = 1.00$ ($F = 3.1752$).

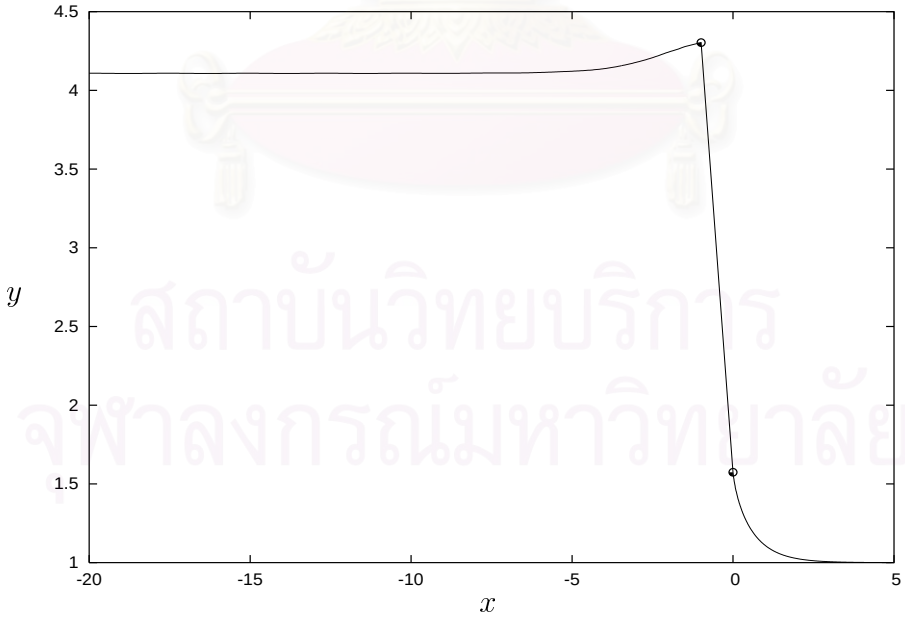

Figure 4.7 (d): $\phi_C = 0.71$ ($F = 2.5704$).

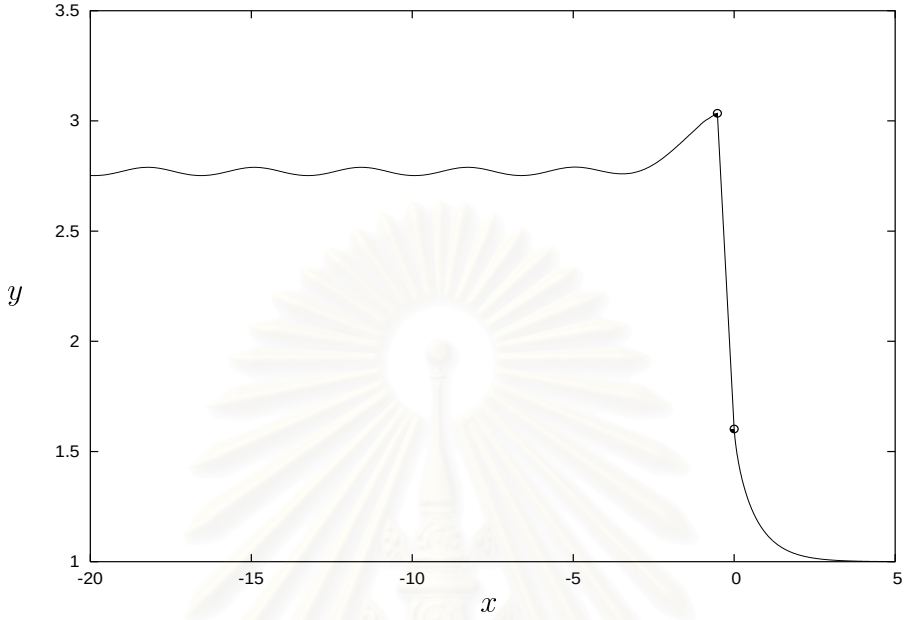

Figure 4.7 (e): $\phi_C = 0.41$ ($F = 2.0172$).

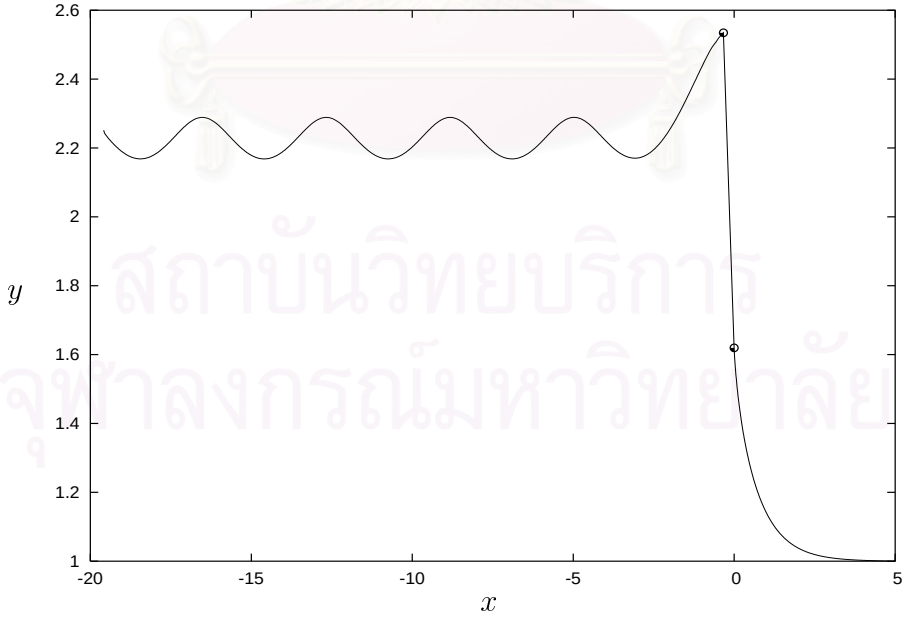

Figure 4.7 (f): $\phi_C = 0.26$ ($F = 1.7518$).

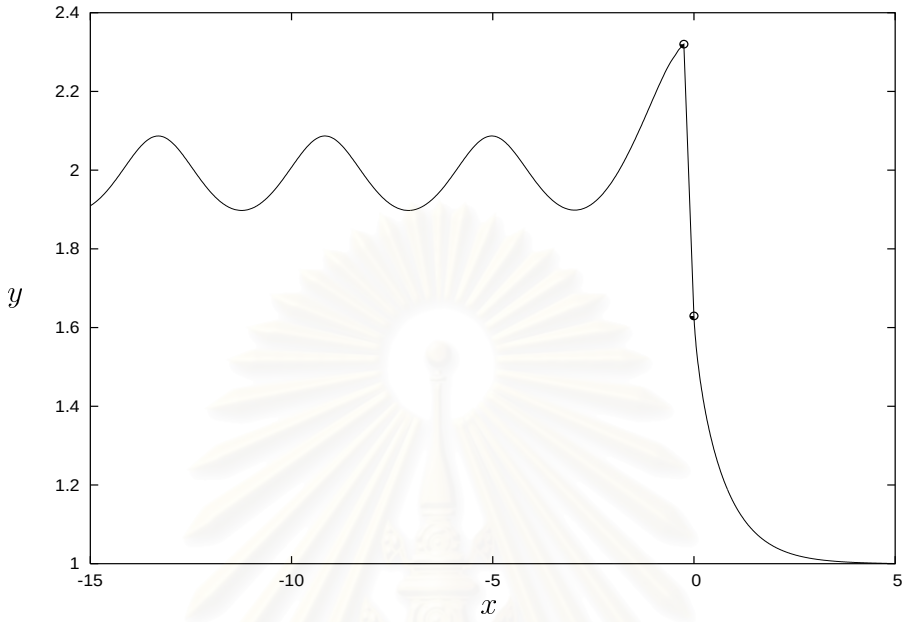

Figure 4.7 (g): $\phi_C = 0.19$ ($F = 1.6250$).

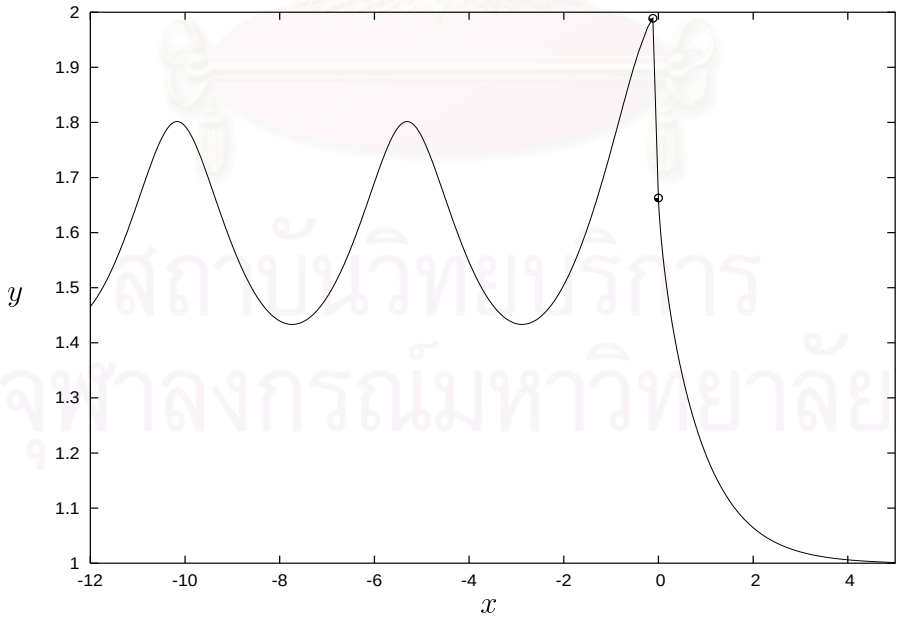

Figure 4.7 (h): $\phi_C = 0.075$ ($F = 1.4064$).

Figure 4.7: Profiles of the free surfaces and the gate when $\gamma = 70°$.

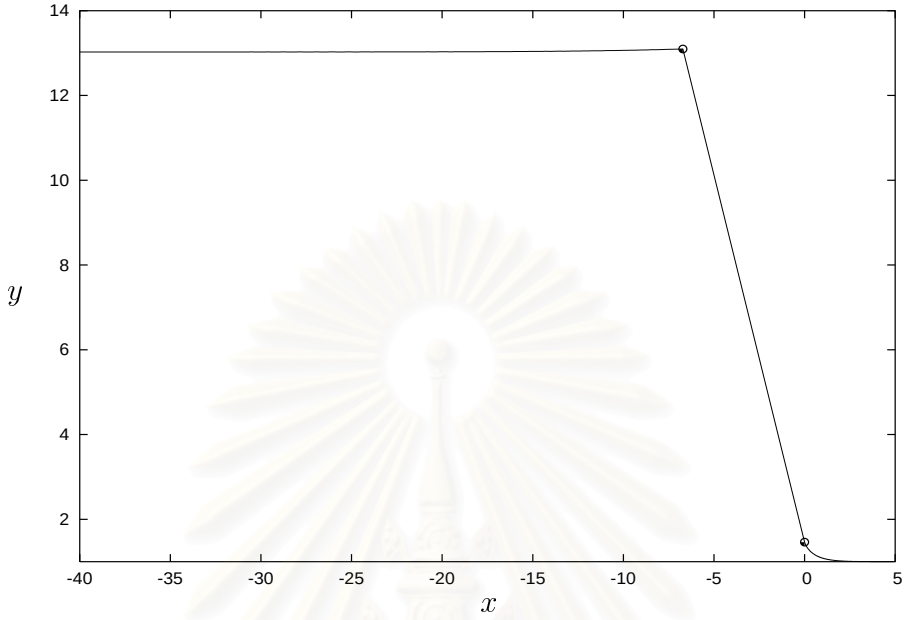

Figure 4.8 (a): $\phi_C = 2.00$ ($F = 4.9189$).

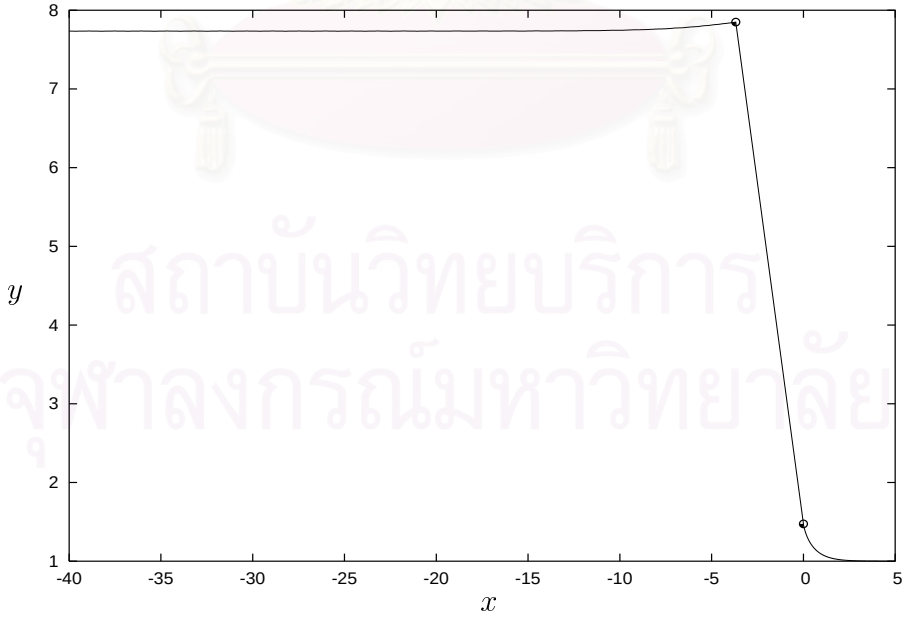

Figure 4.8 (b): $\phi_C = 1.50$ ($F = 3.7011$).

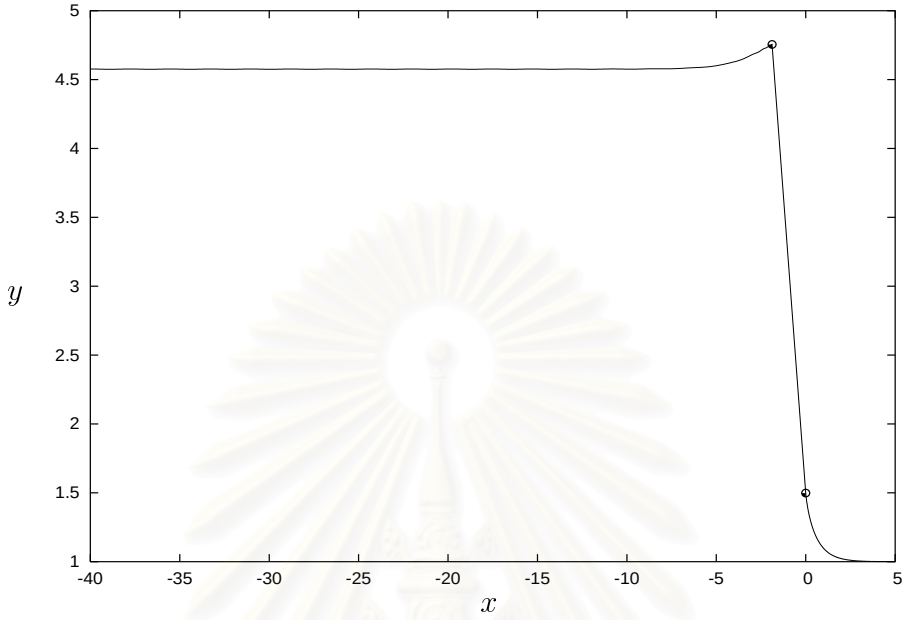

Figure 4.8 (c): $\phi_C = 1.00$ ($F = 2.7404$).

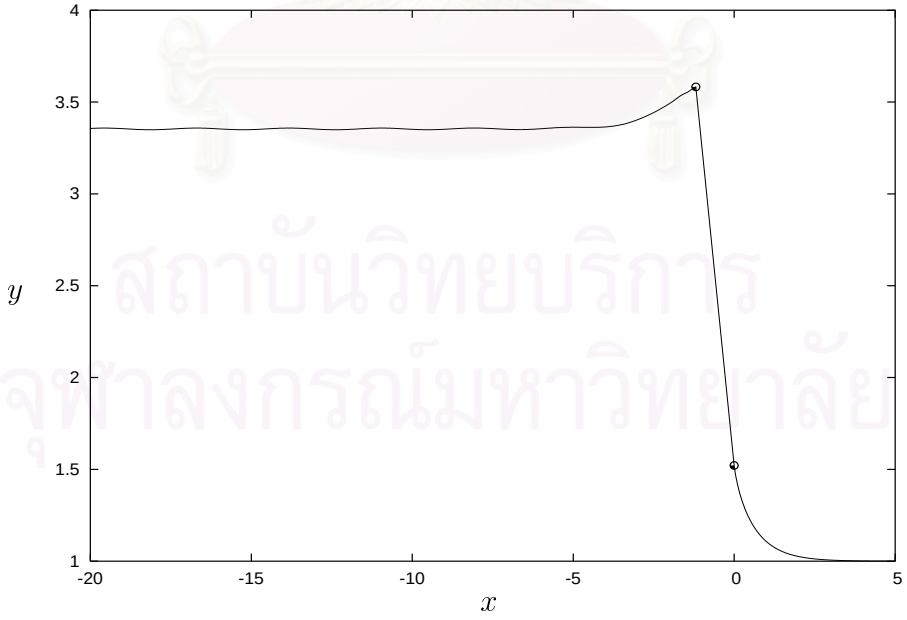

Figure 4.8 (d): $\phi_C = 0.71$ ($F = 2.2726$).

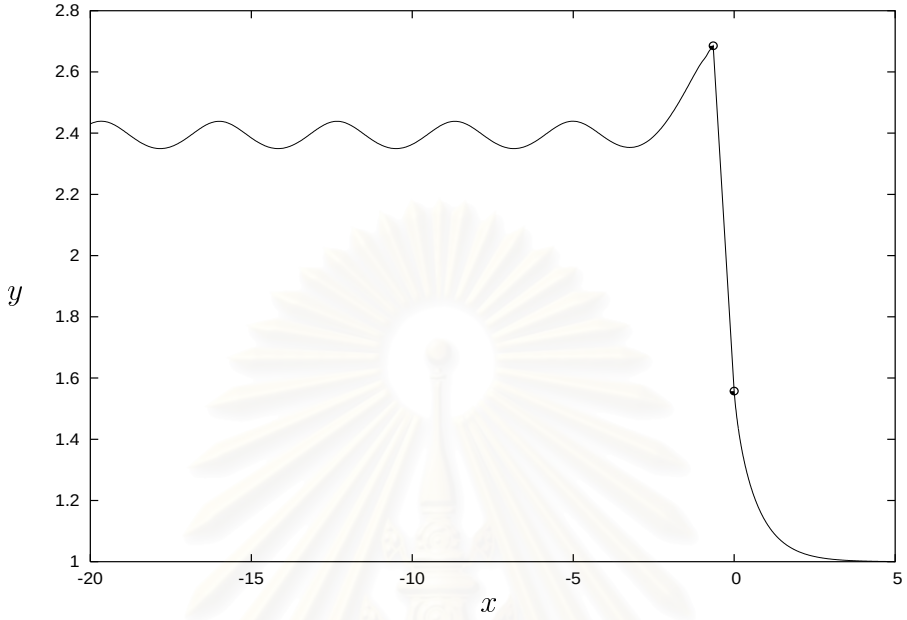

Figure 4.8 (e): $\phi_C = 0.41$ ($F = 1.8360$).

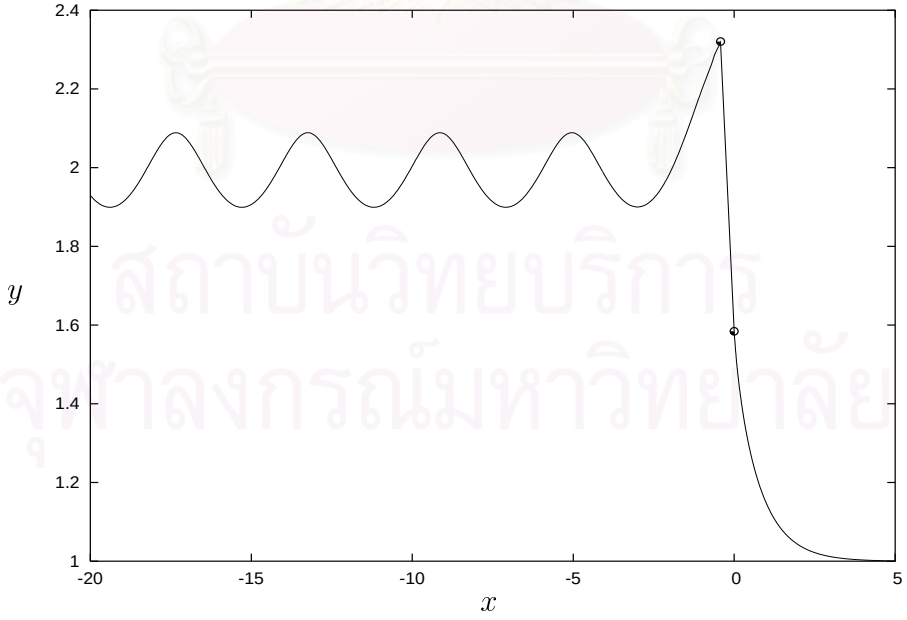

Figure 4.8 (f): $\phi_C = 0.26$ ($F = 1.6250$).

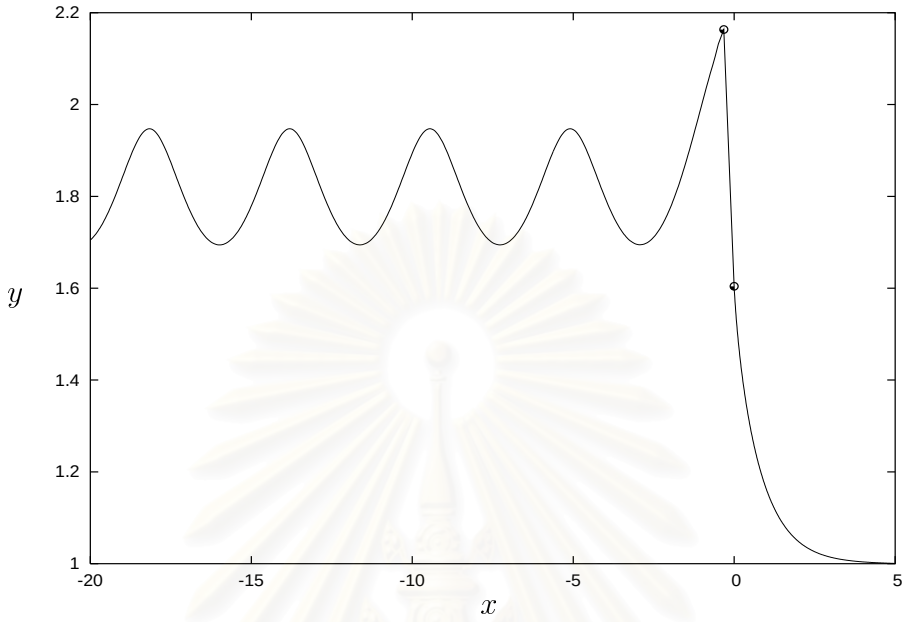

Figure 4.8 (g): $\phi_C = 0.19$ ($F = 1.5256$).

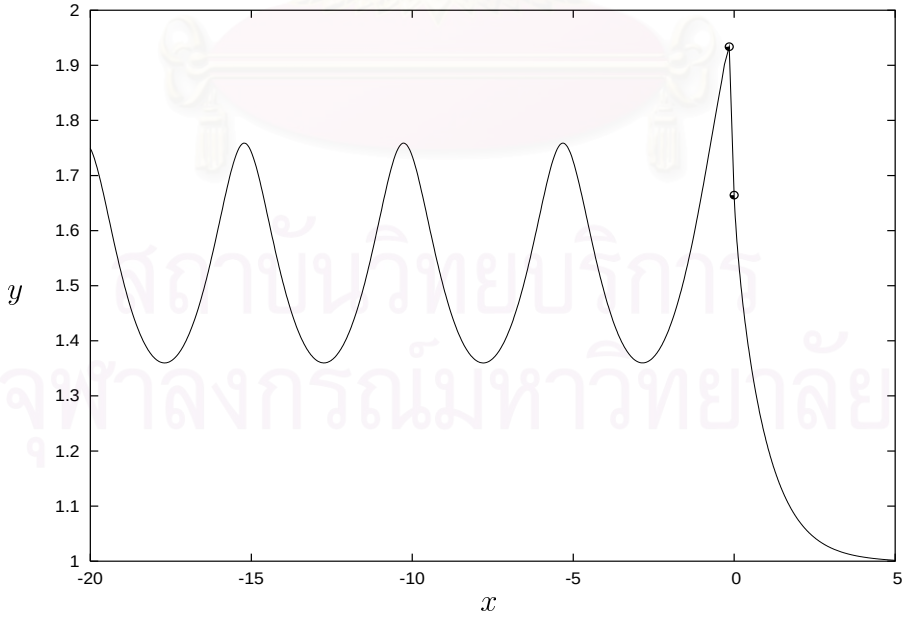

Figure 4.8 (h): $\phi_C = 0.075$ ($F = 1.3641$).

Figure 4.8: Profiles of the free surfaces and the gate when $\gamma = 60°$.

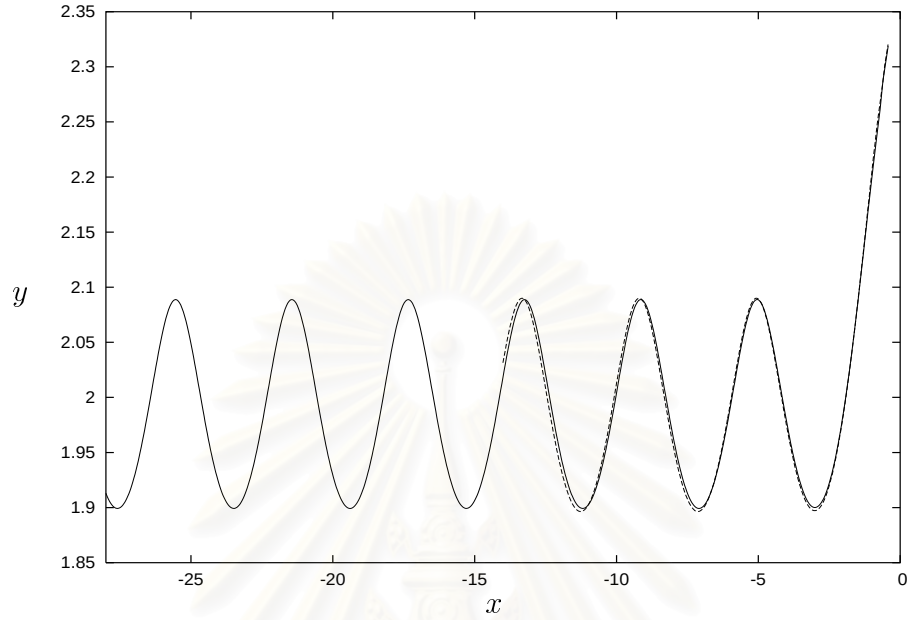

Figure 4.9: Profiles of the upstream free surface with $\Delta_1 = 0.01$ (broken line) and $\Delta_1 = 0.02$ (solid curve) for $\phi_C = 0.26$ and $\gamma = 60°$.

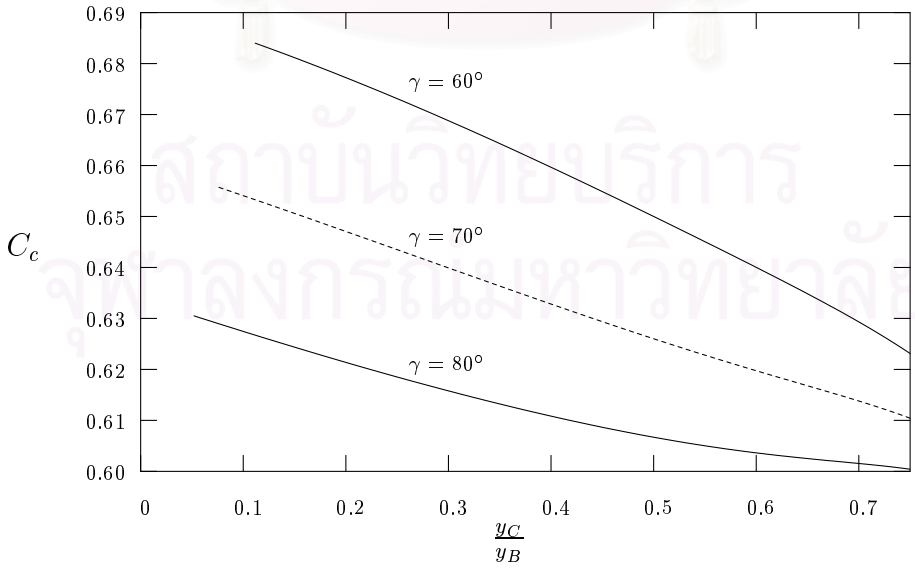

Figure 4.10: Relationship between the contraction coefficient C_c and $\frac{y_C}{y_B}$.

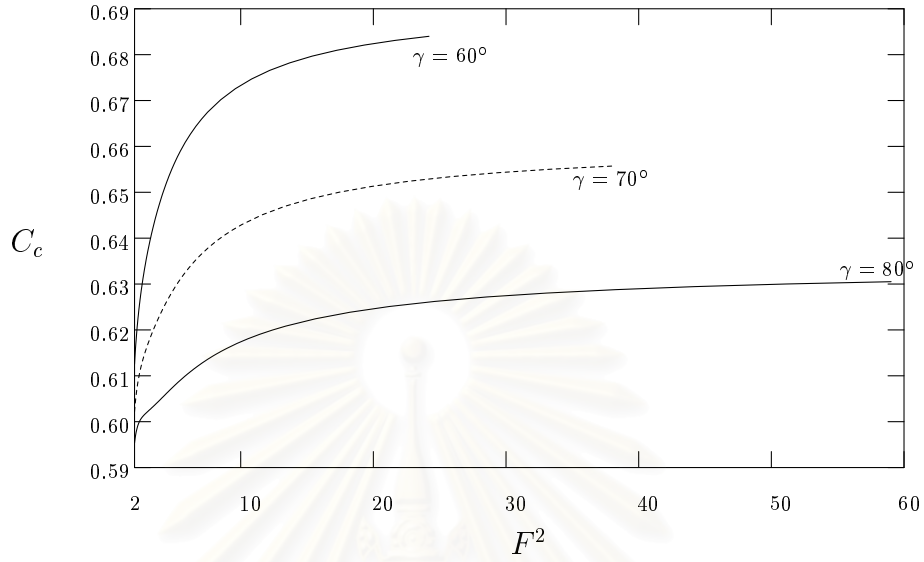

Figure 4.11 (a) $F^2 > 2.0$.

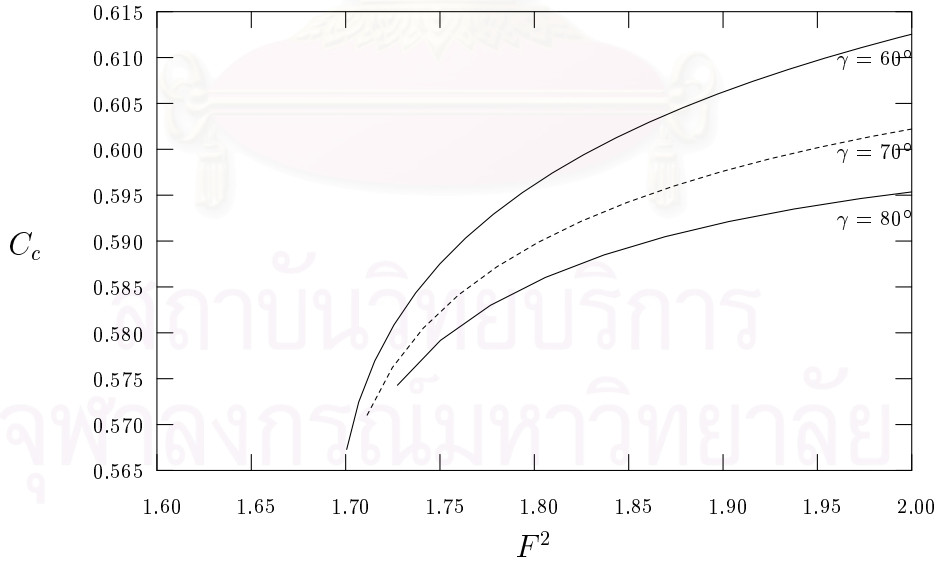

Figure 4.11 (b) $F^2 \leq 2.0$.

Figure 4.11: Relationship between the contraction coefficient C_c and F^2.

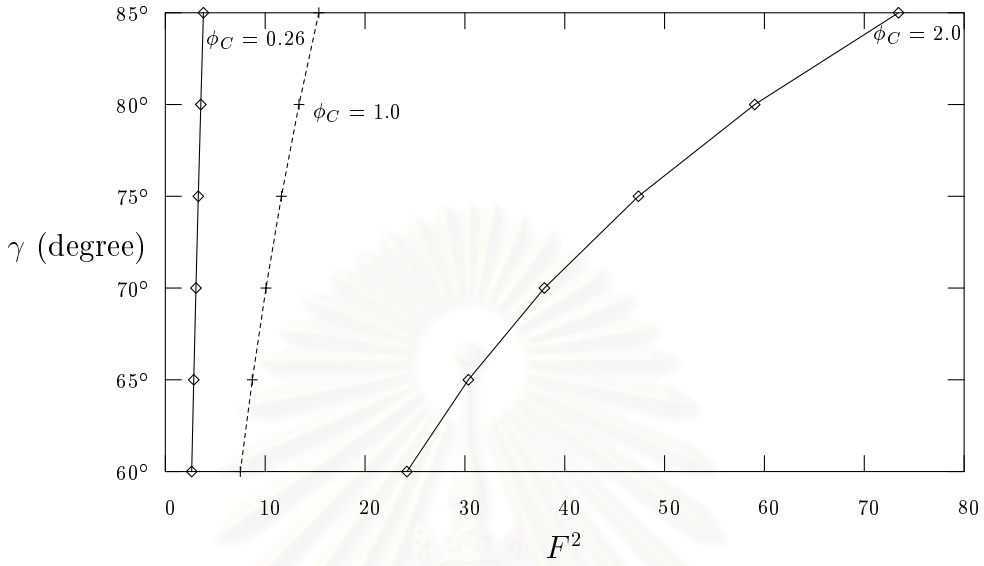

Figure 4.12: The gate inclination γ is shown as a function of F^2.

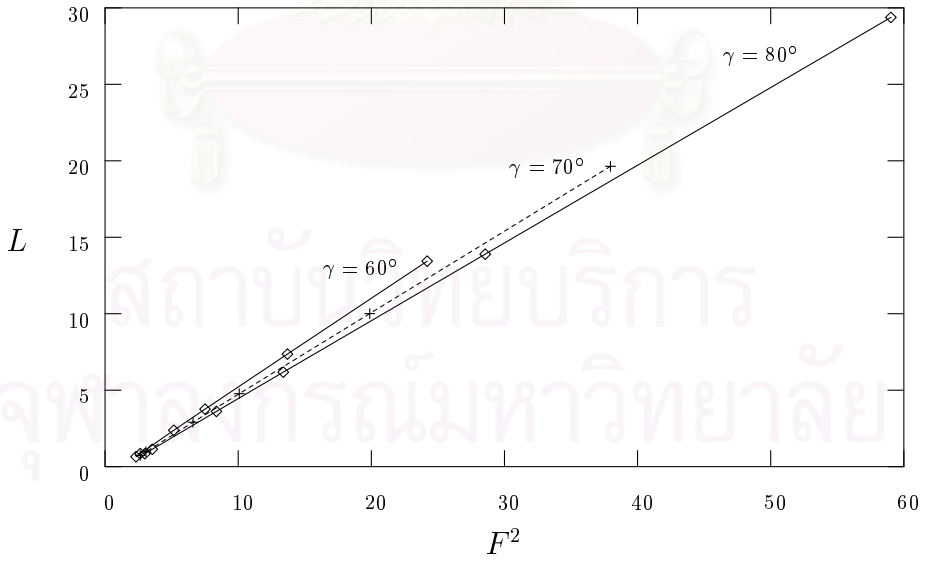

Figure 4.13: The length L of the gate is shown as a function of F^2.

4.3 The Gate Inclination between 0° and 60° ($0^\circ \leq \gamma < 60^\circ$)

In this case, we fixed the value of θ in the neighborhood of the stagnation point to be $\frac{\pi}{3} - \gamma$, i.e. $\theta_1^U = \frac{\pi}{3} - \gamma$.

Typical free-surface profiles are shown in Figures 4.14, 4.15 and 4.16 for $\gamma = 35^\circ,\ 45^\circ$ and 55°, respectively. However, for a given gate inclination γ, solutions exist for the Froude number F greater than some critical value F_γ^*. This critical value F_γ^* depends on the gate inclination γ. For small γ, it is difficult to find the numerical solution because the free surface near upstream separation can no longer satisfy the prescribed stagnation point behavior.

Amplitude of the waves increases as F decreases. For larger value of F, the amplitude of waves remains finite (see Figure 4.17). In addition, for a fixed value of F, amplitude of the waves increases as the gate inclination decreases. In Figure 4.18 we present numerical values of the contraction coefficient C_c versus y_C/y_B. The contraction coefficient C_c increases as γ decreases. It is found that both C_c and L are increasing functions of F^2 for a fixed values of γ (see Figures 4.19 and 4.20). In Figure 4.21, we present numerical values of the gate inclination γ versus F^2 for various values of ϕ_C. For a fixed ϕ_C, F^2 decreases as γ decreases.

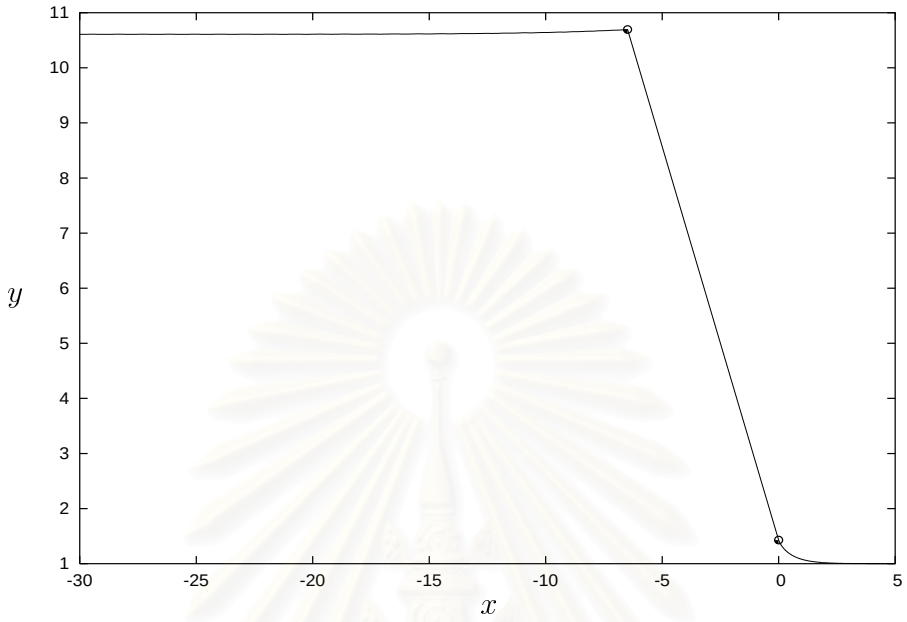

Figure 4.14 (a): $\phi_C = 2.00$ ($F = 4.4036$).

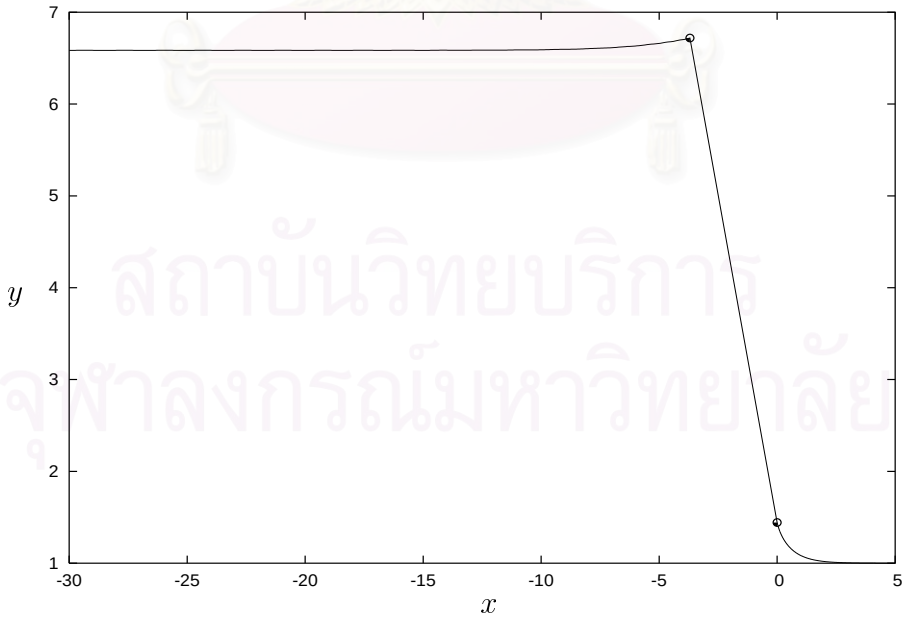

Figure 4.14 (b): $\phi_C = 1.50$ ($F = 3.3821$).

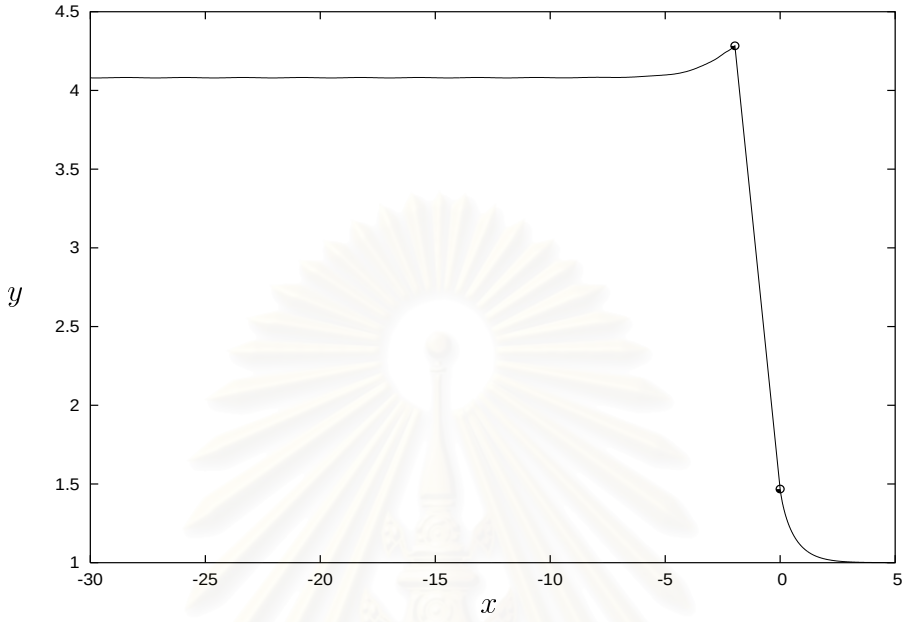

Figure 4.14 (c): $\phi_C = 1.00$ ($F = 2.5627$).

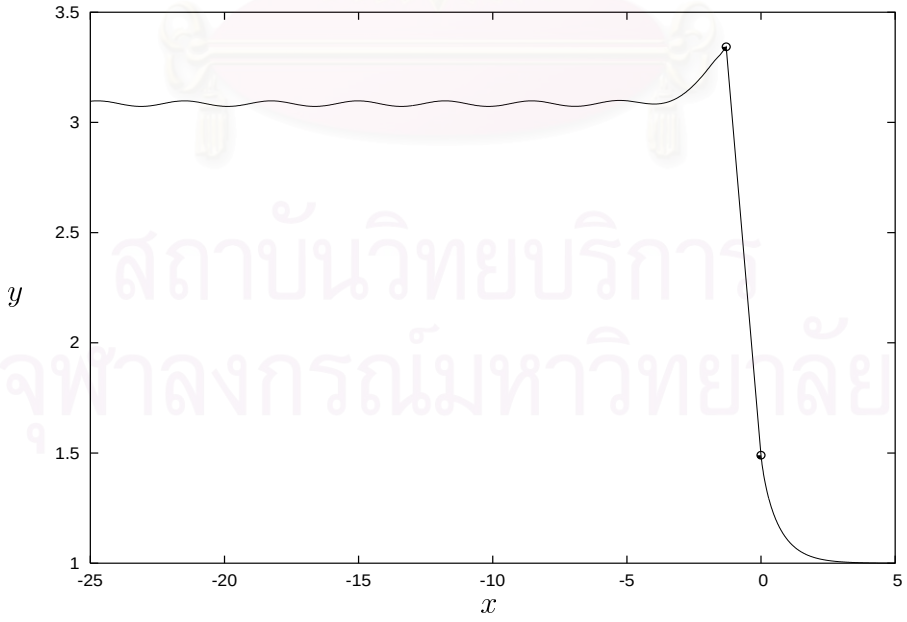

Figure 4.14 (d): $\phi_C = 0.71$ ($F = 2.1647$).

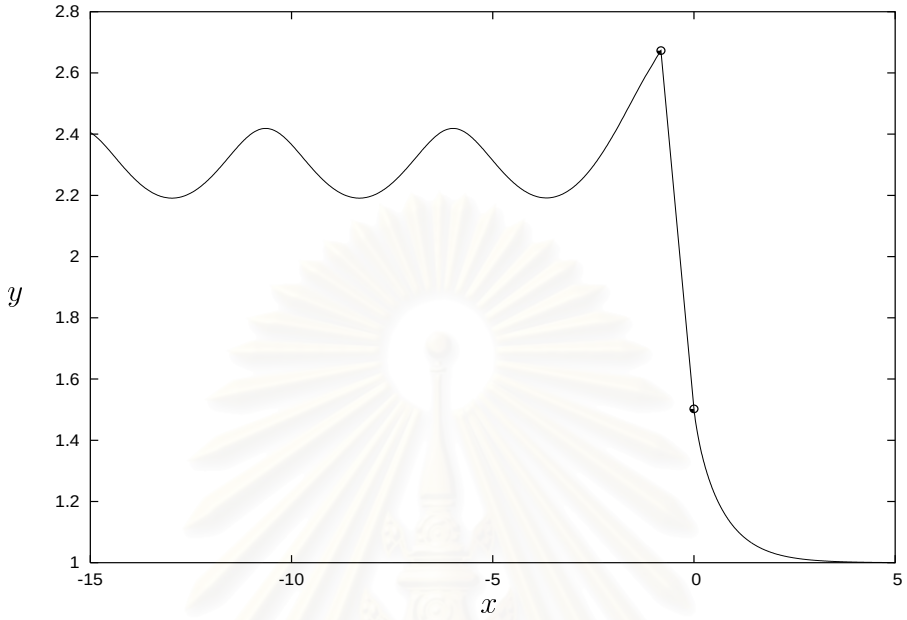

Figure 4.14 (e): $\phi_C = 0.41$ ($F = 1.8291$).

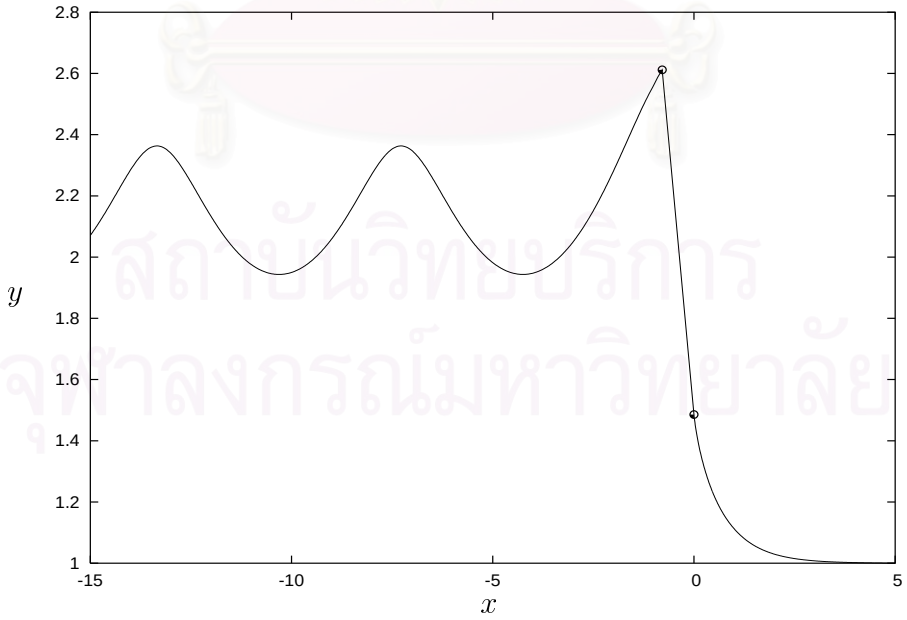

Figure 4.14 (f): $\phi_C = 0.35$ ($F = 1.7954$).

Figure 4.14: Profiles of the free surfaces and the gate when $\gamma = 55°$.

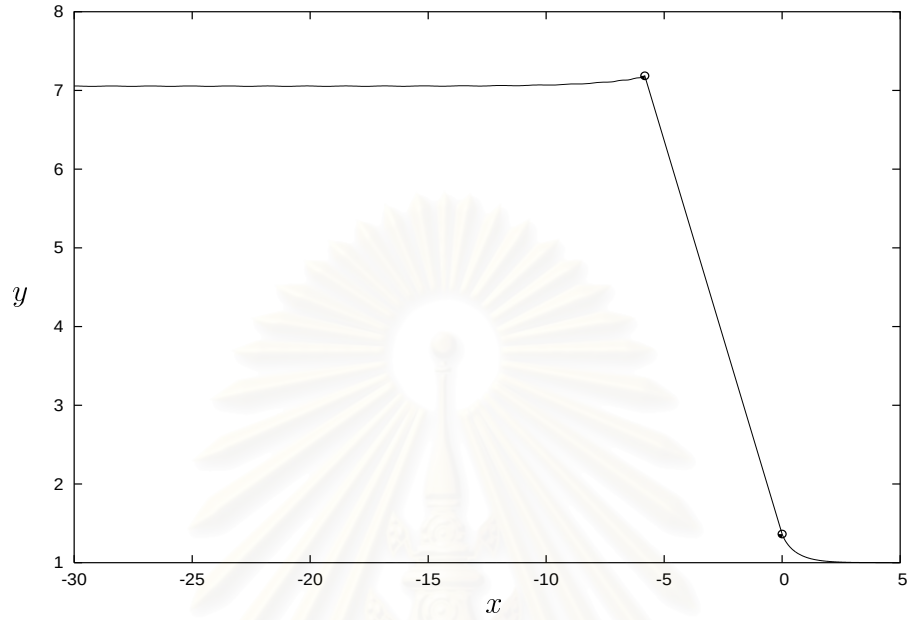

Figure 4.15 (a): $\phi_C = 2.00$ ($F = 3.5175$).

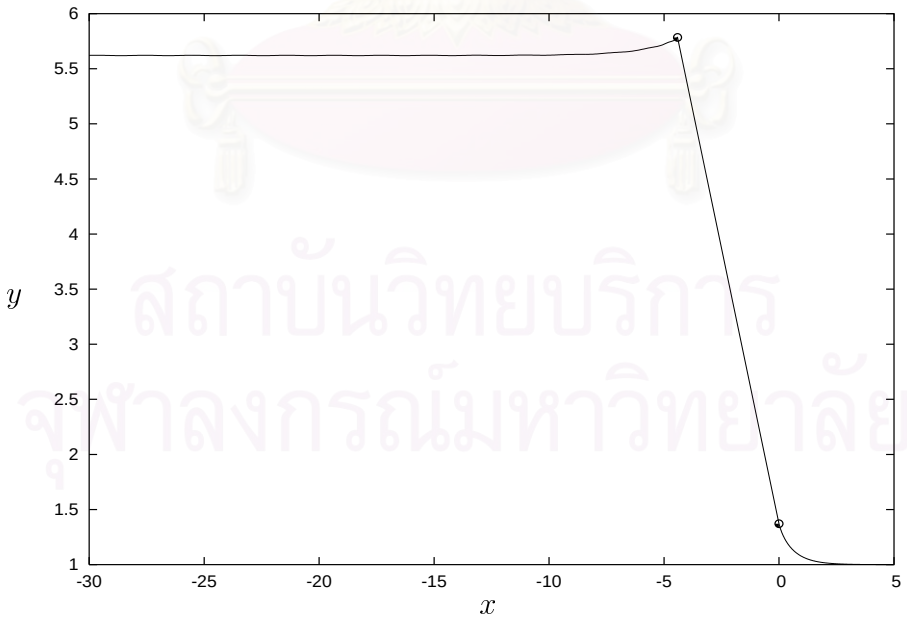

Figure 4.15 (b): $\phi_C = 1.70$ ($F = 3.0934$).

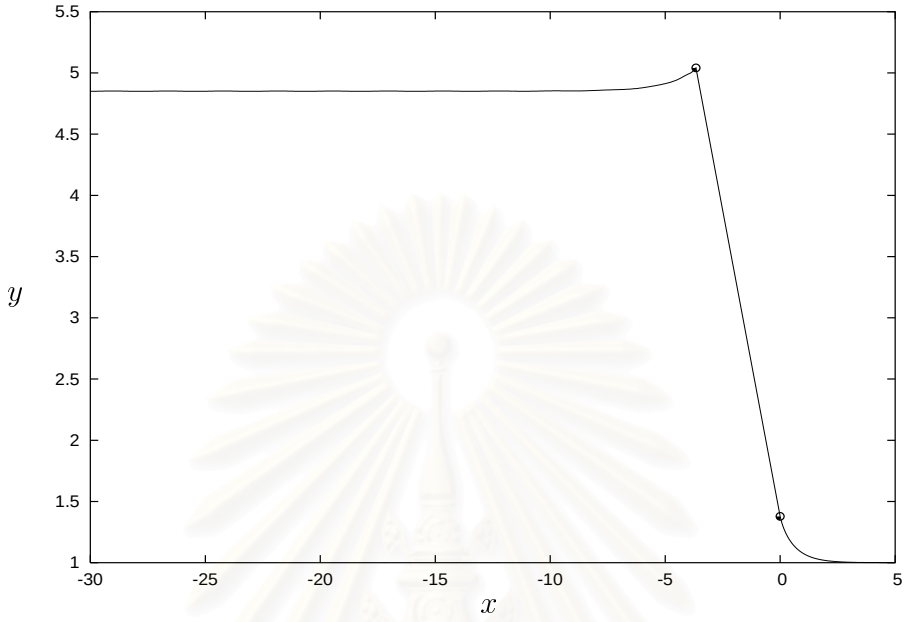

Figure 4.15 (c): $\phi_C = 1.50$ ($F = 2.8431$).

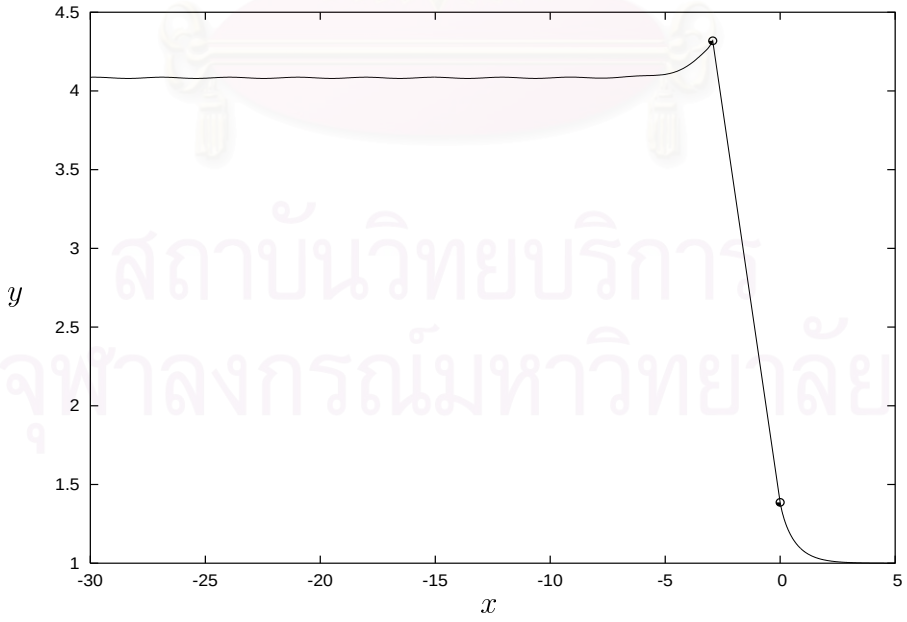

Figure 4.15 (d): $\phi_C = 1.25$ ($F = 2.5763$).

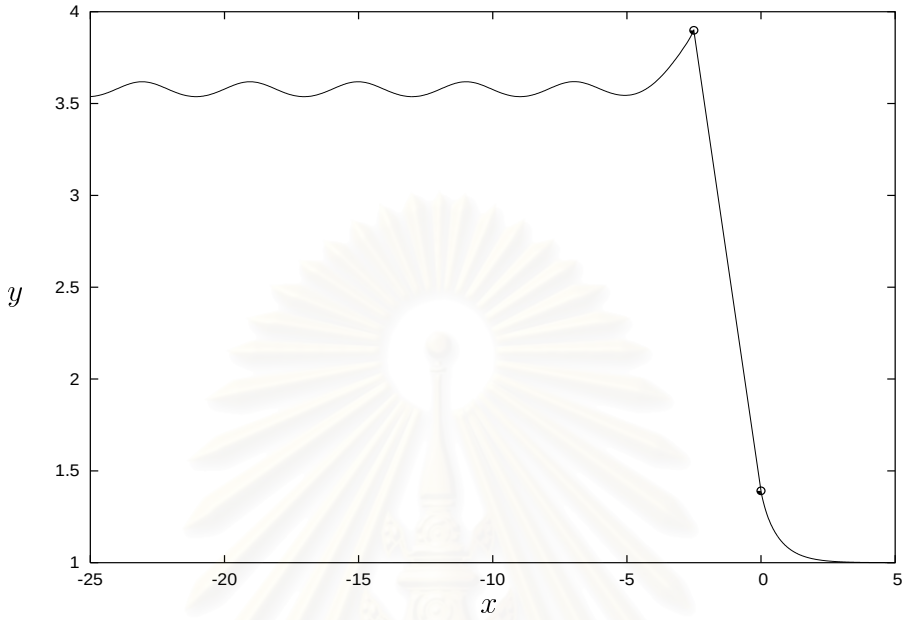

Figure 4.15 (e): $\phi_C = 1.00$ ($F = 2.4077$).

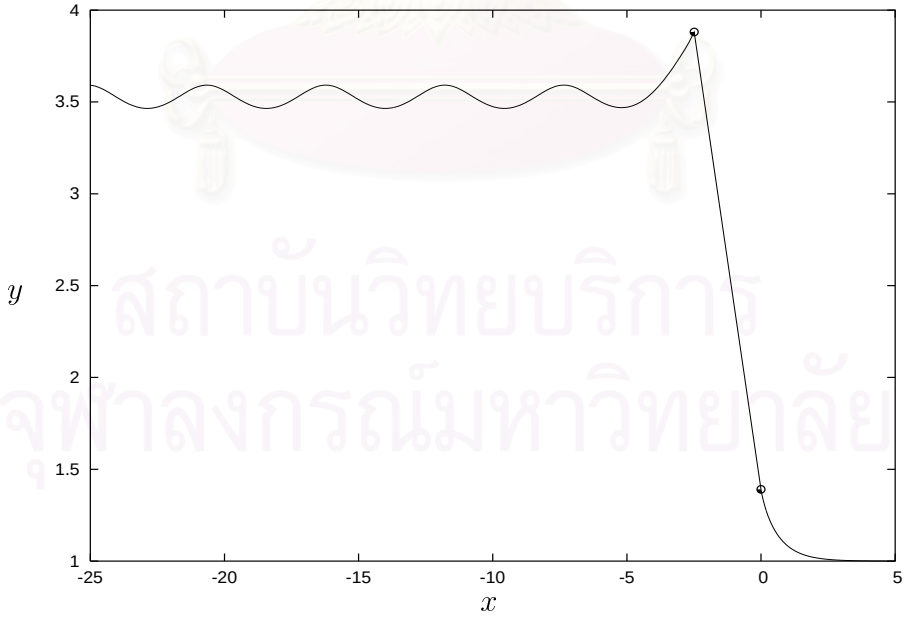

Figure 4.15 (f): $\phi_C = 0.95$ ($F = 2.4005$).

Figure 4.15: Profiles of the free surfaces and the gate when $\gamma = 45°$.

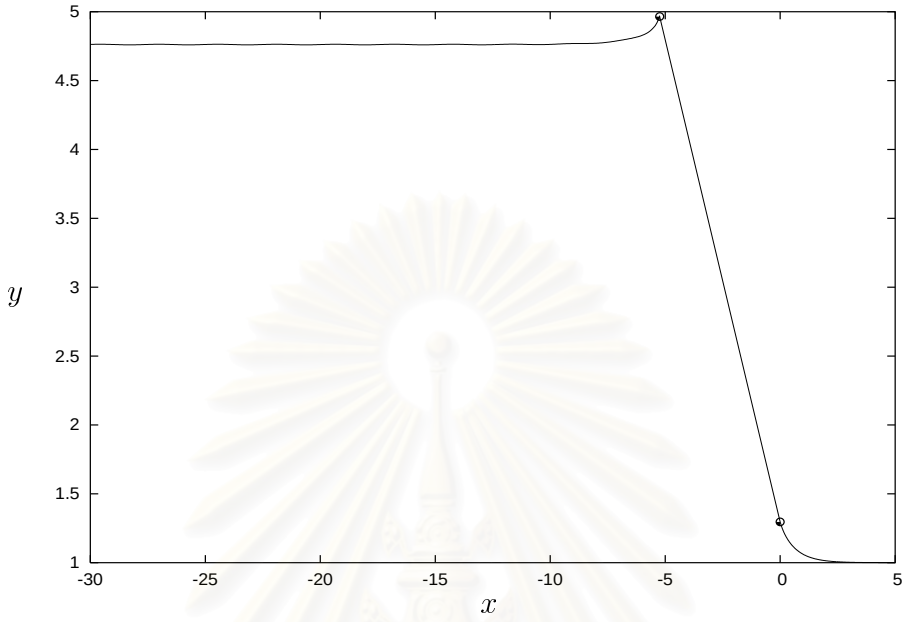

Figure 4.16 (a): $\phi_C = 2.00$ ($F = 2.8161$).

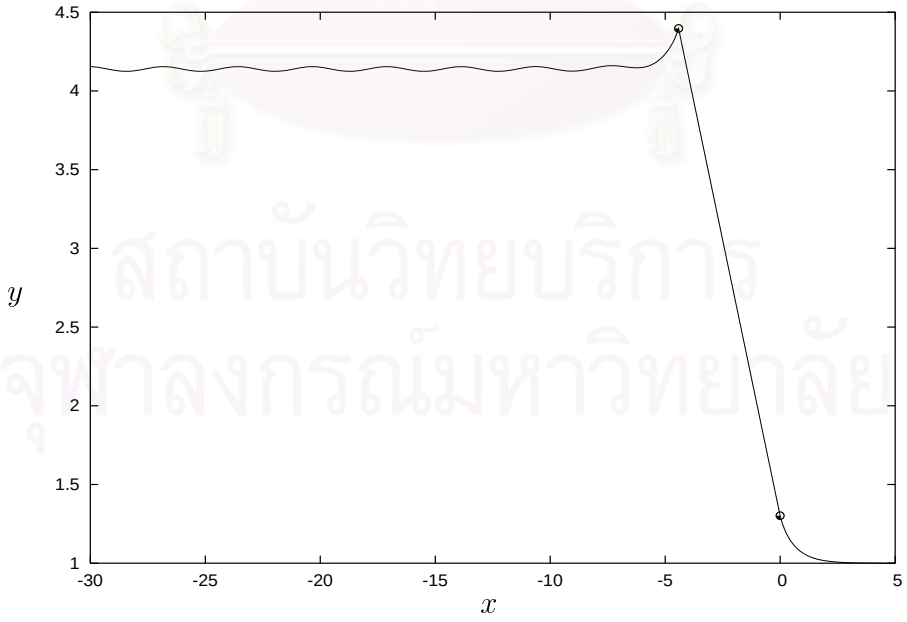

Figure 4.16 (b): $\phi_C = 1.70$ ($F = 2.6066$).

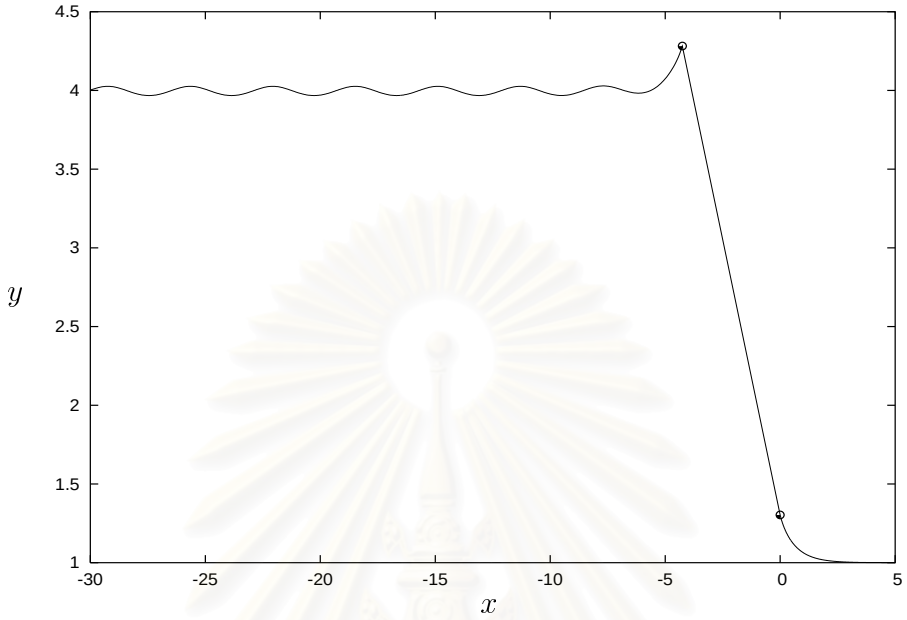

Figure 4.16 (c): $\phi_C = 1.60$ ($F = 2.5622$).

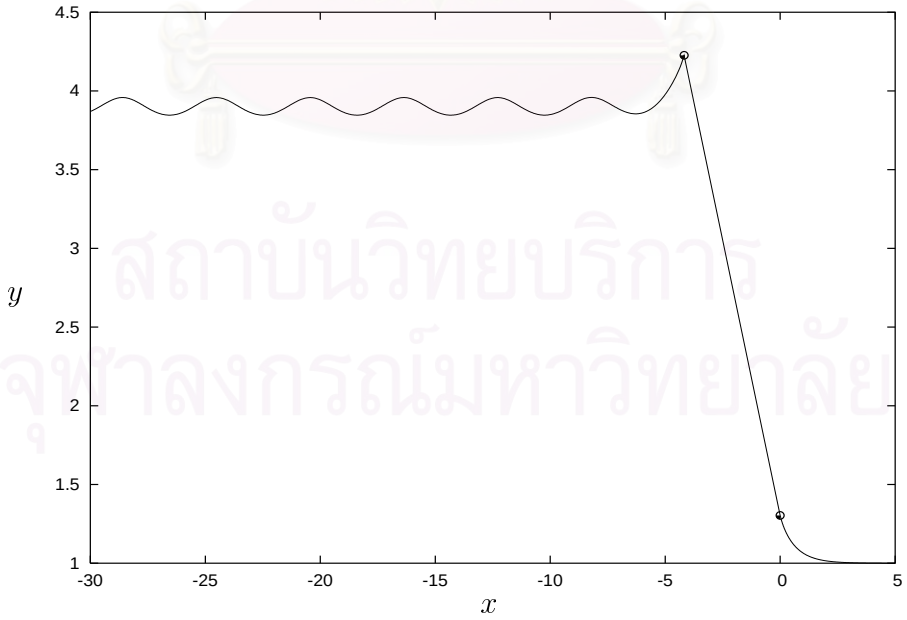

Figure 4.16 (d): $\phi_C = 1.50$ ($F = 2.5403$).

Figure 4.16: Profiles of the free surfaces and the gate when $\gamma = 35°$.

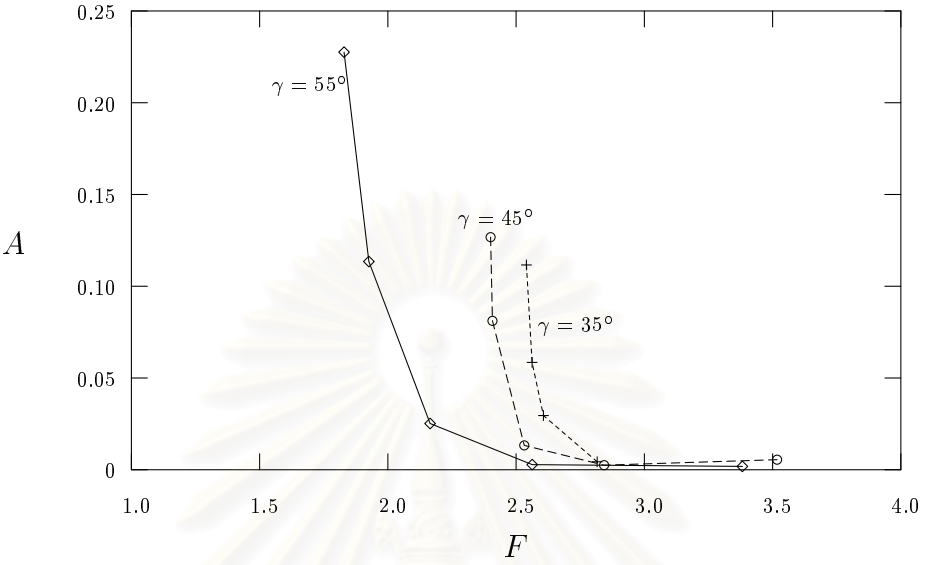

Figure 4.17: The amplitude A of the waves versus F.

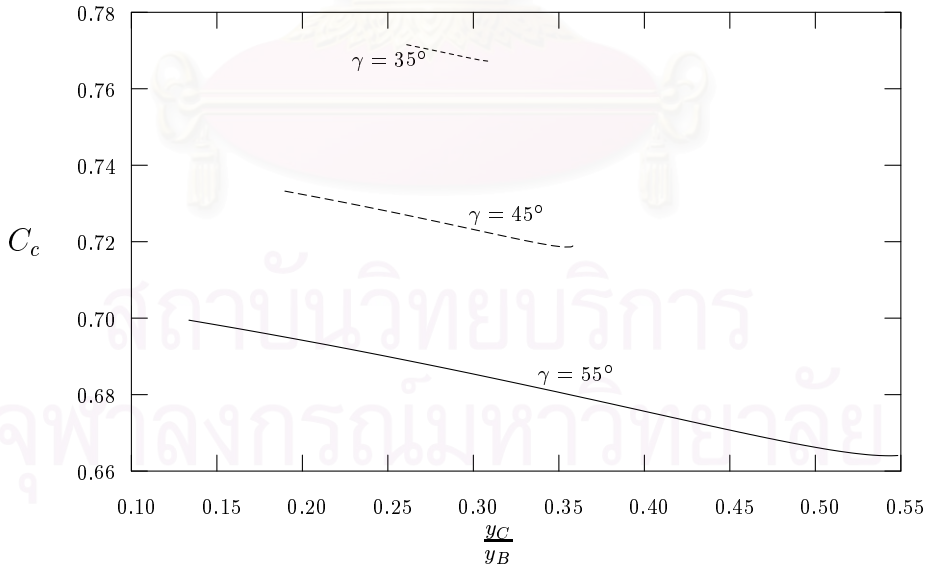

Figure 4.18: Values of the contraction coefficient C_c versus $\frac{y_C}{y_B}$.

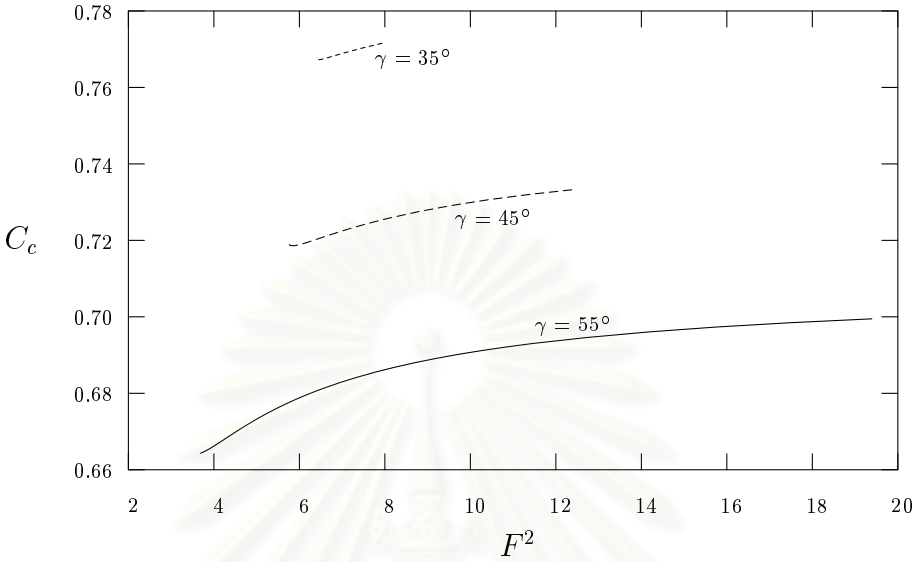

Figure 4.19: Values of the contraction coefficient C_c versus F^2.

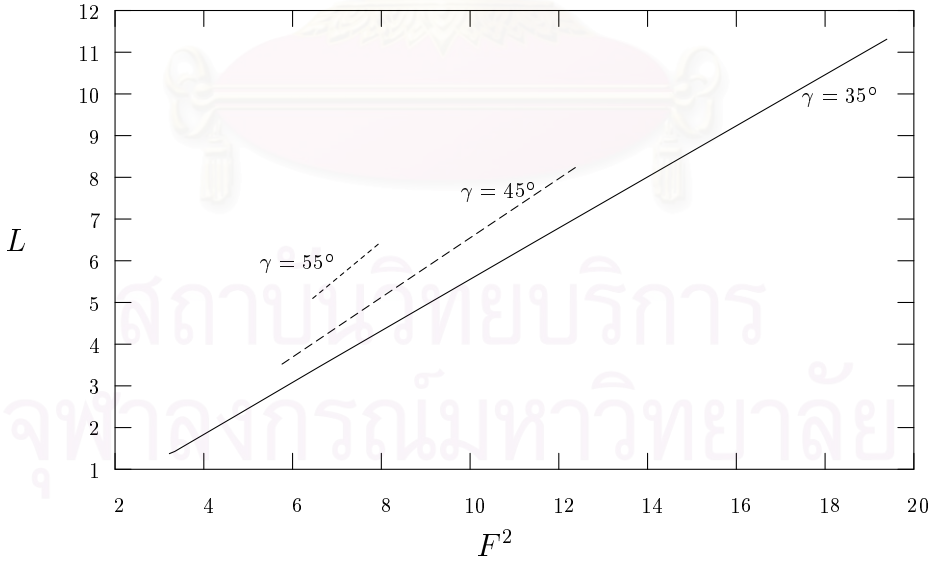

Figure 4.20: The length L of the gate versus F^2.

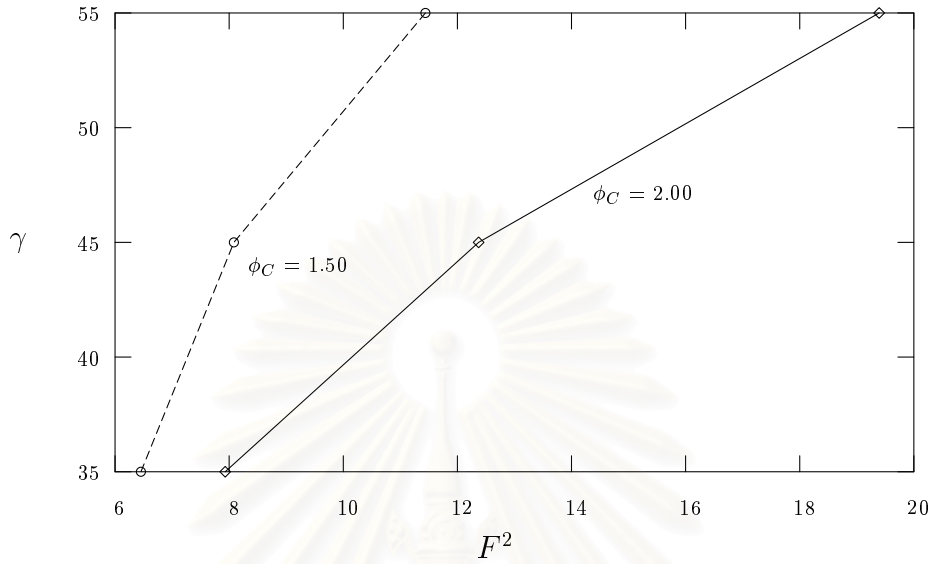

Figure 4.21: The gate inclination γ versus F^2.

CHAPTER V

Numerical Results of Free-Surface Flows under an Inclined Sluice Gate with Smooth Attachment

In this Chapter, we consider the problem of flows under a gate for which the free surfaces leave tangentially at both separation points. The value of θ at both upstream and downstream separation points are $-\gamma$ ($\theta_1^U = \theta_1^D = -\gamma$). In the previous work of Asavanant and Vanden-Broeck (1996), they obtained results for small angles of gate inclination and small values of the downstream Froude numbers. They could not obtain solutions with waves on upstream free surface. Here we can find solution for larger values of gate inclination and all numerical solutions contain waves on the upstream. The numerical scheme derived in chapter III is used to compute solutions for various values of ϕ_C and γ. Most of the results presented here are obtained with $N_1 = 1261, N_2 = 801, \Delta_1 = 0.02$ and $\Delta_2 = 0.01$.

Typical free-surface profiles are shown in Figures 5.1, 5.2 and 5.3 for $\gamma = 6^\circ,\ 7^\circ$ and 8°, respectively. These waves tend to develop narrow crests and broad troughs showing the nonlinearity of waves as F increases (see Figures 5.2 (a) to 5.2 (e)). Magnified portions of the free surface near the upstream separation point are shown in Figures 5.4 and 5.5 for $\gamma = 7^\circ$ and 8°, respectively. As we can see, the numbers of points on the first crest near the upstream separation decrease as F increases. This is a possible cause of numerical difficulties to obtain the converged solutions.

Numerical values of the contraction coefficient C_c and F^2 shown in Figure 5.6.

The contraction coefficient C_c is an increasing function of F^2 for a fixed value of γ. However the contraction coefficient C_c increases as the ratio of y_C and y_B decreases (see Figure 5.7). For a fixed the ratio $\frac{y_C}{y_B}$ or F^2, C_c increases as the gate inclination γ decreases. As F^2 increases, level of crests of the waves approaches the maximum level y^* of the free surface, i.e., $y^* = \frac{F^2}{2} + 1$ (see Figure 5.8).

Figure 5.9 shows that the amplitude A of the waves, defined as the difference between the levels of a successive crest and trough, increases as F_U decreases. Here F_U is an upstream Froude number, defined as

$$F_U = \frac{V}{\sqrt{gD}}.$$

where V is the average upstream velocity and D is the average upstream depth. The Froude number F and F_U are related by the identity

$$F_U^2 = \frac{F^2}{8}\left[\left(\frac{8}{F^2}+1\right)^{\frac{1}{2}} - 1\right]^3$$

(Binnie,1952).

In addition, the steepness s of the waves, defined as the ratio of heights between a crest and a trough and the wavelength, is shown to be a decreasing function of F_U in Figure 5.10. As F_U decreases to the critical value F_U^*, the elevation of the crests tends to the maximum level $\frac{{F_U^*}^2}{2} + 1$ and the waves reach their limiting configuration characterized by a 120° angle at the crests. In order to obtain these critical values, it is necessary to have a finer mesh to resolve the sharp crests. This requires an extensive use of computer time. The dot-dash curve in this figure corresponds to the highest waves computed by Cokelet (1977).

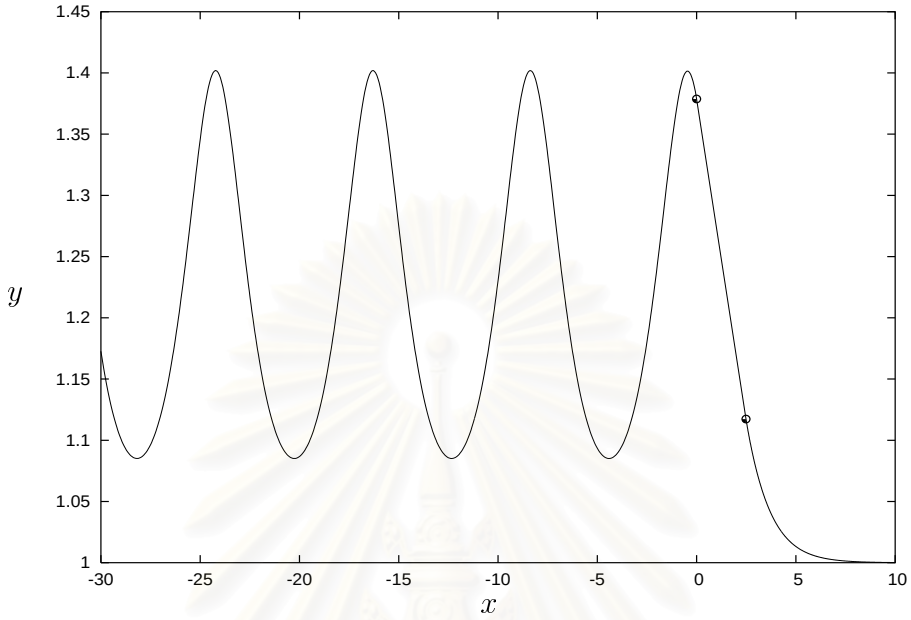

Figure 5.1 (a): $\phi_C = 2.00$ ($F = 1.1882$).

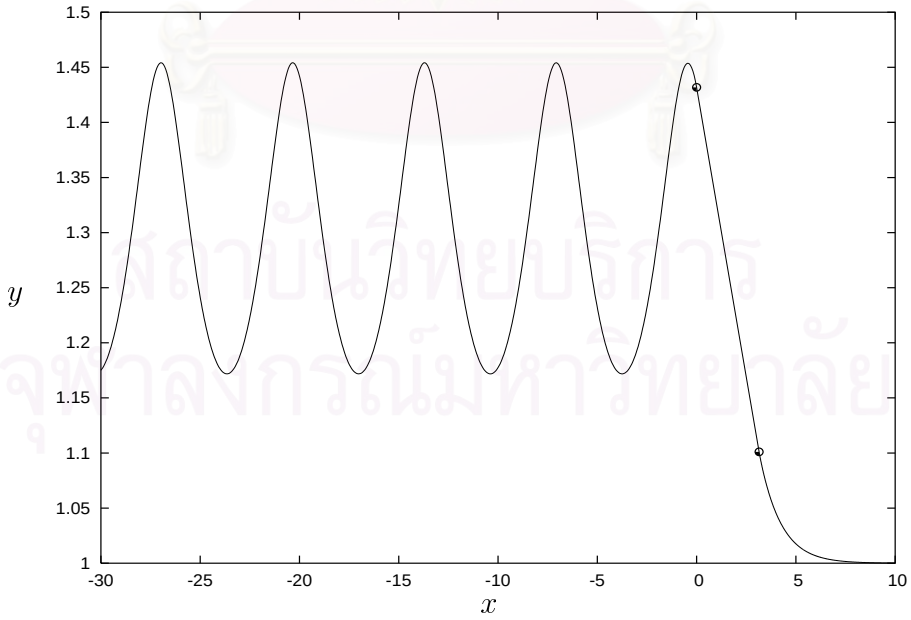

Figure 5.1 (b): $\phi_C = 2.50$ ($F = 1.2273$).

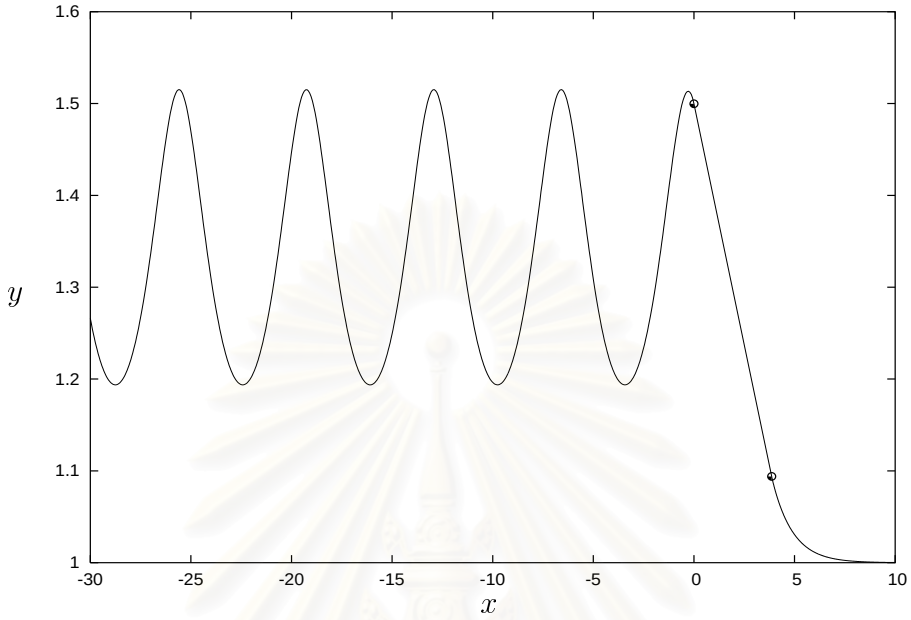

Figure 5.1 (c): $\phi_C = 3.00$ ($F = 1.2543$).

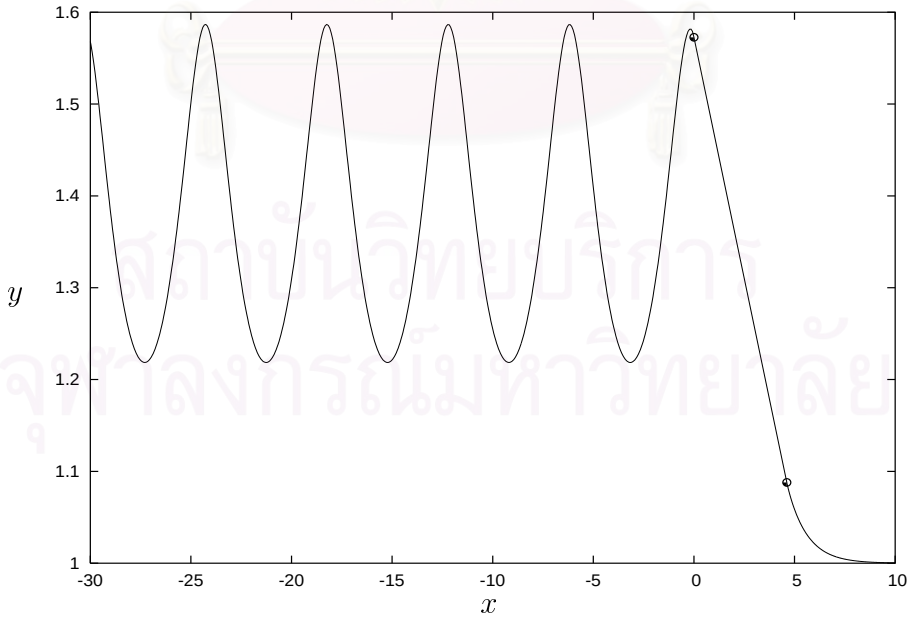

Figure 5.1 (d): $\phi_C = 3.50$ ($F = 1.2848$).

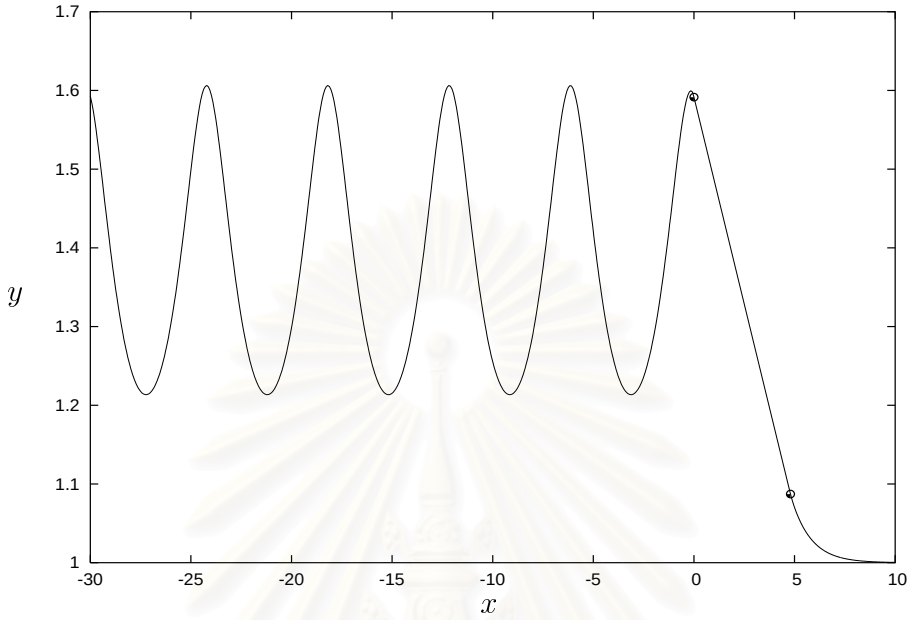

Figure 5.1 (e): $\phi_C = 3.618$ ($F = 1.2897$).

Figure 5.1: Profiles of the free surfaces and the gate when $\gamma = 6°$.

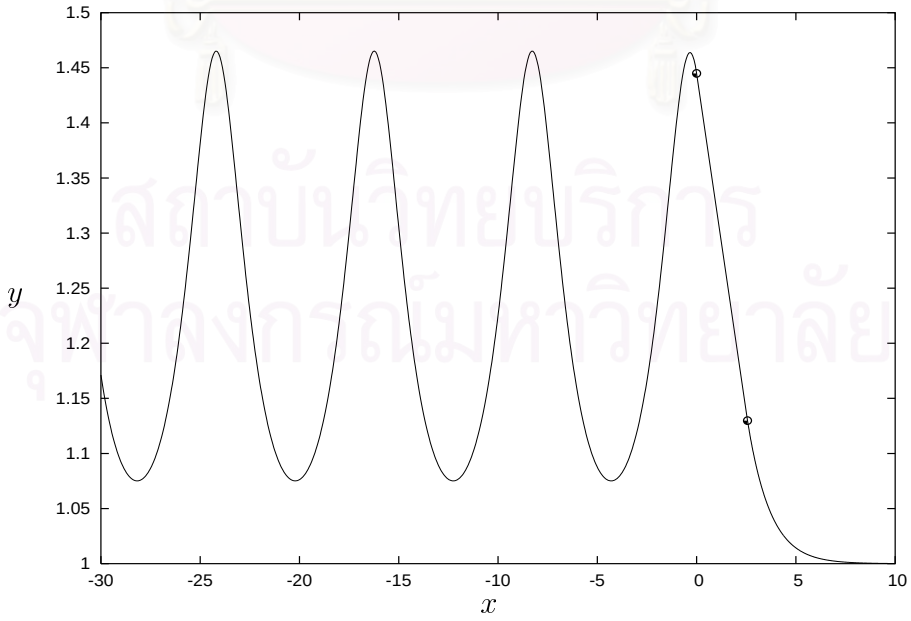

Figure 5.2 (a): $\phi_C = 2.00$ ($F = 1.2102$).

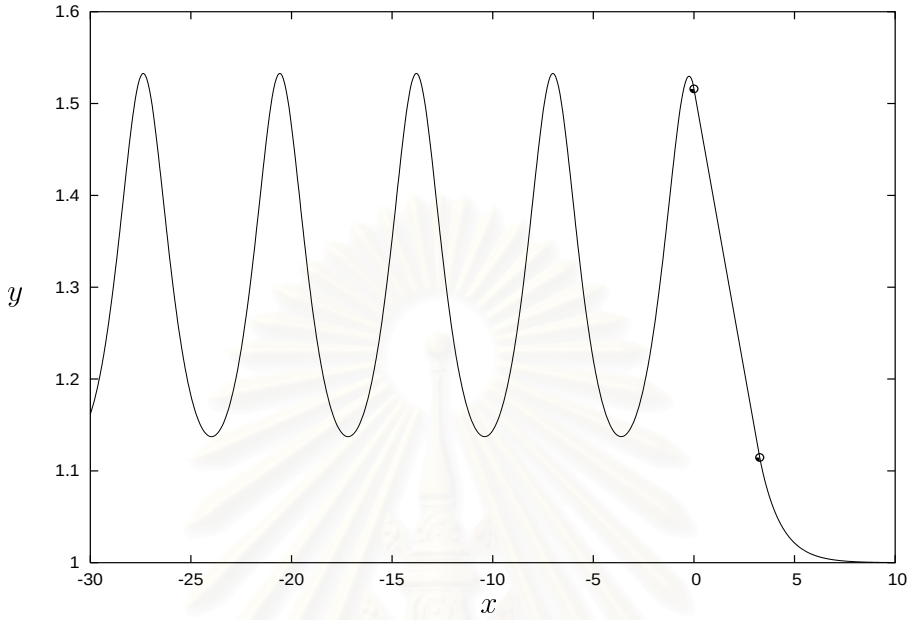

Figure 5.2 (b): $\phi_C = 2.50$ ($F = 1.2466$).

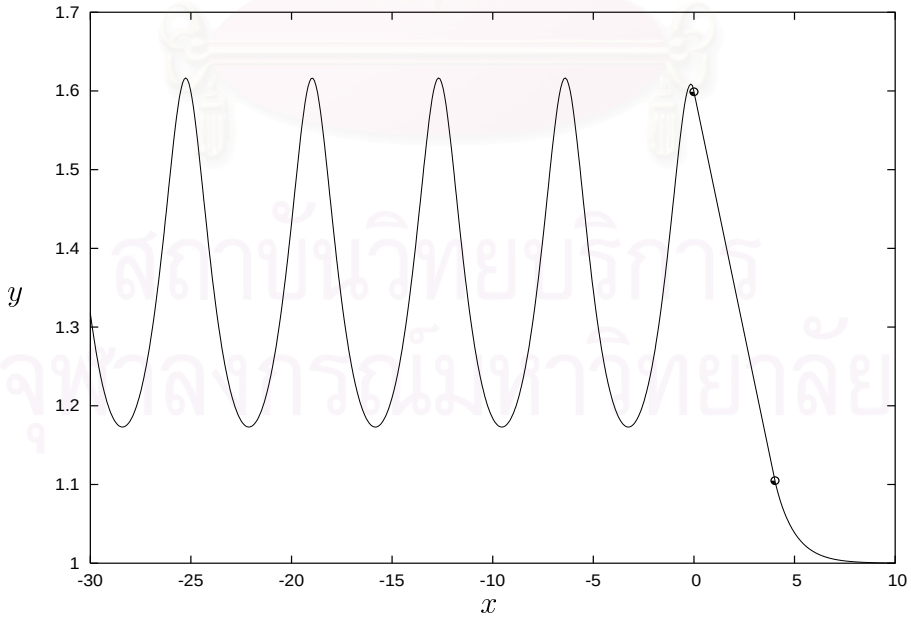

Figure 5.2 (c): $\phi_C = 3.00$ ($F = 1.2827$).

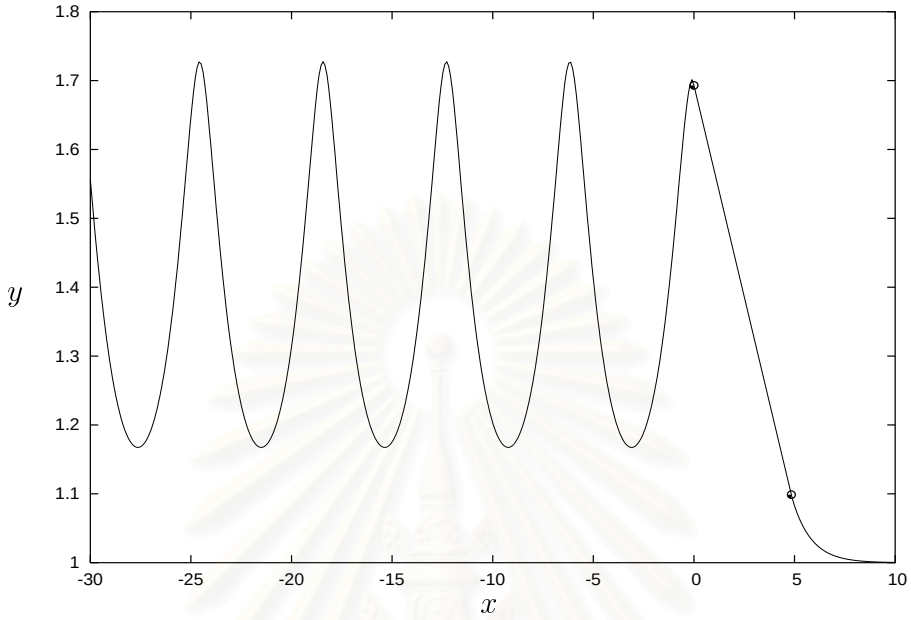

Figure 5.2 (d): $\phi_C = 3.50$ ($F = 1.3145$).

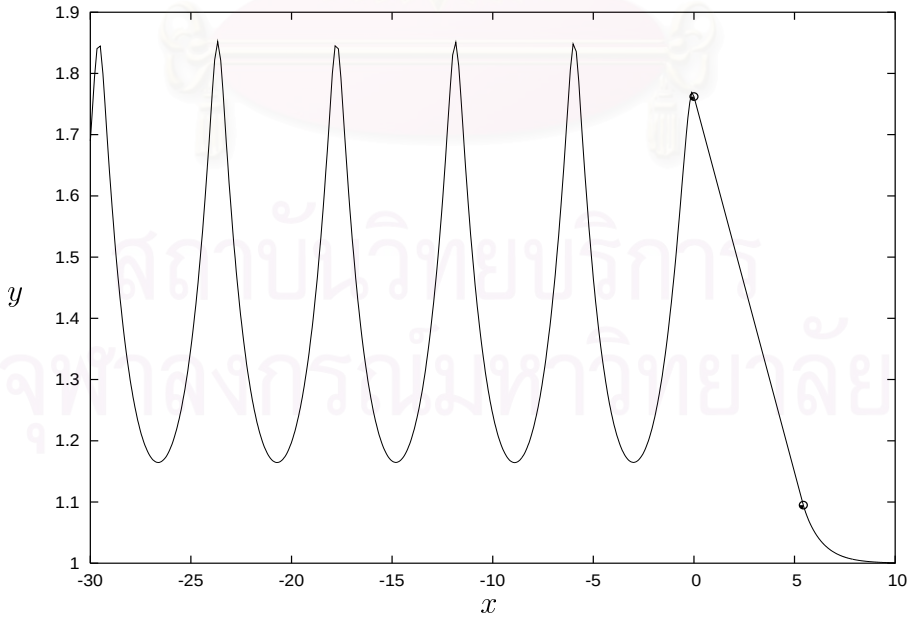

Figure 5.2 (e): $\phi_C = 3.844$ ($F = 1.3389$).

Figure 5.2: Profiles of the free surfaces and the gate when $\gamma = 7°$.

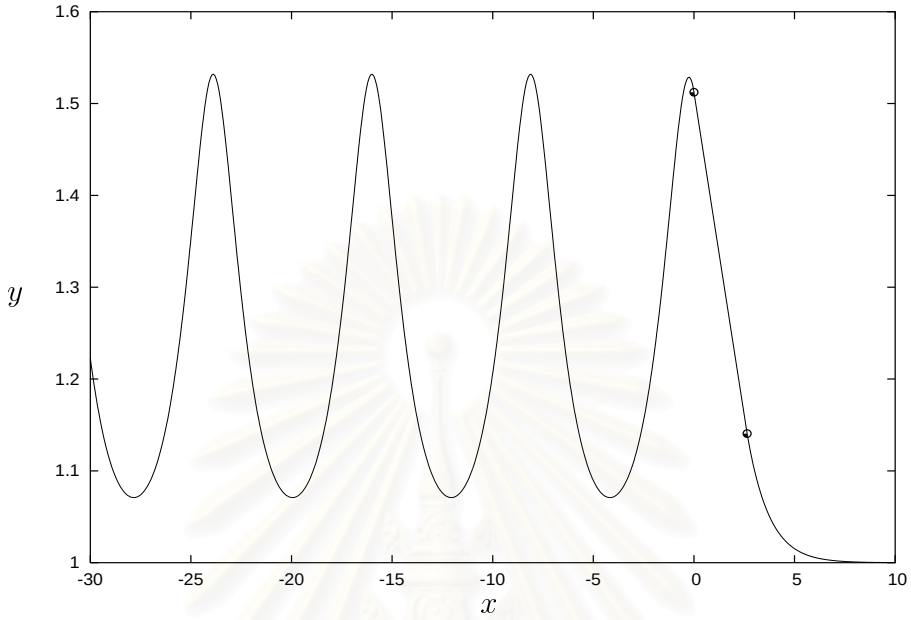

Figure 5.3 (a): $\phi_C = 2.00$ ($F = 1.2337$).

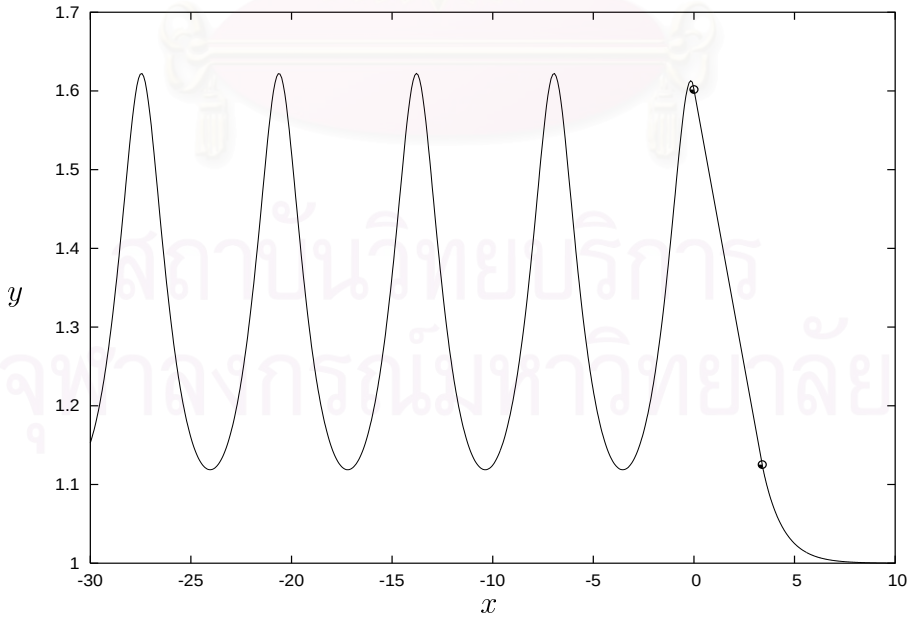

Figure 5.3 (b): $\phi_C = 2.50$ ($F = 1.2725$).

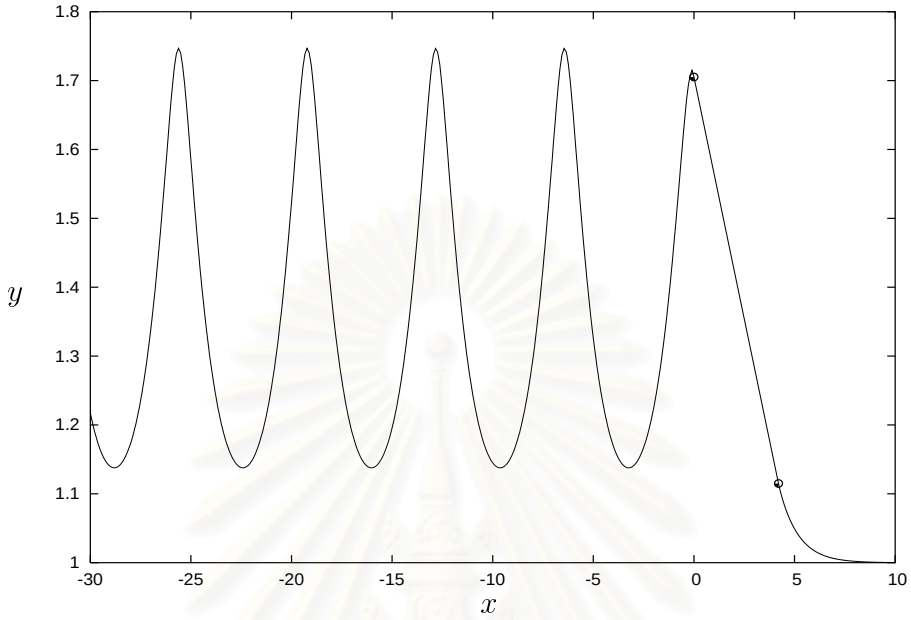

Figure 5.3 (c): $\phi_C = 3.00$ ($F = 1.3129$).

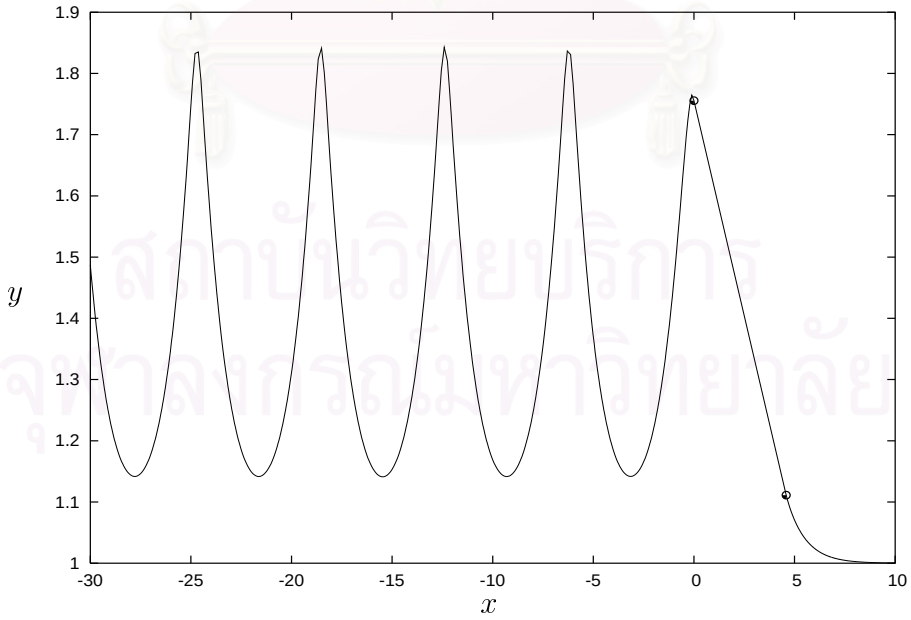

Figure 5.3 (e): $\phi_C = 3.224$ ($F = 1.3319$).

Figure 5.3: Profiles of the free surfaces and of the gate when $\gamma = 8°$.

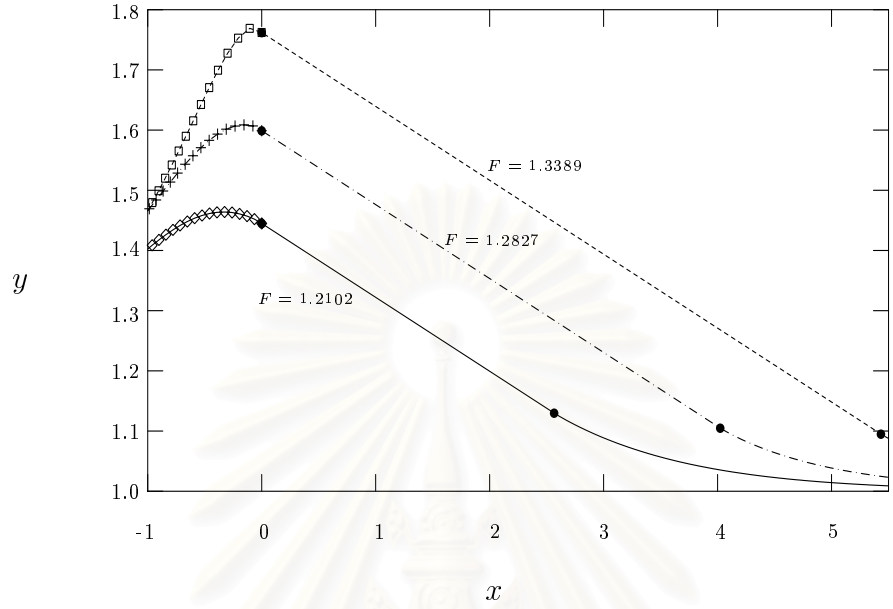

Figure 5.4: Blow up of the free surface near upstream separation point of Figure 5.2 (a), (c) and (e).

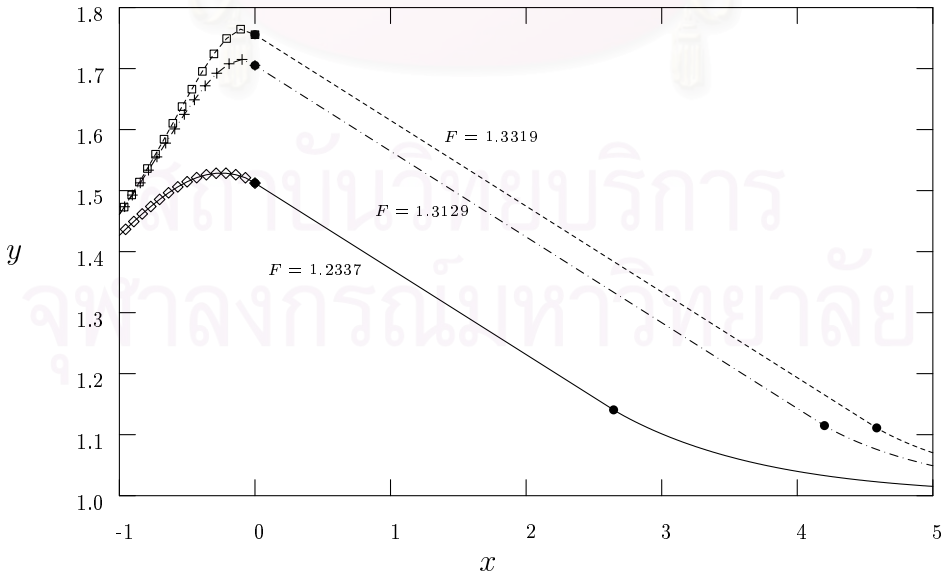

Figure 5.5: Blow up of the free surface near upstream separation point of Figure 5.3 (a), (c) and (e).

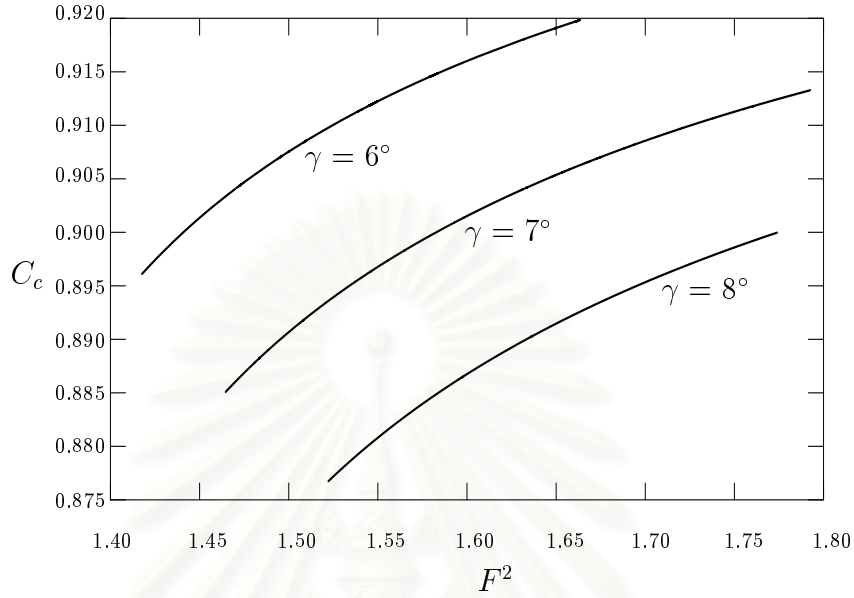

Figure 5.6: Values of the contraction coefficient C_c versus F^2.

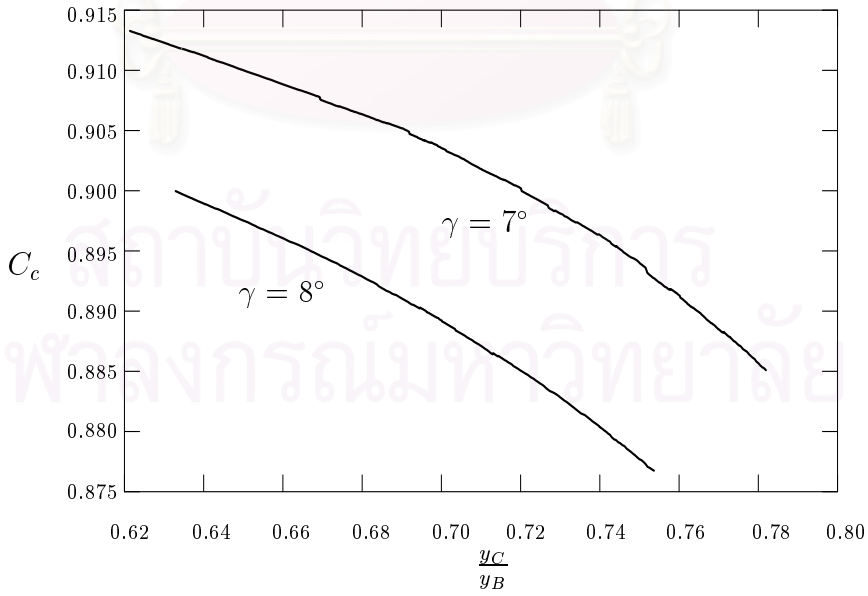

Figure 5.7: Values of the contraction coefficient C_c versus $\frac{y_C}{y_B}$.

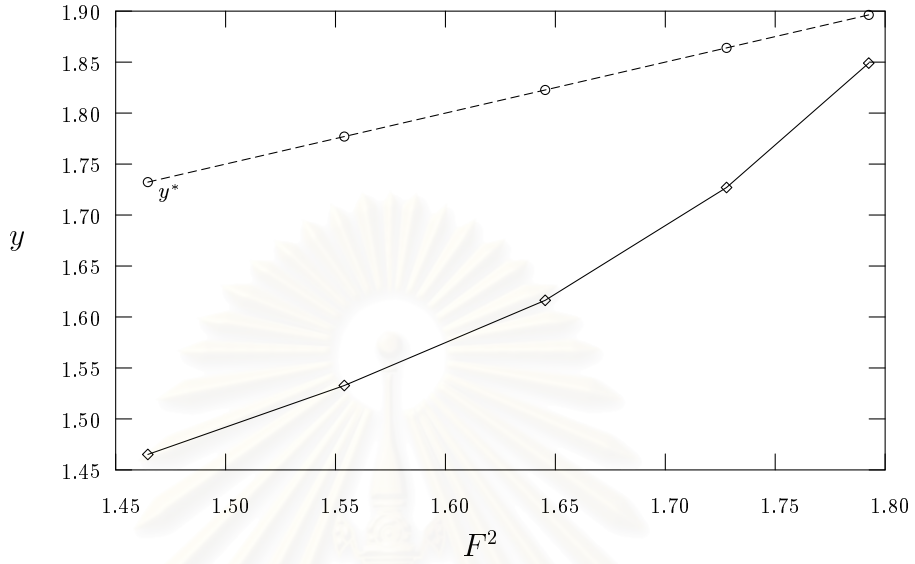

Figure 5.8: Numerical value of y at waves crests versus F^2 for $\gamma = 7°$. As $y^* = \frac{F^2}{2} + 1$ is the maximum level.

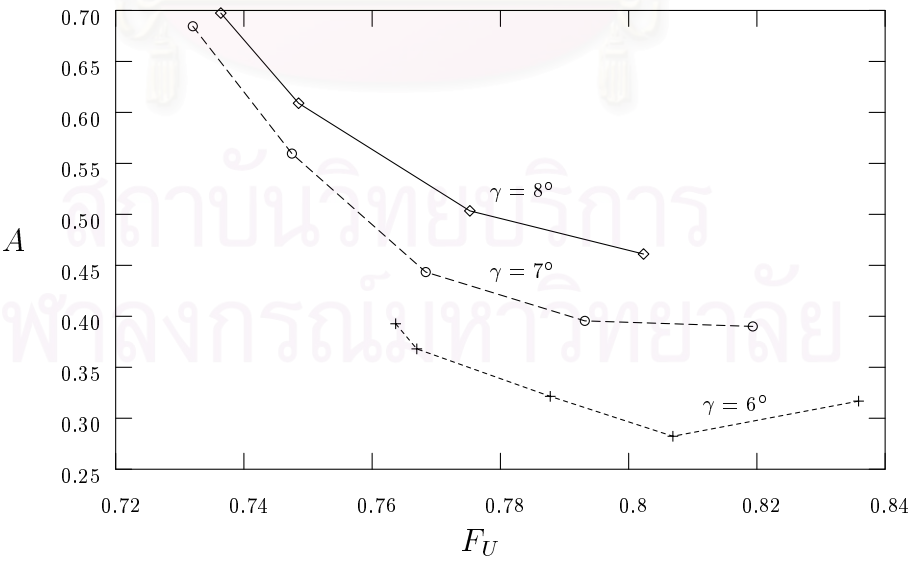

Figure 5.9: The amplitude A of the waves versus the upstream Froude number F_U.

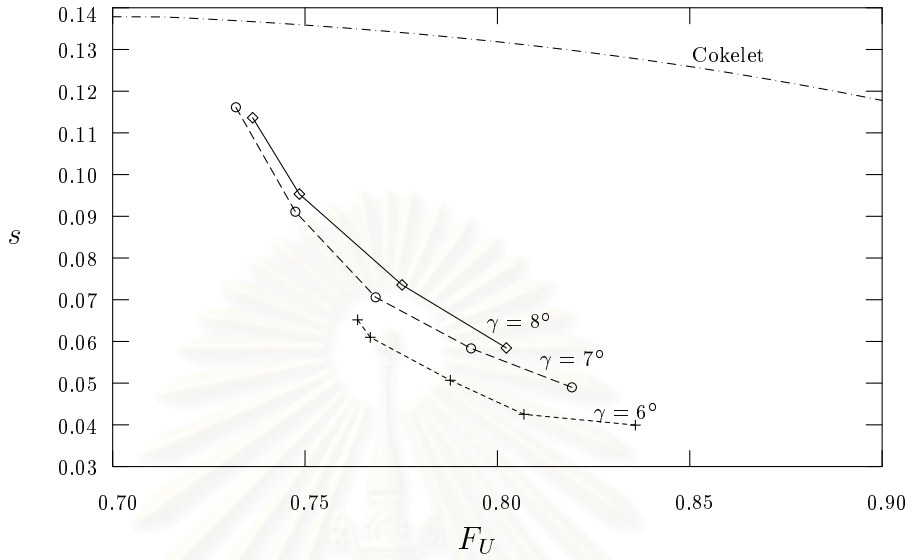

Figure 5.10: The steepness s of the waves versus the upstream Froude number F_U. The dot-dash curve corresponds the limiting cases characterized by a 120° angle at the crests (Cokelet 1977).

CHAPTER VI

Conclusions

We have presented accurate numerical solutions for the free-surface flows under an inclined sluice gate by using boundary integral method. The results show that there are two-parameter families of solutions, the gate inclination γ and ϕ_C.

When a stagnation recurs at the upstream separation, the angle between the upstream free surface and the gate can be either 90° or 120°. Results of the vertical sluice gate ($\gamma = 90°$) treated by Vanden-Broeck (1997) are completely recovered. This constitutes a check on our numerical scheme. It is found that numerical solutions can be found for all value of $\gamma \in (\chi, 90°)$. Here χ is some lower bound depending on ϕ_C. Amplitude of the upstream waves appears to be a decreasing function of ϕ_C or the downstream Froude number F for a given γ. For large F, amplitude of the waves is finitely small and cannot see in figures. In addition, the contraction coefficient C_c and gate length L decrease as F decreases.

Finally, we consider the inclined sluice gate problem with free surfaces leave tangentially at both separation points. The main cause of numerical solution divergence is numbers of mesh on the upstream first crests. Another one is crests of the waves reach limiting configuration characterized by a 120° angle. As the upstream Froude number F_U decreases or F increases, amplitude A and steepness s of the waves increase to the limiting values of Cokelet (1977).

In general, the behavior of the downstream flow can be described by at least two possible pattern, namely: hydraulic jump and jet flow. In this thesis, the downstream jet flow is assumed in all calculations.

For further study, one can include the surface tension effect into the problem. This effect could help explain the value of contact angle between the upstream free surface and the gate. One may use other numerical methods to solve this problem or perform experiments to confirm these results.

REFERENCES

[1] Asavanant, J. *Nonlinear free surface flow under a gate and flow over an obstruction.* Bangkok: TRF, 2000.

[2] Asavanant, J. and Vanden-Broeck, J. M. Free-surface supercritical splashless flows past a two-dimensional symmetrical rectilinear body. *Eur. J. Mech. B/Fluids* 17 (1998): 811-822.

[3] Asavanant, J. and Vanden-Broeck, J. M. Nonlinear free-surface flow emerging from vessels and flows under a sluice gate. *J. Aust. Math. Soc.* B 38 (1996): 63-86.

[4] Benjamin, T. B. On the flow in channels when rigid obstacles are placed in the stream. *J. Fluid Mech.* 1 (1956): 227-248.

[5] Cheng, A. H.-D.; Liggett, J. A. and Liu, P. L.-F. Boundary calculations of sluice and spillway flows. *J. of Hydr. Div.* 107 (1981): 1163-1178.

[6] Cokelet, E. D. Steep gravity waves in water of arbitrary uniform depth. *Phil. Trans. R. Soc. Lond.* A 286 (1977): 183-230.

[7] Dagan, G. and Tulin, M. P. Two-dimensional free-surface gravity flow past blunt bodies. *J. Fluid Mech.* 51 (1972): 529-543.

[8] Defina, A. and Susin, F. M. Hysteretic behavior of the flow under a vertical sluice gate. *Phys. Fluids* 15 (2003): 2541-2548.

[9] Fangmeier, D. D. and Strelkoff, T. S. Solution for gravity flow under a sluice gate. *ASCE J. Eng. Mech. Div.* 94 (1968): 153-176.

[10] Hocking, G. C. and Vanden-Broeck, J. M. Draining of a fluid of finite depth into a vertical slot. *Appl. Math. Modelling* 21 (1997): 634-649.

[11] Masliyah, J. H.; Nandakumar, K.; Hemphill, F. and Fung, L. Body-fitted coordinates for flow under sluice gates. *J. Hydr. Eng.* 111 (1985): 922-933.

[12] Maleewong, M. *Computation of free-surface flows under the influence of pressure distribution.* Master's Thesis, Department of Mathematics, Faculty of Science, Chulalongkorn University, 1999.

[13] Naghdi, P. M. and Vongsarnpigoon, L. Steady flow past a sluice gate. *Phys. Fluids* 29 (1986): 3962-3970.

[14] Petrila, T. Mathematical model for the free surface flow under a sluice gate. *Appl. Math. Comput.* 125 (2002): 49-58.

[15] Tooley, S *The effects of surface tension on free surface flows intersecting rigid walls.* Doctoral Dissertation, School of Mathematics, University of East Anglia, 2002.

[16] Vanden-Broeck, J. M. Flow under a gate. *Phys. Fluids* 29 (1986): 3148-3151.

[17] Vanden-Broeck, J. M. Numerical calculations of the free-surface flow under a sluice gate. *J. Fluid Mech.* 330 (1997): 339-347.

[18] Vanden-Broeck, J. M. and tuck, E. O. Flow near the intersection of a free surface with a vertical wall. *SIAM J. Appl. Math.* 51 (1997): 1-13.

[19] Xianyun, W. and Chigong, W. Boundary integral equation - Inverse method for free surface gravity flows. *Scientia Sinica* 9 (1987): 992-1008.

APPENDIX

APPENDIX

Monacella (1961) proved that a singularity in the Cauchy principal value integrals can be ignored in the numerical integration. This is achieved by spacing the mesh points symmetrically with respect to the pole. We show here by using the trapezoidal rule to compute the Cauchy principal value integral. We can also use the Simpson's rule to approximate such integral.

Let f be a continuous function. We approximate the integral of f over a finite interval $[a, b]$ by partitioning $[a, b]$ into N subintervals with $t_0 = a$ and $t_N = b$. Thus

$$\int_a^b f(t)dt \approx \sum_{i=0}^{N} f(t_i)hw_i. \tag{1}$$

Here $h = \frac{b-a}{N}$ and

$$w_i = \begin{cases} \frac{1}{2} & , i = 0 \quad \text{and} \quad N \\ 1 & , \text{otherwise.} \end{cases} \tag{2}$$

We consider a function $\dfrac{f(t)}{t-x}$ with $f(x) \neq 0$ and $x \in (a, b)$. The integral of $\dfrac{f(t)}{t-x}$ over the variable t is of Cauchy principal value form. For any $\epsilon > 0$, we can write this integral as

$$\int_a^b \frac{f(t)}{t-x}dt = \lim_{\epsilon \to 0} \left[\int_a^{x-\epsilon} \frac{f(t)}{t-x}dt + \int_{x+\epsilon}^b \frac{f(t)}{t-x}dt \right]. \tag{3}$$

To compute this integral, we rewrite the integral on the left hand side of (3) as

$$\int_a^b \frac{f(t)}{t-x}dt = \int_a^b \frac{f(t)-f(x)}{t-x}dt + f(x)\int_a^b \frac{1}{t-x}dt. \tag{4}$$

Next we consider $N+1$ equally spaced mesh point $t_i, i = 0, \ldots, N$. Thus x is the midpoint between t_i and t_{i+1} for $i = 0, 1, \ldots, N-1$. There are two possible cases to be taken into account: (i)$x = \frac{b-a}{2}$ and (ii) $x \neq \frac{b-a}{2}$.

Case (i) $x = \frac{b-a}{2}$.

It can easily be shown that $\int_a^b \frac{1}{t-x}dt = 0$. Thus (4) becomes

$$\int_a^b \frac{f(t)}{t-x}dt = \int_a^b \frac{f(t)-f(x)}{t-x}dt. \tag{5}$$

Using the trapezoidal rule, we approximate the integral on the right hand side of (5) by

$$\begin{aligned}\int_a^b \frac{f(t)}{t-x}dt &\approx \sum_{i=0}^{N} \frac{f(t_i)-f(x)}{t_i-x}hw_i \\ &= \sum_{i=0}^{N} \frac{f(t_i)}{t_i-x}hw_i - \sum_{i=0}^{N} \frac{f(x)}{t_i-x}hw_i \\ &= \sum_{i=0}^{N} \frac{f(t_i)}{t_i-x}hw_i. \end{aligned} \tag{6}$$

The $\sum_{i=0}^{N} \frac{f(x)}{t_i-x}hw_i = 0$ because x is midpoint of the interval $[a,b]$. Equation (6) suggests that the Cauchy principal value integral can be approximated as if it were an ordinary integral.

Case (ii) $x \neq \frac{b-a}{2}$.

Assuming that x is a midpoint on any interval $[c,d] \subset [a,b]$. We now rewrite (3) as

$$\int_a^b \frac{f(t)}{t-x}dt = \int_a^c \frac{f(t)}{t-x}dt + \int_c^d \frac{f(t)}{t-x}dt + \int_d^b \frac{f(t)}{t-x}dt. \tag{7}$$

The first and third integral on the right hand side of (7) are not Cauchy principal values. Thus they can be approximated by trapezoidal rule. The second integral is a Cauchy principal value with x as a midpoint of the interval $[c,d]$. The discussion in case (i) shows that it can also be evaluated by the trapezoidal rule. Therefore

$$\int_a^b \frac{f(t)}{t-x}dt \approx \sum_{i=0}^{N} \frac{f(t_i)}{t_i-x}hw_i$$

Which is the same as (6). Thus, the singularity is subtracted from the Cauchy principal value integral leaving nonsingular integrals to evaluate as claimed.

VITA

Acting Sec. Lt. Panat Guayjarernpanishk was born on February 16, 1976 in Ubonratchathani, Thailand. He received a Bachelor of Science in Mathematics (2^{nd} Class Degree Honours) from Department of Mathematics, Faculty of Science, Chaing Mai University in 1996. He had worked for four years at Faculty of Science, Ubonratchathani University before he started of master at Chulalongkron University and by the University Development Commission (U.D.C.) Scholarship. He is interested in numerical analysis and computational fluid dynamics.